STATUS REPORTS

to the

RECYCLED PAPER

AND

SURFACE AND COLLOID SCIENCE

PROJECT ADVISORY COMMITTEE

March 27, 1997

INSTITUTE OF PAPER SCIENCE AND TECHNOLOGY

Atlanta, Georgia

ANNUAL RESEARCH REVIEW

RECYCLED PAPER

AND

SURFACE AND COLLOID SCIENCE

March 27, 1997

February 13, 1997

TO: MEMBERS OF THE RECYCLED PAPER AND SURFACE AND COLLOID SCIENCE PROJECT ADVISORY COMMITTEES

Attached for your review are the Status Reports for the projects to be discussed at the Recycled Paper and Surface Colloid Science Project Advisory Committee meeting. The Program Review is scheduled for Thursday, March 27, 1997, at 8:00 a.m. - 12:00 p.m. and the PAC Committee Meeting will meet from 1:00 p.m. to 5:00 p.m.

Please note that the meeting is being held at the Institute of Paper Science and Technology.

We look forward to seeing you at this time.

Sincerely,

David I. Orloff, Ph.D.
Professor of Engineering & Director
Engineering and Paper Materials Division

DIO/map

Attachments

Institute of Paper Science and Technology, Inc.

500 10th Street, N.W.
Atlanta, GA 30318-5794

Telephone 404-894-5700
FAX# 404-894-IPST (4778)

RECYCLE/SURFACE AND COLLOID SCIENCE
PROJECT ADVISORY COMMITTEE

IPST Liaison: Dr. David Orloff (404) 894-6649; FAX (404) 894-1496
RAC Liaison: Mr. Walter Rew (218) 327-6272; FAX (218) 327-6392

Dr. Giancarlo A. Cavagna *(1997)
Research Associate
Westvaco Corporation
11101 Johns Hopkins Road
Laurel, MD 20723
(301) 497-1347
(301) 497-1309 FAX

Mr. W. Bruce Darlington *(1997)
Senior Research Fellow
The Mead Corporation
Central Research
Post Office Box 1700
Chillicothe, OH 45601-5700
(614) 772-3055
(614) 772-3595 FAX

Dr. Robert De Jong *(1999)
James River Corporation
1915 Marathon Avenue
Post Office Box 899
Neenah, WI 54957-0899
(414) 729-8555
(414) 729-8161 FAX

Mr. Anil Dewan *(1999)
Director, Mechanical Pulping /Recycle Fiber
Champion International Corporation
West Nyack Road
West Nyack, NY 10994-1738
(914) 578-7240
(914) 578-7175 FAX

Dr. Susan M. Ehrhardt *(1996)
Project Manager
Hercules Incorporated
Research Center - Lancaster Pike
500 Hercules Road
Wilmington, DE 19808-1599
(302) 995-3109
(302) 995-4565 FAX

Mr. Joseph M. Fernandez *(1998)
Senior Research Engineer
Potlatch Corporation
Fiber Research & Development
20 N. 22nd Street
Post Office Box 503
Cloquet, MN 55720
(218) 879-2374
(218) 879-2375 FAX

Ms. Susan Freeland *(1999)
Fiber Science Department
Weyerhaeuser Company
WTC 2B22
Tacoma, WA 98477
(206) 924-6414
(206) 924-6324 FAX

Mr. Pierre Gagnon *(1998)
St. Laurent Paperboard Inc.
Research Center
15400 Cherbrooke East
Montreal, CANADA H1A 3S2
(514) 642-9251
(514) 498-3411 FAX

Mr. David Grimes *(1998)
Senior Research Engineer
Beloit Corporation
Pittsfield Research Center
448 Hubbard Avenue
Pittsfield, MA 01201-3822
(413) 445-3266
(413) 499-3155 FAX

Mr. Herbert Holik *(1999)
Head of R&D Stock Preparation
Voith Sulzer
Stoffaubereitung GmbH
Postfach 2120
Ravensburg, D 88191 GERMANY
4 90 751832402
4 90 751833030 FAX

Dr. Gregory J. Hollod *(1996)
Vice President of Health, Safety
and Environmental
Riverwood International Corporation
3350 Cumberland Circle
Suite 1600
Atlanta, GA 30339
(770) 644-3223
(770) 644-2925 FAX

Mr. James Lynn Jonakin *(1999)
Director of Technology
MacMillan Bloedel Inc.
Post Office Box 336
Pine Hill, AL 36769-0336
(334) 963-4391
(334) 963-4850 FAX

Recycle/Surface and Colloid Science PAC (cont.)

Dr. Michael Juang *(1996)
Senior Research Chemist
Boise Cascade Corporation
4435 North Channel Avenue
Portland, OR 97217-7652
(503) 286-7452
(503) 286-7467 FAX

Mr. Maury Keesler *(1997)
Director, New Product & Strategic Development
Wisconsin Tissue Mills, Inc.
Post Office Box 489
Menasha, WI 54952
(414) 725-7031
(414) 727-3743 FAX

Mr. Kasy King *(1998) (Vice Chairman)
Manager, Pulp & Paper Technology
Appleton Papers Inc.
Post Office Box 359
Appleton, WI 54912-0359
(414) 749-8878
(414) 730-7243 FAX

Dr. Veli V. Lapinoja *(1997)
Director, Pulp and Paper Engineering
Georgia-Pacific Corporation
133 Peachtree Street, NE
Post Office Box 105605
Atlanta, GA 30303-5605
(404) 652-4618
(404) 584-1466 FAX

Mr. Philip N. Liberato *(1996)
Manager, Process and Product Development
Chesapeake Corporation
19th & Main Streets
Post Office Box 311
West Point, VA 23181-0311
(804) 843-5553
(804) 843-5409 FAX

Mr. Bob McIntyre *(1999)
Asten, Inc.
209 Bareton Drive
Raleigh, NC 27615

Dr. Robert Moran *(1999)
Vice President, Manufacturing Services
Bowater Incorporated
55 East Camperdown Way
Post Office Box 1028
Greenville, SC 29602
(864) 282-9371
(864) 282-9570 FAX

Mr. Christopher D. Perry *(1998)
Technical Specialist
Buckman Laboratories International, Inc.
1256 N. McLean Blvd.
Memphis, TN 38108
(901) 272-6473
(901) 272-8585 FAX

Mr. Michael A. Pikulin
Group Leader
Union Camp Corporation
R&D Division
Post Office Box 3301
Princeton, NJ 08543-3301
(609) 844-7224
(609) 844-7323 FAX

Mr. Erland C. Porter, Jr. *(1998)
Technical Director
Repap Wisconsin Inc.
433 North Main Street
Kimberly, WI 54136-1490
(414) 788-3511
(414) 788-8609 FAX

Mr. Walter Rew *(1999)
Technical Director
Blandin Paper Company
115 First Street, SW
Grand Rapids, MN 55744-3407
(218) 327-6272
(218) 327-6392 FAX

Dr. Nigel Sanders *(1998)
Project Manager
Specialty Minerals Inc.
9 Highland Avenue
Bethlehem, PA 18017
(610) 861-3457
(610) 861-3412 FAX

Recycle/Surface and Colloid Science PAC (cont.)

Mr. Peter Seifert *(1997)
Corporate Vice President, Research
& Product Planning
The Black Clawson Company
605 Clark Street
Middletown, OH 45042
(513) 424-7400
(513) 424-3845 FAX

Dr. Steven J. Severtson *(1998)
Chemist
Nalco Chemical Company
One Nalco Center
Naperville, IL 60563-1198
(630) 305-1000
(630) 305-2982 FAX

Dr. Jeffrey S. Shaw *(1995)
Manager
3M Company
Paper Technology Center
Building 230-2F-10
St. Paul, MN 55144
(612) 733-0980
(612) 736-0237 FAX

Mr. Richard J. Spangenberg *(1998) (Chairman)
Director, Recycling Research
Weyerhaeuser Company
WTC 2F39
Tacoma, WA 98477-0001
(206) 924-6501
(206) 924-6541 FAX

Dr. Michael R. St. John *(1999)
Research Associate
Nalco Chemical Company
One Nalco Center
Naperville, IL 60563-1198
(708) 305-2349
(708) 305-2982 FAX

Dr. David White *(1998)
James River Corporation
1915 Marathon Avenue
Neenah, WI 54957-0899
(414) 729-8466
(414) 729-8023 FAX

Mr. Louis K. Wilhelm *(1999)
Recycling Manager
P.H. Glatfelter Co.
1655 Bergstrom Road
Neenah, WI 54956
(414) 727-2200
(414) 727-2305 FAX

RECYCLE & SURFACE AND COLLOID SCIENCE PROJECT ADVISORY COMMITTEE MEETING

March 27, 1997

Institute of Paper Science and Technology
Atlanta, Georgia

PROGRAM REVIEW AGENDA

Seminar Room

8:00 a.m. - 8:10 a.m.	Opening Remarks and Antitrust Statement		Dick Spangenberg
8:10 a.m. - 8:15 a.m.	Welcome by Vice President of Research		Gary Baum
8:15 a.m. - 8:30 a.m.	Overview of IPST Recycle/Surface Science Research		David Orloff
8:30 a.m. - 9:30 a.m.	Project F00903	Flotation Deinking Fluid Mechanics	Ted Heindel
9:30 a.m. - 9:50 a.m.	Break		
9:50 a.m. - 11:00 a.m.	Project F00904	Fiber Carry Over Reduction in Flotation Deinking	Yulin Deng
11:00 a.m. - 12:00 p.m.	Project F00902	Effect of Shear on Stickie Deposition and Agglomeration	Sujit Banerjee

Seminar Room

1:00 p.m. - 3:30 p.m.	Recycled Paper and Surface and Colloid Science Discussions

RECYCLE & SURFACE AND COLLOID SCIENCE PROJECT ADVISORY COMMITTEE MEETING

March 27, 1997

Institute of Paper Science and Technology
Atlanta, Georgia

COMMITTEE DISCUSSIONS AGENDA

Seminar Room (Room 114)

1:00 p.m.	Convene - Antitrust Statement - New Members - Acceptance of Agenda	Spangenberg
1:15 p.m.	Small Group Review of Project Comments	
	• Flotation Deinking Fluid Mechanics	DeJong, Dewan, Seifert
	• Fiber Carry Over Reduction in Flotation Deinking	King, Sanders, White
	• Effect of Shear on Stickie Deposition and Agglomeration	Cavanaga, Grimes, Severtson
2:00 p.m.	Break	
2:15 p.m.	Re-Convene and Summary of Reviews	Review Leaders
3:15 p.m.	Other Business Date for Fall Meeting	Spangenberg
3:30 p.m.	Adjourn	

TABLE OF CONTENTS

FLOTATION DEINKING FLUID MECHANICS

STATUS REPORT

FOR

PROJECT F00903

Ted Heindel

March 27, 1997

Institute of Paper Science and Technology
500 10th Street, N.W.
Atlanta, Georgia

Project Title:	**FLOTATION DEINKING FLUID MECHANICS**
Project Code:	DEINKFLOW
Project Number:	F00903
Division:	Engineering and Paper Materials
Project Staff:	Ted Heindel, Adele Emery, Fred Bloom
Project Budget (FY96-97):	$122,174
Reporting Period:	March 1996 to March 1997

1 OBJECTIVE

The objective of this project is to increase flotation efficiency by maximizing contaminant removal from wastepaper while minimizing fiber loss. This objective will be realized by developing a better understanding of the fundamental processes involved in flotation separation.

2 SUMMARY

This report summarizes the progress of this study over the past year in the areas of modeling the overall flotation separation process and measuring the bubble size distribution in a pulp suspension. The report that follows begins by reviewing the goals for this period. The focus will then change to two specific areas, flotation modeling and bubble size determination. Within each area, a brief summary as to why this work is important to the pulp and paper industry will be presented. Then, selected results obtained over the current period will be highlighted. Finally, goals for the next period will be stated, and the report will end with a short conclusion.

3 GOALS

The project goals for the current period (March 1996 to March 1997), which were presented at the Project Review on March 20, 1996, involved:

<u>Flotation Modeling</u>

1. Use the identified parametric ranges of the flotation parameters to evaluate the various flotation performance assessment parameters defined in the simplified flotation model and determine which parameters are most influential.

Status: Completed.

2. Extend the simplified flotation model by relaxing some of the incorporated assumptions.

   Status: Three additional models have been outlined.

3. Compare predictions from the first model to those from the extended models.

   Status: Delayed until April 1997.

4. Identify, with the help of a PAC subcommittee, experiments that we should conduct to verify our flotation model and begin designing these experiments.

   Status: Initiated process.

5. Summarize our advances in flotation modeling in a formal Member Company report.

   Status: Completed, Project F00903 Report 2 issued November 25, 1996 [1].

Bubble Size Determination

1. Conclude the flash x-ray radiographic measurements to determine the effect pulp fibers have on bubble size.

   Status: Completed.

2. Issue a formal report to the Member Companies upon completion of this experiment.

   Status: Completed, Project F00903 Report 3 issued February 3, 1997 [2].

4 DISCUSSION

Project discussion will focus on the two areas addressed in this research program: modeling the overall flotation separation process and bubble size measurements in a pulp suspension. Details of the progress made in these two areas are contained in this section.

4.1 Flotation Modeling

4.1.1 Introduction – Flotation Modeling Significance

Since flotation is influenced by many parameters (e.g., bubble size, particle size, particle density, contact angle, surface tension, turbulent energy density, etc.), modeling can be used to isolate specific effects. Flotation models can also be used to identify, among other things, which parameters affect contaminant removal and which ones do not (under specific conditions), what the parametric trends may be for given situations, and how to improve system performance for given flotation constraints. These predictions can be performed before expensive system trials are initiated to determine if desired results can be expected for the given change in operating conditions.

4.1.2 The "Simplified" Flotation Model (Model #1)

A first-generation model of the overall flotation deinking process has been developed in Report 1 of this project [3]; it includes the overall probability that a free (ink) particle will successfully intercept and adhere to an air bubble that is initially void of particles, as well as the probability that a bubble/particle aggregate will become unstable and split to yield an additional free (ink) particle. This model assumes that the bubbles and particles are spherical, the total number of particles is constant (n_p = constant), the total number of bubbles is constant (n_B = constant), the total number of particles that attach to an individual bubble is 1 ($n_p^a = n_B^a$), and the total number of bubbles is greater than the total number of particles ($n_B > n_p$). This model will be referred to as Model #1.

Results from this model have been utilized to predict four different flotation cell performance measures: (1) flotation efficiency as a function of time; (2) flotation efficiency at infinite flotation time; (3) flotation efficiency after a given flotation time; and (4) the time required to reduce the number of free (ink) particles in a representative unit volume by a given amount. These predictions are summarized in Report 2 of this project [1]. A general summary will be provided here, and details can be found in Report 2.

Our first-generation model is described by a kinetic-type equation governing the number of (ink) particles in a volume element and can be written as

$$\frac{dn_p^f}{dt} = -k_1 n_p^f n_B^f + k_2 n_B^a \tag{1}$$

where the initial condition $n_p^f(0)$, given at t = 0 (i.e., the number of free particles at time t = 0), is known. The first term on the right-hand side represents the overall probability that a free particle (n_p^f) will successfully attach to a bubble that is initially free of particles (n_B^f). The second term is a measure of the probability that a bubble/particle aggregate (an air bubble that has a particle attached to it – n_B^a) will become unstable and split to yield a "new" free particle. The "kinetic" constants k_1 and k_2 are positive numbers described by the following relationships:

$$k_1 = ZP_cP_{asl}P_{tpc}P_{stab} \tag{2}$$

$$k_2 = P_{destab} = 1 - P_{stab} \tag{3}$$

where Z is the collision frequency between the particles and bubbles; P_c is the probability of collision between a particle and bubble; P_{asl} is the probability of adhesion by sliding; P_{tpc} is the probability of three-phase contact; P_{stab} is the probability of stability of a bubble/particle aggregate; and P_{destab} is the probability of destabilization of a bubble/particle aggregate. Various formulations of the collision frequency and the distinct probabilities are discussed in detail in Report 1 [3], and specific values used in this study are summarized in Report 2 [1].

From the solution of Eq. (1), four different performance parameters have been identified: (1) flotation efficiency as a function of time; (2) flotation efficiency at infinite flotation time; (3) flotation efficiency after a given flotation time; and (4) the time required to reduce the number of free (ink) particles in a representative unit volume by a given amount. The solution to Eq. (1), as well as these performance parameters, are described in detail in Report 2 [1].

To obtain flotation cell performance predictions, selected bubble, particle, and fluid parameters must be identified. The parameters used in this study are outlined in Table 1. The rationale behind these parametric values is discussed in Report 2, where detailed results are also found.

Predictions that result from the solution of Eq. (1) can be utilized to generate figures representing the flotation efficiency as a function of time. Two such figures are presented in Figs. 1 and 2 for selected bubble and particle radii, respectively. To generate these figures, all other parameters are held constant at their standard conditions (i.e., see Table 1). As shown in Fig. 1, for the given fixed conditions, increasing the flotation time in a representative unit volume increases flotation efficiency until an asymptotic limit is reached, which is very low for $R_B = 0.1$ mm (asymptotic limit of approximately 0.06), but increases as bubble radius increases. Increasing R_B also reduces the time period required to reach the asymptotic limit of 1 when $R_B \geq 0.5$ mm for the given conditions.

The effect particle radius has on flotation efficiency as a function of time is shown in Fig. 2. Particle radii greater than 200 μm (i.e., calculations at $R_p = 300$ and 500 μm) are not shown in Fig. 2 because at the larger particle radii, the correlation for P_{stab} results in $P_{stab} < 0$ for the given conditions, which implies the bubble and particle will not form a stable aggregate under these conditions. When $R_p = 200$ μm, flotation efficiency is very high at $t = 0.1$ sec, but asymptotes to a value less than 1 (≈ 0.98). Therefore, approximately 2% of the particles with $R_p = 200$ μm will not form a stable bubble/particle aggregate and will not be removed. As the particle radius decreases, a longer time period is required for the flotation efficiency to asymptote to a constant

value, which approaches 1. Even when R_p = 1 μm, flotation efficiency asymptotes to 1. However, particles this small are typically not removed in conventional flotation cells. This apparent discrepancy between the model and actual operation can be explained by focusing on how long the actual required time period is for the efficiency to asymptote to 1 for R_p = 1 μm – well over 6000 seconds. Hence, a particle with R_p = 1 μm *must* remain in the unit volume for almost *1.7 hours* to eventually collide with and attach to a bubble. This is highly unlikely in actual flotation cell operation because the stock will typically remain in a unit volume for a much shorter time period, which may even be less than 1 second (depending on the definition of a representative unit volume, which may be large or very small). For example, when $t \approx 100$ seconds, the flotation efficiency is approximately 0.12 for R_p = 1 μm, which is a very poor removal efficiency, and when $t \approx 1$ second for the same conditions, the flotation efficiency is nearly 0.

Another way to look at efficiency is to fix the flotation time and determine how the efficiency varies with changes in selected parameters. Figure 3 represents a typical plot where the flotation time has been fixed at 1 second, and flotation efficiency is predicted as a function of particle radius for selected values of bubble radii. Small particles are not removed very effectively, if at all, after 1 second. Increasing the particle radius results in an increase in the efficiency until a maximum is reached over a given particle size range, which depends on the given conditions, then the efficiency rapidly declines toward zero. The rapid decline is due to the failure of the larger particles in forming stable bubble/particle aggregates. The shape of these curves is similar to that typically presented when flotation efficiency is plotted as a function of particle size, where flotation is performed for a given time period. Therefore, our predictions are at least in qualitative agreement with experimental and operational observations.

Similar curves to those presented here and the two other flotation cell performance parameters can be found in Report 2 [1]. The general conclusions from this report are summarized in Tables 2-5. They are:

- Table 2 summarizes the predictions for flotation efficiency as a function of time. Model #1 predicts that flotation efficiency will increase as flotation time increases and will asymptote to a constant value given a long enough flotation time. In general, for the given conditions addressed in this study, varying R_B, R_p, ε, ϕ^*_{crit}, n_B, or n_p, while holding all other parameters fixed, produced families of similarly shaped curves. Altering ρ_p or θ over the ranges considered in this study, while holding all other parameters fixed, resulted in no significant effect on flotation efficiency as a function of time.
- The general trends of flotation efficiency at infinite flotation time are summarized in Table 3. In general, for the considered conditions, the flotation efficiency at infinite flotation time will approach 1 for large bubble radii, small particle radii, all particle densities, all turbulent energy densities, large contact angles, large critical attachment angles, a large number of bubbles, and a large number of particles. Deviations from these general trends do exist and depend on the selected parameters. Note that infinite flotation time may be on the order of seconds (or less) for some conditions, but on the order of hours for others. Therefore, the above trends would result only if the specified conditions would remain constant in a representative unit volume for the required time period. Hence, these trends imply the best efficiencies under the given operating conditions.
- The overall trends predicted for flotation efficiency after a flotation time of 1 second are summarized in Table 4. In general, these results reveal that flotation efficiency after a flotation time of 1 second is sensitive to most parameters considered in this study, with increasing the respective parameter generally resulting in an increase in the efficiency. However, when the bubble/particle aggregate becomes unstable, the efficiency drops drastically toward zero.
- Table 5 summarizes the common trends for the time required to reduce the total number of free particles in a representative unit volume by a factor of two ($t_{1/2}$). In general, $t_{1/2}$ decreases (or remains constant) as the considered parameters are increased. The decrease in $t_{1/2}$ is most sensitive to bubble radius, particle radius, critical attachment angle, number of bubbles, and

number of particles and can be more than several orders of magnitude. Deviations from this general trend typically result from the destabilization of the bubble/particle aggregate.

4.1.3 Model Extensions

Our "simplified" flotation model (Model #1) includes various assumptions in order to obtain a solution. We have begun to relax selected assumptions and have outlined three additional models based on the assumptions listed in Table 6. Predictions based on some of these models will soon be initiated, and results will be reported in a similar fashion to those in Report 2. Details of the specific model will also be presented at this time.

4.1.4 Publications

At the March 20, 1996, PAC Meeting, members expressed their desire that I interact with other individuals doing similar research. To accomplish this, I attended the 1996 TAPPI Pulping Conference, October 27-31, 1996. To allow further interactions and permit discussion of my work with other researchers before the two-year moratorium expires, I was given permission to publish the more fundamental areas of this work early. To this end, two papers have been accepted for publication, one at the 1997 TAPPI Recycling Symposium [4], and one in the journal of *Mathematical and Computer Modelling* [5]. An additional paper is currently under review [6].

4.2 Bubble Size Determination

In general, air/water/fiber systems like those common to flotation deinking are opaque, and visualizing what the air bubbles are doing in the bulk flow is very difficult, if not impossible. Flash x-ray radiography (FXR) has been utilized in this project to visualize gas flows in pulp suspensions at consistencies commonly found in the mill. Report 3 [2] of this project summarizes this procedure and presents results for bubble size measurements in an ONP system. Selected results will be highlighted here. Additionally, preliminary observations of the bubble dynamics in a bleached kraft system will also be presented.

4.2.1 Introduction - Bubble Size Importance

Controlling the air bubble size, quantity, ascension path, and coalescence rate in a pulp slurry is important for effective control of flotation separation. In addition to flotation deinking, this information can also be used to improve bleaching performance and clarifier operations. Bubble behavior is very important to flotation deinking because it has a direct effect on the contaminant removal efficiency. For example, a bubble must be large enough to produce a sufficient buoyant force to rise through the fiber network. However, if the bubble is too large, the overall bubble surface area will be significantly reduced for a given total air volume, which reduces the area contaminant particles can attach to. Additionally, large bubbles may reduce flotation efficiency by promoting the formation of discrete regions in the suspension where the majority of the air rises (defined as channeling), leaving some regions deficient of air bubbles. Ideally, a homogeneous system would provide for more efficient flotation than a heterogeneous system. However, a systematic flow regime study has yet to be performed due to the complexities of this system. Furthermore, other parameters important for optimizing flotation, such as bubble size and bubble rise velocity, are not known for actual operating consistencies typically found in flotation deinking.

4.2.2 Visualizing Gas Bubbles in a Pulp Suspension

The FXR system allows stop-motion pictures of gas bubbles in an opaque system to be captured on film. To verify this technique, video and FXR images of an air/water system under the same operating conditions were recorded and analyzed for bubble size distribution. Details can be found in Report 3 [2]. The video analysis resulted in a larger average equivalent bubble diameter than that recorded with the FXR technique. The discrepancy in recorded bubble diameter distributions between the two imaging techniques for identical experimental conditions is schematically described in Fig. 4. In the video analysis, the high intensity light used to record the bubble images is reflected off the bubble surface and is recorded on the video film as a sharp contrast between the bubble and fluid medium interface (Fig. 4a). The resulting high contrast at the bubble/fluid

interface is ideal for image analysis. In comparison, the amount of x-rays transmitted (or absorbed) and eventually incident on the x-ray film is a function of the depth of material the x-rays pass through. The amount of x-rays transmitted along a cord passing near the bubble periphery is less than the amount transmitted along a cord through the bubble center because the x-rays pass through more water near the bubble periphery, and water absorbs approximately 1000 times more x-rays than air. This results in a gray-scale variation from the bubble center (a very dark region because more x-rays pass through this region) to the bubble edge (a lighter region because more x-rays are adsorbed by the water). Upon image analysis, this produces a loss of bubble projected area onto the film due to a lack of image contrast at the bubble/fluid interface (Fig. 4b).

Hence, actual equivalent bubble diameters may not be recorded with the current experimental facility. However, relative bubble sizes can be determined and compared to those obtained with differing experimental conditions. For example, FXR can be used to determine if bubbles are larger or smaller when one system parameter is varied.

4.2.3 Bubble Size Measurements - ONP

Flash x-rays of an air/water system (0% consistency) and an air/water/ONP fiber system at 0.1, 0.5, 1.0, and 1.5% consistency were obtained at four locations in a planar bubble column for a fixed air flow rate of 0.25 slpm (standard liters per minute). Two different air injection techniques, identified as *gasket* or *sparger*, were studied in this investigation. No additional system chemistry (i.e., soaps, collectors, etc.) was added during the tests. Qualitative observations and bubble size distribution measurements are detailed in Report 3 [2]. Selected results are presented here.

Air was injected though a single hole drilled with a 0.34 mm diameter drill bit in a 3.18 mm thick n-butyl rubber gasket, which became self-sealing when the air flow was turned off. Figure 5 shows a composite of four x-ray images taken of the column when air was injected into a water column (0% consistency). Air was introduced from a central location at the column base, as indicated in the figure. The small dark dots represent air bubbles as they rise through the column.

The original x-rays reveal that the bubbles are ellipsoidal in shape (a detail which may not be apparent when the image is digitized and reduced for presentation). The air bubbles rise in a serpentine pattern and become well-dispersed toward the top of the water column.

Adding ONP fibers to the system at a consistency of 1% (Fig. 6) has a significant effect on the air flow patterns in the column. The bubbles in the original x-rays reveal a shape that is more spherical than the bubbles observed in the pure water situation. The 1% consistency slurry also results in a rather large effective viscosity, promoting bubble coalescence, which produces air bubbles that are much larger than those previously observed. In addition, the relatively high viscosity impairs bubble dispersion, and the rising air bubbles remain in a confined region. The air bubble confinement is the beginning of channeling in this system, a phenomenon where air bubbles rise only in selected regions and other regions have no interaction with the ascending air. This channeling phenomenon can lead to a reduction in flotation cell performance because there could be regions in the flotation cell with a high concentration of contaminants but very few bubbles.

Air was also introduced into the bubble column by an alternate method. A bronze pneumatic filter designed to remove particles larger than 40 μm was used as an air sparger. A length of Tygon tubing was attached to the sparger and placed on the column bottom. Air was introduced through the Tygon tubing, which was positioned adjacent to the column wall such that it did not interfere with the column flow patterns.

As shown in Fig. 7, when the sparger is used for air injection, the general flow patterns for the air/water (0% consistency) system are similar to those observed when a single-hole gasket is used for air injection. Specifically, the bubbles are ellipsoidal in shape, rise in a serpentine fashion, and disperse as they ascend through the column. The main difference between the sparger and gasket air injection techniques at 0% consistency is bubble size, with the sparger producing a smaller average equivalent bubble diameter [2].

Figure 8 reveals the air bubble flow patterns for a consistency of 1% with the sparger air injection technique. The bubbles appear to be very large upon introduction into the system as shown in the x-ray for Position 1. Most are still spherical in shape, but some are observed to be spherical-capped (e.g., like a bullet nose). As the bubbles rise, they may coalesce with adjacent bubbles to form larger bubbles, and this is observed in the x-rays from Positions 3 and 4. The rising bubbles are also confined to a narrow channel region.

Figure 9 shows a compilation of x-rays at column Position 2 for the 5 different consistencies and 2 different air injection techniques investigated in this study. The air flow rate was held constant at 0.25 slpm for all test conditions. It is apparent that as the ONP consistency increases, the bubbles become less numerous, larger, and less dispersed.

Bubble size measurements were obtained for both air injection techniques from the x-rays taken at Position 2 for systems with 0, 0.1, 0.5, and 1.0% consistency. Bubble size distributions were obtained from these measurements with at least 700 bubbles making up each sample size. This typically required 6 to 18 x-rays to be taken of Position 2 with the desired experimental conditions. More x-rays were required as the fiber consistency increased. Measurements were not taken at 1.5% consistency because only a few large bubbles were recorded at Position 2 for this consistency at the given air flow rate of 0.25 slpm. Numerous (100 or more) x-rays would be required to gather enough bubble measurements for a sufficient sample size, and this was deemed too costly. However, we can conclude by observation that bubble sizes at 1.5% consistency are much larger than those at 1% consistency (i.e., see Fig. 9).

These studies reveal that the average bubble size increases and the bubble size distribution becomes more broad as the ONP consistency increases. This is shown in Figs. 10 and 11 for the gasket and sparger air injection techniques, respectively. When the gasket is used to introduce air into the system, the bubble size distribution does not change considerably until the consistency reaches approximately 1% (Fig. 10). Then, the bubble size distribution shifts slightly to larger equivalent

diameters. The sparger air injection technique does not reveal the same trend (Fig. 11). Increasing the consistency results in a broader bubble size distribution, with the mean value shifting to much larger diameters.

These differences can be explained by how the bubbles leave the region where they are introduced into the system. Increasing the fiber consistency has the same effect as increasing the system effective viscosity, which will increase the viscous drag forces around the bubble as it rises and slow its ascension. The gasket produces relatively large air bubbles in water. The bubbles have a sufficient buoyant force to be removed as soon as they form at the gasket air inlet. The buoyant force associated with these relatively large bubble sizes is sufficient even for fiber consistencies as high as 0.5%. At 1% consistency, the effective viscosity is such that the bubbles are slowed enough so more coalesce to form larger bubbles as they rise. The resulting larger bubbles have an increased buoyant force to rise through the fiber network.

In contrast, the sparger produces relatively small bubbles in water, and they all enter the system in a small region around the sparger head. These bubbles quickly disperse in water to limit any bubble coalescence that may take place. When the fiber consistency increases, particularly to 0.5%, the small bubbles no longer have a sufficient buoyant force to rise through the fiber network. Hence, the small bubbles coalesce upon introduction into the system to form very large bubbles with a sufficient buoyant force to break through the fiber network. Further increases in the fiber consistency increase the bubble size slightly to form yet larger bubbles. This is revealed in the more equivalent bubble diameters reported for the larger bubble size fractions when the sparger is used.

The effect ONP consistency has on the average equivalent bubble diameter is summarized in Fig. 12. Increasing the consistency results in an increase in the average equivalent bubble diameter. These increases are on the order of 0.5 and 1.5 mm for the gasket and sparger air injection techniques, respectively, when the consistency was increased from 0 to 1%. The average

equivalent bubble diameter obtained with video analysis using the gasket air injection technique is also shown for a reference. The significant conclusion from this figure is that the air injection technique can have a substantial influence on the average equivalent bubble diameter and, as shown in Figs. 10 and 11, on the equivalent bubble size distribution. Furthermore, the conclusions drawn at 0% consistency (i.e., an air/water system) may not be the same conclusions at consistencies typically found during flotation deinking.

4.2.4 Bubble Size Measurements - Bleached Kraft

Bubble column experiments using virgin Northern softwood bleached kraft fibers have also been initiated to determine if these longer fibers have a significant influence on the experimental results. The fibers used in this study have a weight-weighted average fiber length of 2.8 mm, compared to 1.4 mm for the ONP. Since this is ongoing research, preliminary results will only be presented here.

Figure 13 shows the combined x-ray images taken at the four column positions with the gasket air injection technique for 0.1% virgin kraft fibers with a 0.25 slpm air injection rate. Observations reveal that the general bubble characteristics and flow patterns do not differ significantly from those observed with 0.1% ONP operating under similar conditions.

When the sparger air injection technique is used with 0.1% virgin kraft (Fig. 14), observations differ from those with 0.1% ONP (i.e., see Report 3 [2]). The bubbles are considerably larger and are much more confined when virgin kraft is used. Table 7 summarizes the preliminary bubble size measurements obtained with the bleached kraft fibers and compares these measurements with those obtained with ONP. The increase in bubble size when the sparger is used is evident in this table. This increase in size is due to the longer kraft fibers creating fiber networks at relatively low consistencies that prevent dispersion of the small bubbles formed by the sparger. These bubbles coalesce upon introduction into the system.

When the consistency is increased to 0.5% bleached virgin kraft, significant changes take place, which are revealed in Figs. 15 and 16, respectively, for the gasket and sparger air injection techniques. The longer fibers create a stronger fiber network, which considerably constrains the bubble rise and dispersion. The result is a significant reduction in the number of bubbles present in the column with the air flow rate of 0.25 slpm, and bubbles that are much larger than those observed with 0.5% ONP (i.e., see Fig. 9 and Report 3 [2]). These results are amplified when the sparger air injection technique is used (Fig. 16). The bubbles are so infrequent that only a single large one is observed at Position 3 in Fig. 16 and none are recorded at Position 4. However, by the "bump" at the air/fluid interface, we hypothesize that a large bubble broke through the surface right before the radiograph was taken at Position 4.

So few bubbles are recorded in the 0.5% virgin kraft with 0.25 slpm air injection rate that to determine a bubble size distribution with a sufficient bubble population size, between 100 and 200 x-rays would have to be taken. This is deemed too costly. Therefore, we will begin experiments in the near future with a much larger air injection flow rate (e.g., 2 slpm).

5 FUTURE GOALS (March 1997 to March 1998)

Goals for the next period (March 1997 to March 1998) can be grouped into two areas and are summarized below.

5.1 Flotation Modeling

1. Perform calculations on determining the initial rate of decrease of the number of particles in a unit volume using Model #1.

2. Perform calculations of flotation performance predictions using Model #2 (see Table 6).

3. Perform calculations of flotation performance predictions using Model #3 (see Table 6).

4. Revisit the model for the probability of adhesion by sliding and develop a better predictive equation that includes other system parameters.

5. Design and build an apparatus to measure selected flotation microprocess probabilities and begin experimentation to validate our model. (Contingent on funding for a Post-Doc position and equipment.)

6. Summarize our flotation modeling progress in a Member Company Report.

5.2 Bubble Size Determination

1. Measure the bubble size in ONP fiber systems at various consistencies and alter the chemistry with fatty acid soaps and synthetic surfactants to levels typical of ONP processing.

2. Measure the bubble size in bleached kraft fiber systems at various consistencies with an air injection rate of 2 slpm. The system chemistry will not be altered. Selected experiments will also be performed with ONP at an air injection rate of 2 slpm so direct comparisons can be made between the two fiber lengths.

3. Measure the bubble size in bleached kraft fiber systems at various consistencies with an air injection rate of 2 slpm and alter the system chemistry to correspond to levels typical of MOW processing.

4. Design and construct a flow loop to be used in the x-ray experiments to allow for both liquid and bubble transport. (Preliminary designs have been completed, and a pump and flowmeter will have to be purchased.)

5. Summarize our progress in measuring bubble size with a Member Company Report.

6 CONCLUSIONS

This report summarized the progress achieved during the last year (March 1996 to March 1997) in the area of flotation modeling and bubble size measurements. Flotation performance predictions based on our first-generation model (Model #1) have been completed, and detailed results were summarized in a Member Company Report [1]. The model predicts general trends when selected parameters are varied, and results are in qualitative agreement with those observed in practice. Bubble size measurements have also been obtained using flash x-ray radiography (FXR) for an ONP suspension at various consistencies. The FXR technique and ONP results were summarized in a Member Company Report [2]. The main conclusions from this report were that bubble size increases with increasing consistency and it is dependent on the air injection technique. In addition, the conclusions drawn in an air/water system (0% consistency) may not be applicable to those actually observed when fibers are present in the system.

7 REFERENCES

[1] Heindel, T.J., and Bloom, F., Mathematical Modeling of the Overall Flotation Deinking Process: Predictions of Selected Performance Parameters, Institute of Paper Science and Technology, Atlanta, GA, Member Company Report, Project F00903, Report 2, (November 25, 1996).

[2] Heindel, T.J., A Method to Visualize Gas Bubbles in a Pulp Suspension, Institute of Paper Science and Technology, Atlanta, GA, Member Company Report, Project F00903, Report 3, (February 3, 1997).

[3] Heindel, T.J., and Bloom, F., Mathematical Modeling of the Overall Flotation Deinking Process, Institute of Paper Science and Technology, Atlanta, GA, Member Company Report, Project F00903, Report 1, (December 8, 1995).

[4] Heindel, T.J., and Bloom, F., "New Measures for Maximizing Ink Particle Removal in a Flotation Cell," *1997 TAPPI Recycling Symposium*, Chicago, Accepted for Publication (April 14-16, 1997).

[5] Bloom, F., and Heindel, T.J., "Mathematical Modelling of the Flotation Deinking Process," *Mathematical and Computer Modelling*, Accepted for Publication (1997).

[6] Bloom, F., and Heindel, T.J., "A Theoretical Model of Flotation Deinking Efficiency," *Journal of Colloid and Interface Science*, In Review (1997).

8 NOMENCLATURE

$\Im_e(t)$	flotation efficiency at any given time period
$\Im_e^{\infty}$	flotation efficiency at an infinite flotation time period
$\Im_e(t=t')$	flotation efficiency at a fixed flotation time of t'
k_1	the rate constant associated with the formation of stable bubble/particle aggregates
k_2	the rate constant associated with the destabilization of bubble/particle aggregates
n_B	total number of bubbles in a representative unit volume
n_B^a	number of bubbles in a representative unit volume that have a particle attached to them
n_B^f	number of bubbles in a representative unit volume that do not have a particle attached to them
n_p	total number of particles in a representative unit volume
n_p^a	number of particles in a representative unit volume that are attached to bubbles
n_p^f	number of free particles in a representative unit volume
P_{asl}	probability of adhesion by sliding
P_c	probability of collision between a particle and a bubble
P_{destab}	probability of destabilization of a bubble/particle aggregate
P_{tpc}	probability of three-phase contact
P_{stab}	probability of stability
R_B	bubble radius
R_p	particle radius
t	time
t'	fixed flotation time
$t_{1/2}$	time required to reduce the number of free particles in a representative unit volume by a factor of two
Z	collision frequency between bubbles and particles
ε	turbulent energy density
μ_ℓ	liquid dynamic viscosity
ρ_ℓ	liquid density
ρ_p	particle density
ϕ^*_{crit}	largest touching angle (< 90°) such that as a particle slides past a bubble, the thin liquid film between the bubble and particle will have sufficient time to thin and rupture
θ	contact angle
σ	surface tension
υ_B	bubble rise velocity

9 TABLES

Table 1: Parametric ranges of the various flotation parameters utilized in this study.

Parameter	Minimum Value Used in the Literature	Maximum Value Used in the Literature	Parametric Range Utilized in this Study	"Standard" Conditions	Calculations Performed At Selected Values
R_p (μm)	1	600	1-500	50	1, 10, 50, 100, 200, 300, 500
R_B (mm)	0.15	2	0.1-5.0	0.5	0.1, 0.3, 0.5, 0.7, 1.0, 3.0, 5.0
ρ_p (g/cm^3)	1	7.5	1.0-3.0	1.3	1.0, 1.1, 1.3, 1.5, 2.0, 3.0
ρ_ℓ (g/cm^3)	1	1	–	1	1
υ_B (cm/s)	1.25	30	–	10	10
μ_ℓ (cP)	1	1	–	1	1
ε (W/kg)	1	130	1-400	10	1, 10, 50, 100, 200, 400
σ (dynes/cm)	35	73	$\sigma=(2R_B)^{5/3}\varepsilon^{2/3}\rho_\ell$	$\sigma=(2R_B)^{5/3}\varepsilon^{2/3}\rho_\ell$	$\sigma=(2R_B)^{5/3}\varepsilon^{2/3}\rho_\ell$
θ (deg)	5	105	5-120	60	20, 40, 60, 80, 100, 120
ϕ^*_{crit} (deg)	33	72	5-85	60	20, 40, 60, 80
n_B	–	–	100-10000	1000	200, 500, 1000, 5000, 10000
n_p	–	–	1-1000	100	1, 10, 50, 100, 500, 975

Table 2: Summary of the general conclusions from the predictions of flotation efficiency as a function of time ($\Im_e(t)$) when the given conditions are satisfied. Note that ↑ implies $\Im_e(t)$ will increase when the specified parameter increases.

Increasing from the Lowest Selected Value to the Highest Selected Value[1]	Effect on $\Im_e(t)$
R_B	↑
R_p	↑[2]
ρ_p	N.A.C.[3]
ε	↑
θ	N.A.C.[4]
ϕ^*_{crit}	↑
n_B	↑
n_p	↑[5]

[1] All other values at standard conditions.
[2] For stable bubble/particle aggregates.
[3] N.A.C. signifies no apparent change.
[4] $\Im_e(t)$ predictions for $\theta = 20°$ are slightly below the predictions for other values of θ.
[5] Until $n_p \rightarrow n_B$.

Table 3: Summary of the general conclusions from the predictions of flotation efficiency at infinite flotation time ($\mathfrak{I}_e^\infty$) when the given conditions are satisfied. Note that ↑ and ↓ implies that $\mathfrak{I}_e^\infty$ will increase or decrease, respectively, for the specified conditions.

	Increasing Value of Given Parameter							
Fixed at Selected Values[1]	R_B	R_p	ρ_p	ε	θ	ϕ^*_{crit}	n_B	n_p
R_B	–	↓[3]	~1[4]	~1[9]	↑[2]	↑	↑	↑[14]
R_p	↑[2]	–	~1[5]	~1[10]	↑[2]	↑	↑	↑[14]
ρ_p	↑[2]	↓[3]	–	~1	↑[2, 13]	↑	↑	↑[14]
ε	↑	↓[3]	~1	–	↑[2, 13]	~1	↑	~1
θ	↑[2]	↓[3]	~1[6]	~1[11]	–	↑	↑	↑[14]
ϕ^*_{crit}	↑	↓[3]	~1	~1[12]	↑[2, 13]	–	↑	↑[14]
n_B	↑	↓[3]	~1[7]	~1[12]	↑[2, 13]	↑	–	↑[14]
n_p	↑	↓[3]	~1[8]	~1[12]	↑[2, 13]	↑	↑	–

[1] All other values at standard conditions.
[2] For stable bubble/particle aggregates.
[3] $\mathfrak{I}_e^\infty$ is typically constant until the bubble/particle aggregate becomes unstable and then it drops over a narrow range of R_p.
[4] Decreases for $R_B = 0.1, 0.3$ mm.
[5] Declines when $R_p = 200$ μm; stable bubble/particle aggregates do not form when $R_p > 200$ μm.
[6] Decreases from $\mathfrak{I}_e^\infty \approx 1$ when $\theta = 20°$.
[7] Decreases from $\mathfrak{I}_e^\infty \approx 1$ when $n_B = 200$.
[8] Decreases from $\mathfrak{I}_e^\infty \approx 1$ when $n_p = 1$.
[9] Increases toward $\mathfrak{I}_e^\infty \approx 1$ for $R_B = 0.1, 0.3$ mm.
[10] Increases toward $\mathfrak{I}_e^\infty \approx 1$ when $R_p = 200$ μm; stable bubble/particle aggregates do not form when $R_p > 200$ μm.
[11] Increases toward $\mathfrak{I}_e^\infty \approx 1$ when $\theta = 20°$.
[12] Slight minimum in $\mathfrak{I}_e^\infty$ at $\varepsilon \approx 5$ W/kg.
[13] Stable bubble/particle aggregates do not form when $\theta \lesssim 10°$.
[14] Until $n_p \rightarrow n_B$.

Table 4: Summary of the general conclusions from the predictions of flotation efficiency at a fixed flotation time of 1 second ($\Im_e(t=1)$) when the given conditions are satisfied. Note that ↑ implies that $\Im_e(t=1)$ will increase for the specified conditions.

	Increasing Value of Given Parameter							
Fixed at Selected Values[1]	R_B	R_p	ρ_p	ε	θ	ϕ^*_{crit}	n_B	n_p
R_B	–	Max.[3]	~Const.[4]	↑	~Const.[8]	↑	↑	↑[9]
R_p	↑[2]	–	~Const.[5]	~Const.[7]	~Const.[8]	↑	↑	↑[9]
ρ_p	↑[2]	Max.[3]	–	↑	~Const.[8]	↑	↑	↑[9]
ε	↑	Max.[3]	~Const.	–	~Const.[8]	↑	↑	↑[9]
θ	↑[2]	Max.[3]	~Const.[6]	↑	–	↑	↑	↑[9]
ϕ^*_{crit}	↑	Max.[3]	~Const.	↑	~Const.[8]	–	↑	↑[9]
n_B	↑	Max.[3]	~Const.	↑	~Const.[8]	↑	–	↑[9]
n_p	↑	Max.[3]	~Const.	↑	~Const.[8]	↑	↑	–

[1] All other values at standard conditions.
[2] For stable bubble/particle aggregates.
[3] Maximum value of $\Im_e(t=1)$ over a range of R_p, which depends on conditions.
[4] $\Im_e(t=1)$ decreases when $R_B = 0.1$ mm.
[5] $\Im_e(t=1)$ decreases when $R_p = 200$ μm; stable bubble/particle aggregates do not form when $R_p > 200$ μm.
[6] $\Im_e(t=1)$ decreases when $\theta = 20°$.
[7] $\Im_e(t=1)$ increases when $R_p = 10, 50$ μm.
[8] $\Im_e(t=1)$ increases over a limited contact angle range, depending on conditions, and then remains constant.
[9] Until $n_p \rightarrow n_B$.

Table 5: Summary of the general conclusions from the predictions of the time required to reduce the number of free particles in a representative unit volume by a factor of two ($t_{1/2}$) when the given conditions are satisfied. Note that ↓ implies that $t_{1/2}$ will decrease for the specified conditions.

	Increasing Value of Given Parameter							
Fixed at Selected Values[1]	R_B	R_p	ρ_p	ε	θ	ϕ^*_{crit}	n_B	n_p
R_B	–	↓[2]	~Const.	↓	~Const.[5]	↓	↓	↓
R_p	↓[2]	–	~Const.[3]	↓	~Const.[5]	↓	↓	↓
ρ_p	↓[2]	↓[2]	–	↓	~Const.[5]	↓	↓	↓
ε	↓[2]	↓[2]	~Const.	–	~Const.[5]	↓	↓	↓
θ	↓[2]	↓[2]	~Const.[4]	↓	–	↓	↓	↓
ϕ^*_{crit}	↓[2]	↓[2]	~Const.	↓	~Const.[5]	–	↓	↓
n_B	↓[2]	↓[2]	~Const.	↓	~Const.[5]	↓	–	↓
n_p	↓[2]	↓[2]	~Const.	↓	~Const.[5]	↓	↓	–

[1] All other values at standard conditions.
[2] For stable bubble/particle aggregates.
[3] $t_{1/2}$ increases when $R_p = 200\ \mu m$; stable bubble/particle aggregates do not form when $R_p > 200\ \mu m$.
[4] $t_{1/2}$ increases when $\theta = 20°$.
[5] $t_{1/2}$ decreases over a limited contact angle range, depending on conditions, and then remains constant.

Table 6: Summary of the assumptions incorporated into the various flotation performance models.

Model Assumptions			
Model #1	**Model #2**	**Model #3**	**Model #4**
n_p = constant	n_p = constant	n_p = constant	$n_p = n_p(t)$
n_B = constant	n_B = constant	n_B = constant	$n_B = n_B(t)$
$n_p^a = n_B^a$	$n_p^a \geq n_B^a$	$n_p^a \geq n_B^a$	$n_p^a \geq n_B^a$
$n_B > n_p$	$n_B > n_p$	$n_B < n_p$	$n_B < n_p$ or $n_B > n_p$

Table 7: ONP and bleached kraft comparison of bubble size measurements obtained with the gasket and sparger air injection techniques for an air/water/0.1% fiber system.

Test Conditions:	System Slurry Charge: 3.2 liters (to the 80 cm mark) Air Flow Rate: 0.25 slpm Added Chemicals: None Column Position: 2 Consistency: 0.1%			
Equivalent Diameters	**Air Injection Technique**			
	Gasket		**Sparger**	
	ONP	Bleached Kraft	ONP	Bleached Kraft
Average (mm)	3.1	2.8	2.3	3.9
Median (mm)	3.0	2.7	2.3	3.9
Minimum (mm)	1.0	1.0	1.0	1.0
Maximum (mm)	6.4	5.4	6.8	6.9
Standard Deviation (mm)	1.0	0.7	0.8	1.0
Sauter Mean Diameter (mm)	3.6	3.2	2.9	4.3
Bubble Population Size	978	759	799	752

10 FIGURES

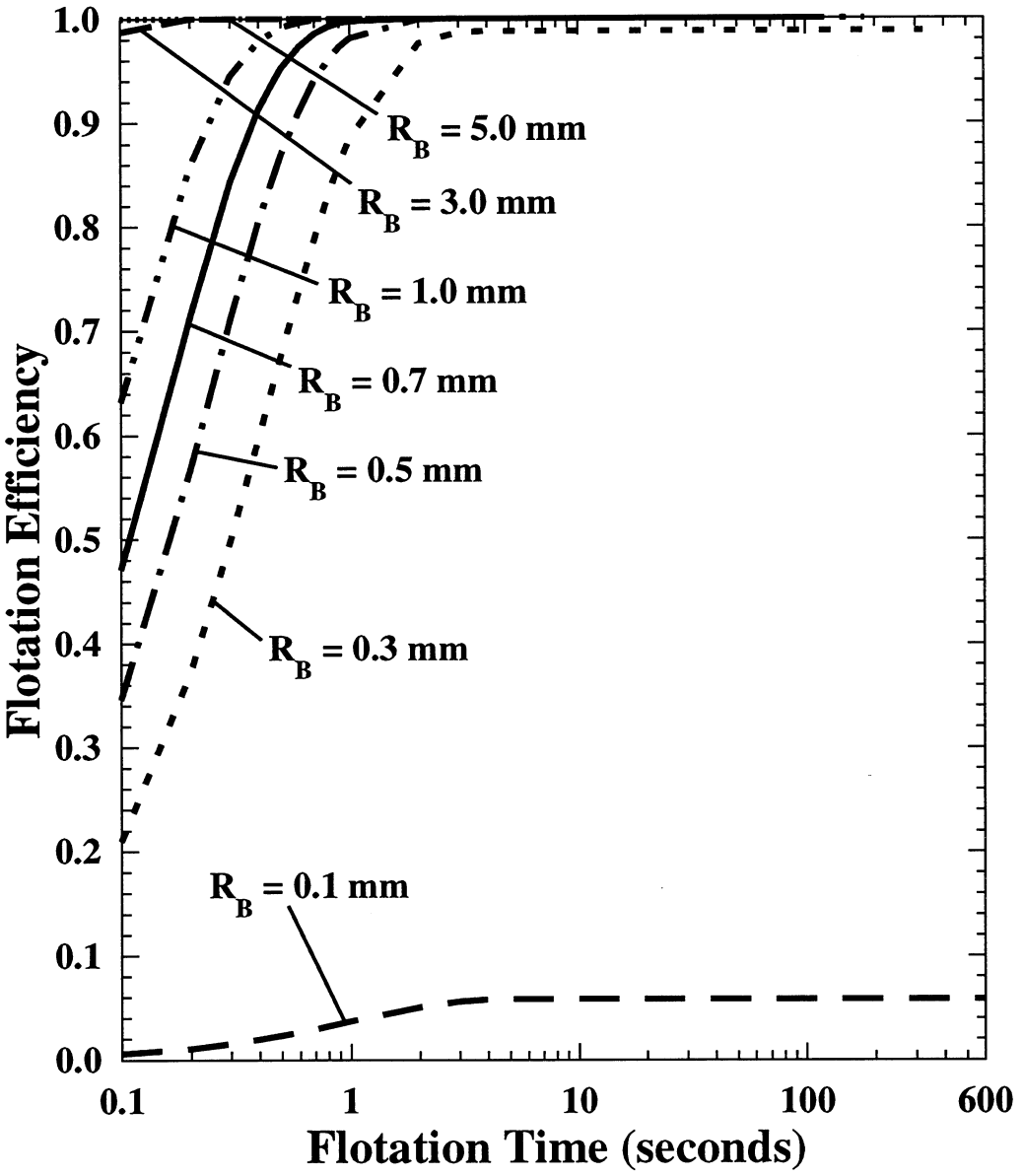

Figure 1: Flotation efficiency as a function of time for selected bubble radii, R_B. All other independent variables are held at standard conditions: R_p = 50 μm, ρ_p = 1.3 g/cm^3, ε = 10 W/kg, θ = 60°, ϕ^*_{crit} = 60 °, n_B = 1000, and n_p = 100.

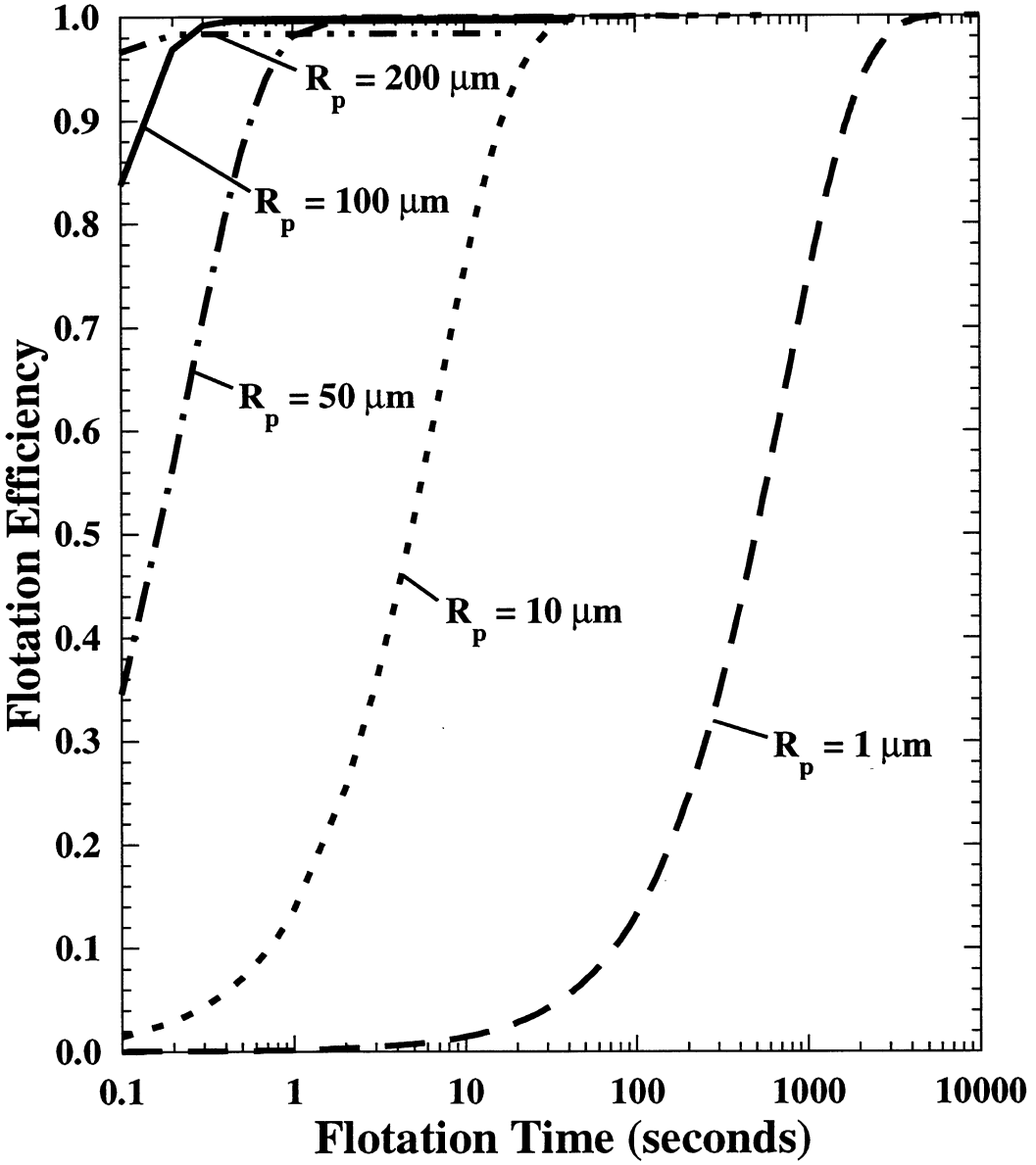

Figure 2: Flotation efficiency as a function of time for selected particle radii, R_p. All other independent variables are held at standard conditions: $R_B = 0.5$ mm, $\rho_p = 1.3$ g/cm^3, $\varepsilon = 10$ W/kg, $\theta = 60°$, $\phi^*_{crit} = 60$ °, $n_B = 1000$, and $n_p = 100$.

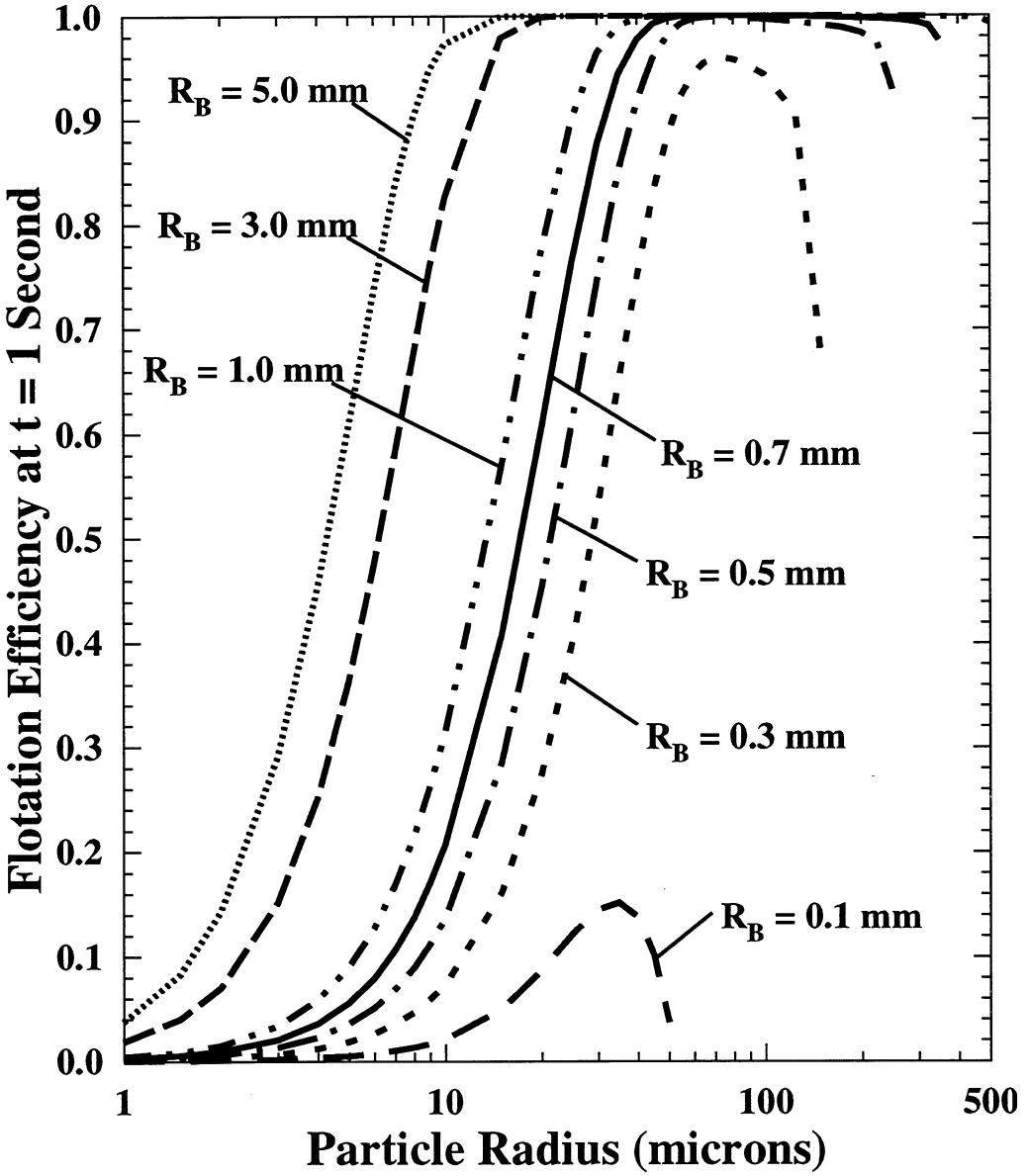

Figure 3: Flotation efficiency at t = 1 second as a function of particle radius, R_p, for selected bubble radii, R_B. All other independent variables are held at standard conditions: ρ_p = 1.3 g/cm^3, ε = 10 W/kg, θ = 60°, ϕ^*_{crit} = 60°, n_B = 1000, and n_p = 100.

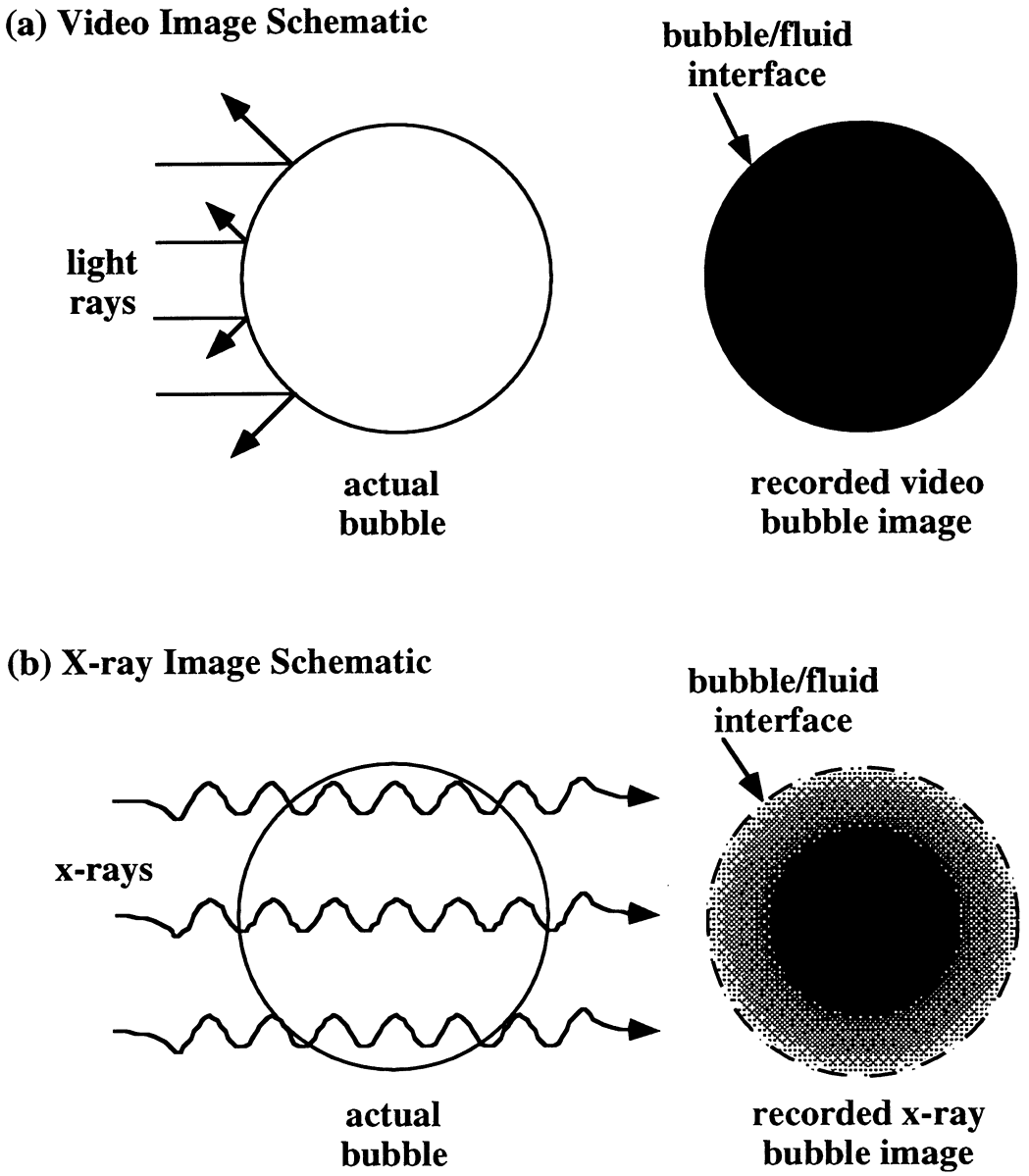

Figure 4: Schematic diagram of identical air bubbles recorded by the video and x-ray imaging techniques.

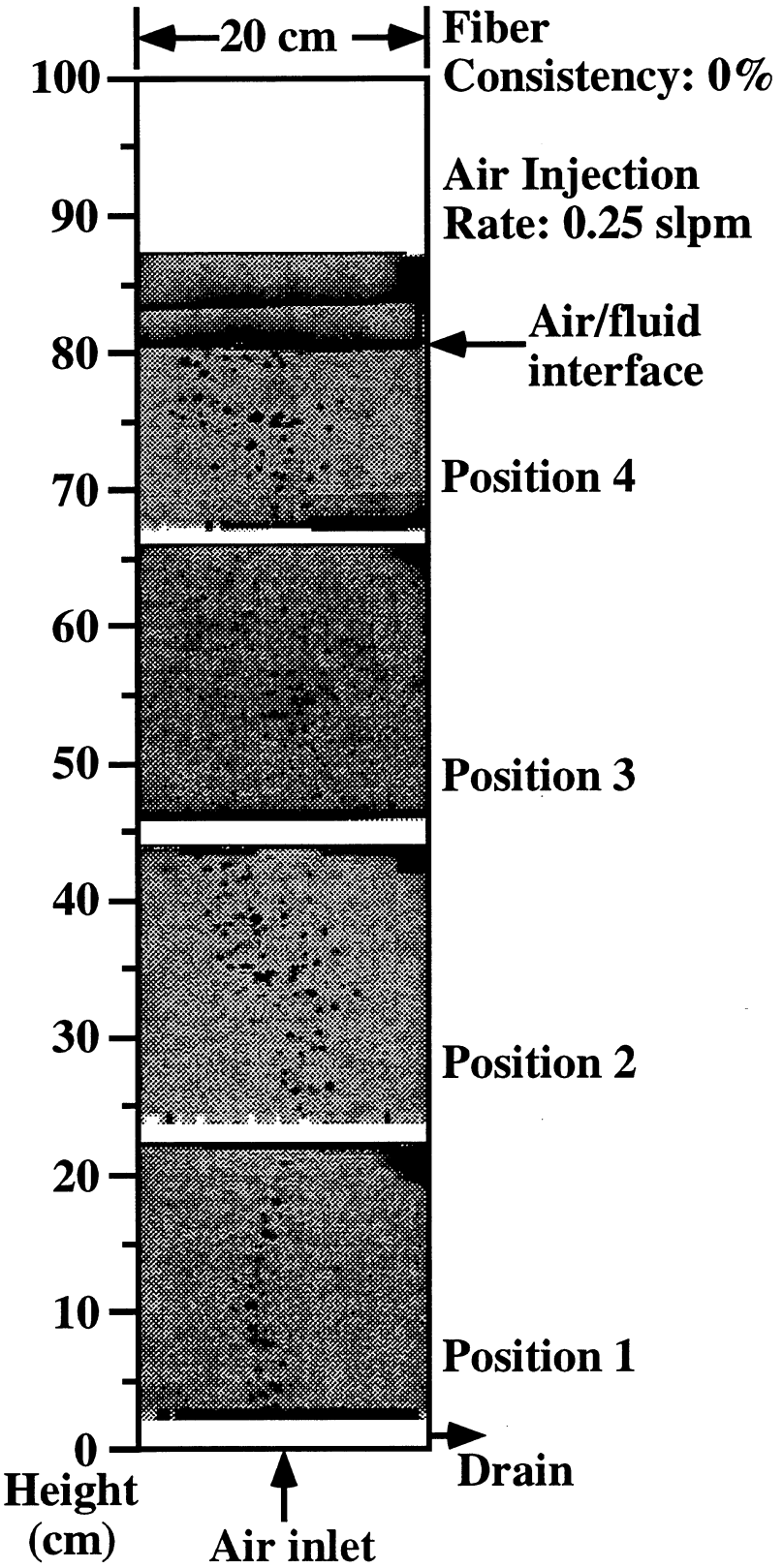

Figure 5: X-ray composite of air bubble flow patterns in an air/water (0% consistency) system with air injected through a single-holed gasket at the bottom of the column.

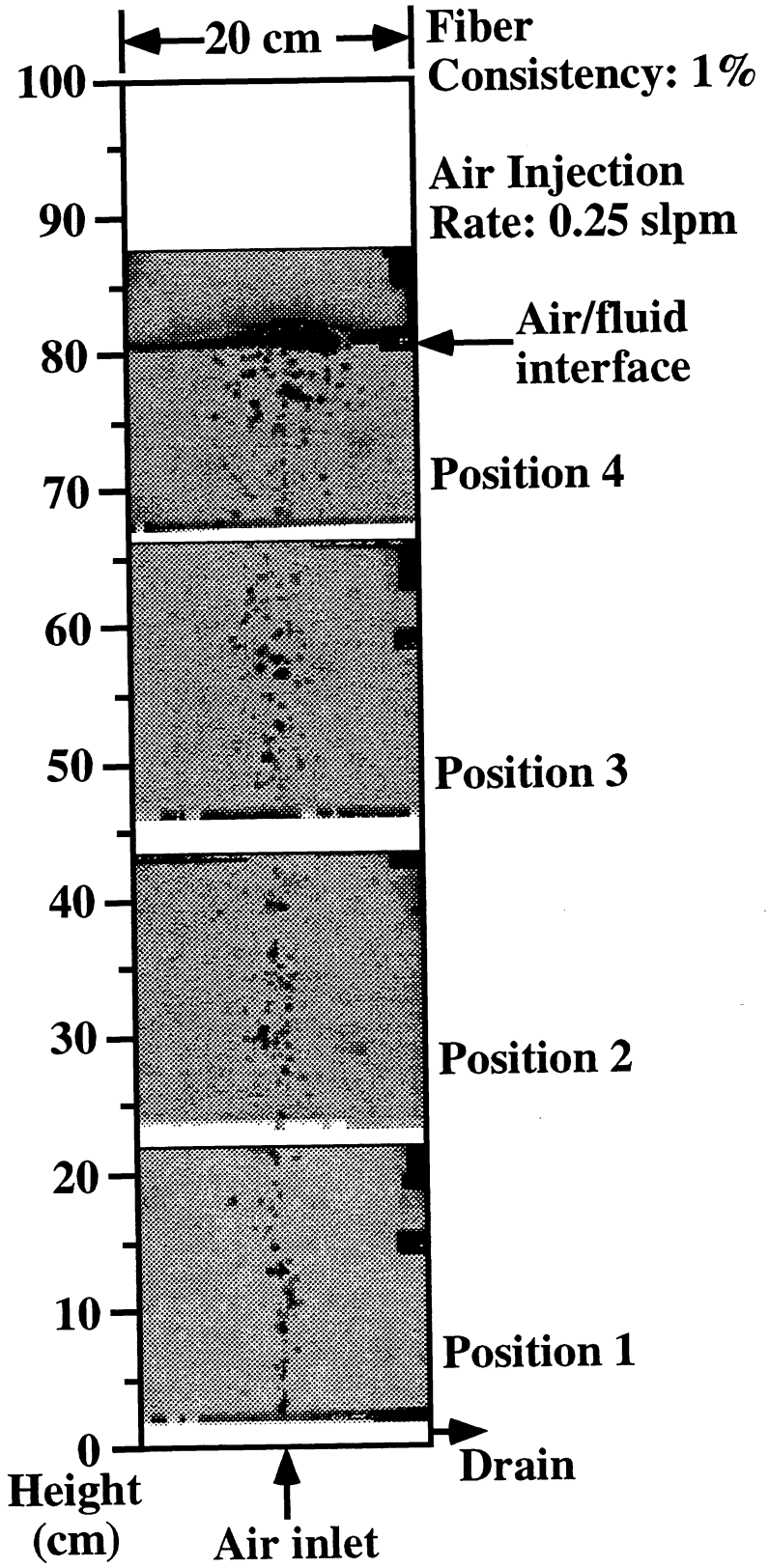

Figure 6: X-ray composite of air bubble flow patterns in an air/water/1% ONP system with air injected through a single-holed gasket at the bottom of the column.

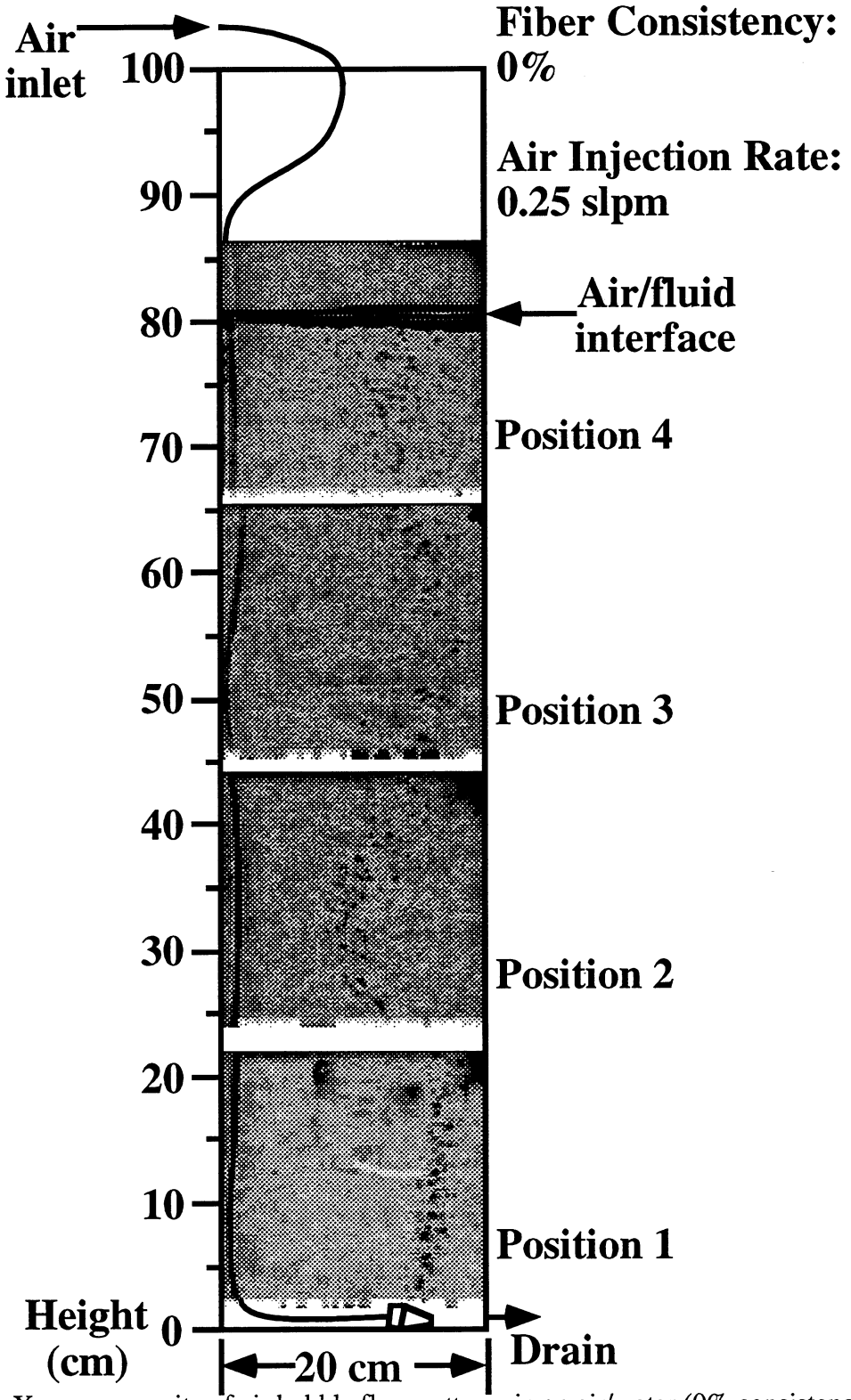

Figure 7: X-ray composite of air bubble flow patterns in an air/water (0% consistency) system with air injected through a sparger with 40 μm openings.

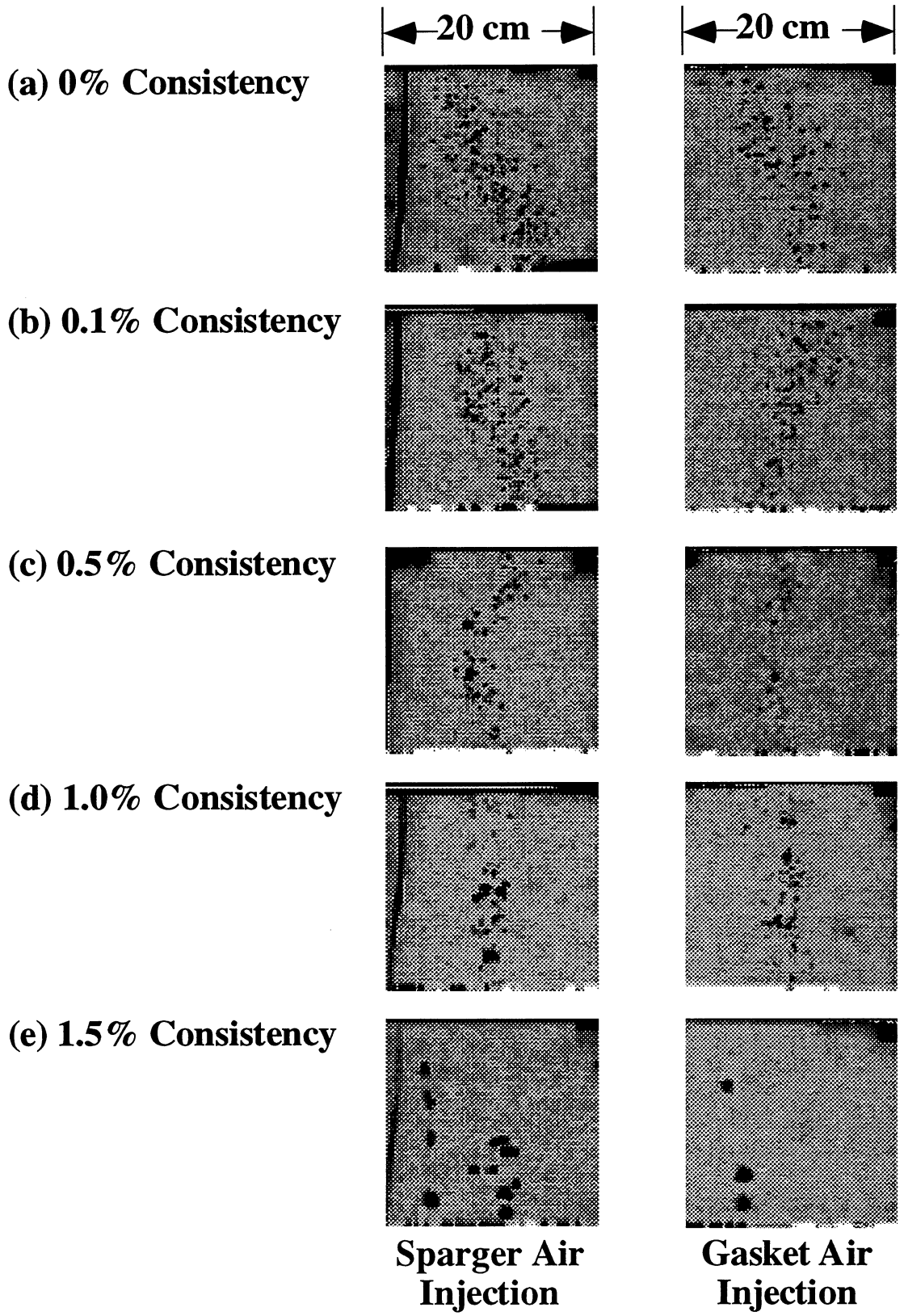

Figure 9: X-ray comparisons at Position 2 for all ONP consistencies considered in this study with two different air injection methods.

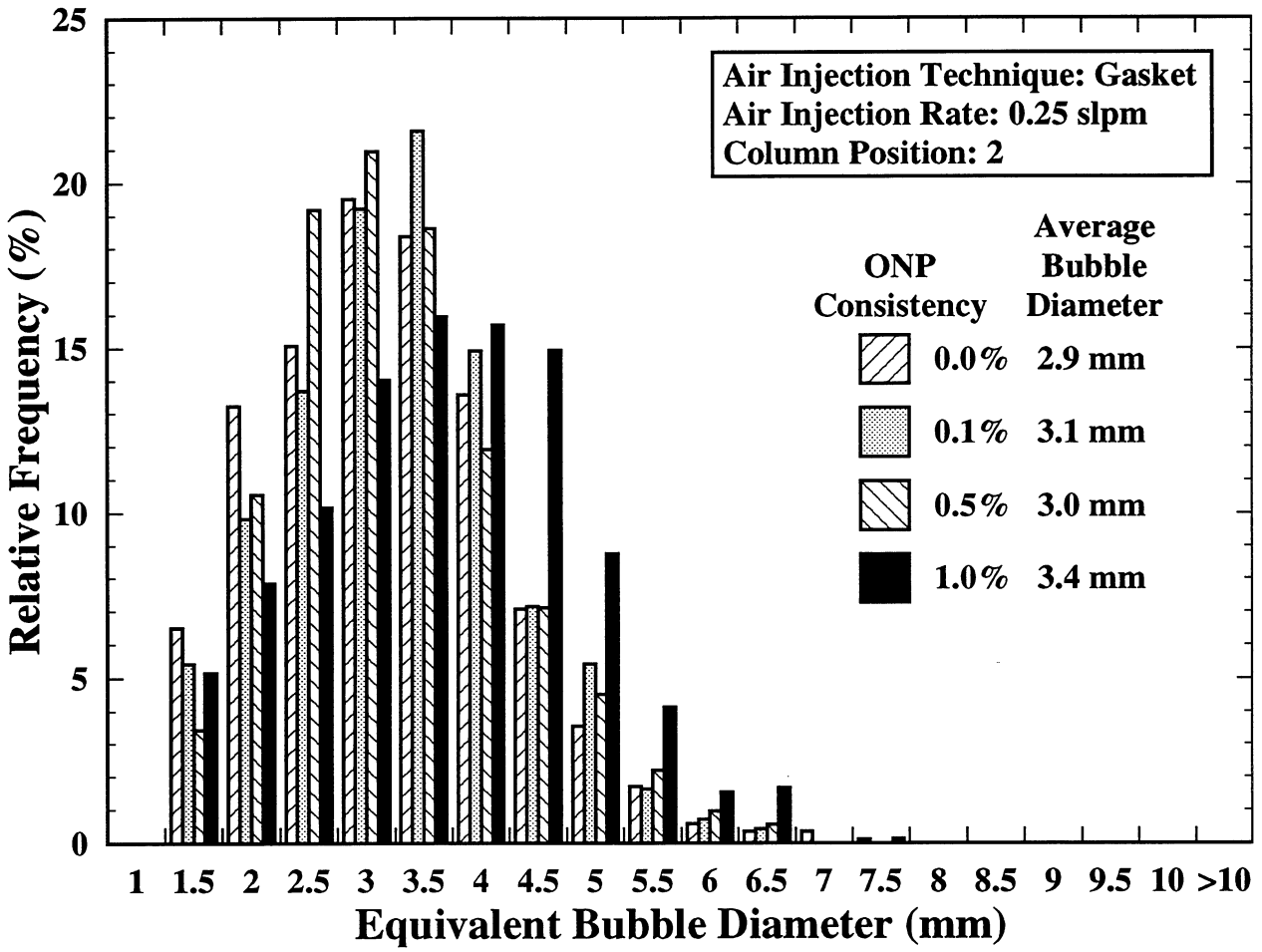

Figure 10: Bubble size distributions obtained with the gasket air injection technique for various ONP consistencies.

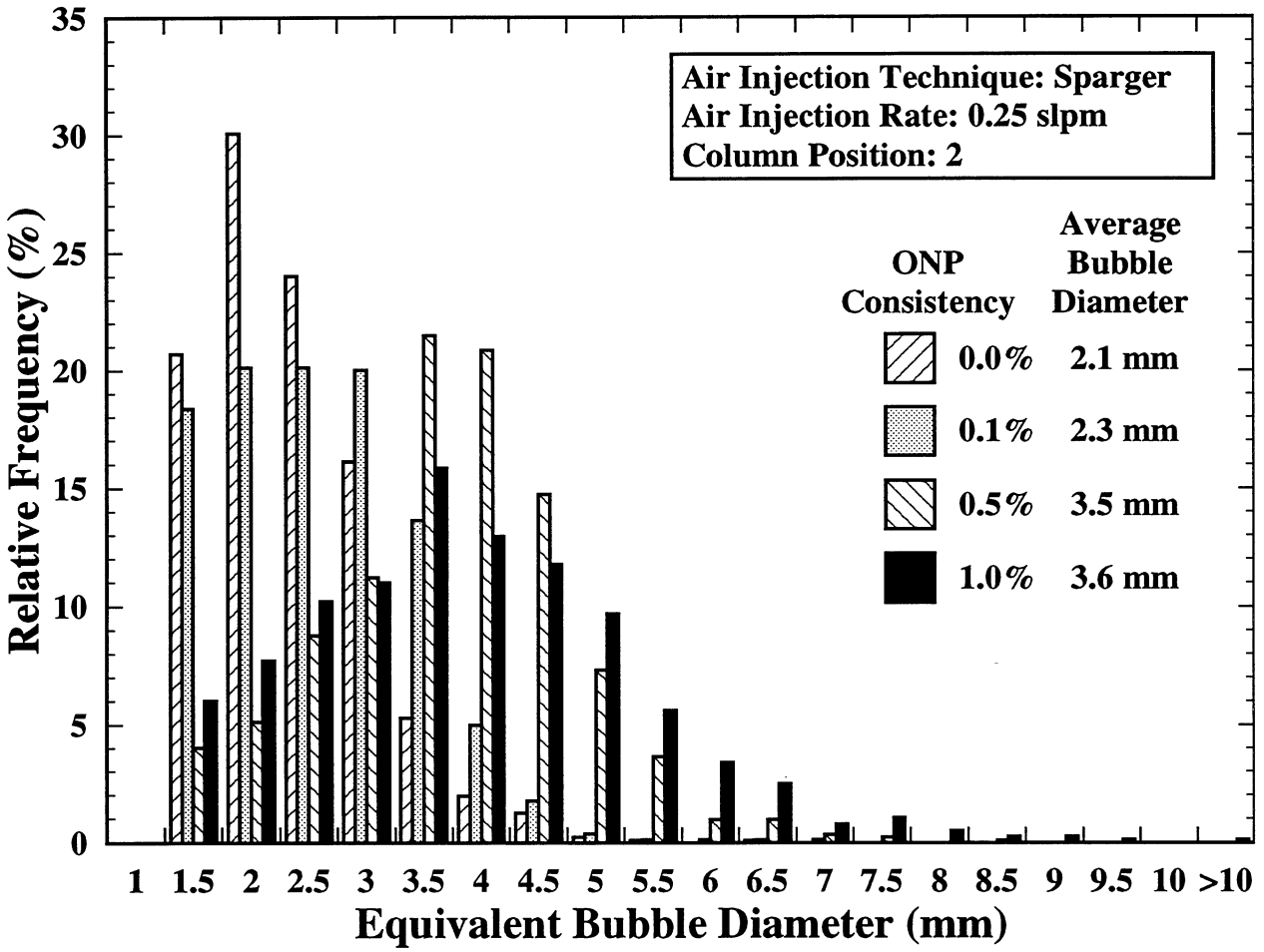

Figure 11: Bubble size distributions obtained with the sparger air injection technique for various ONP consistencies.

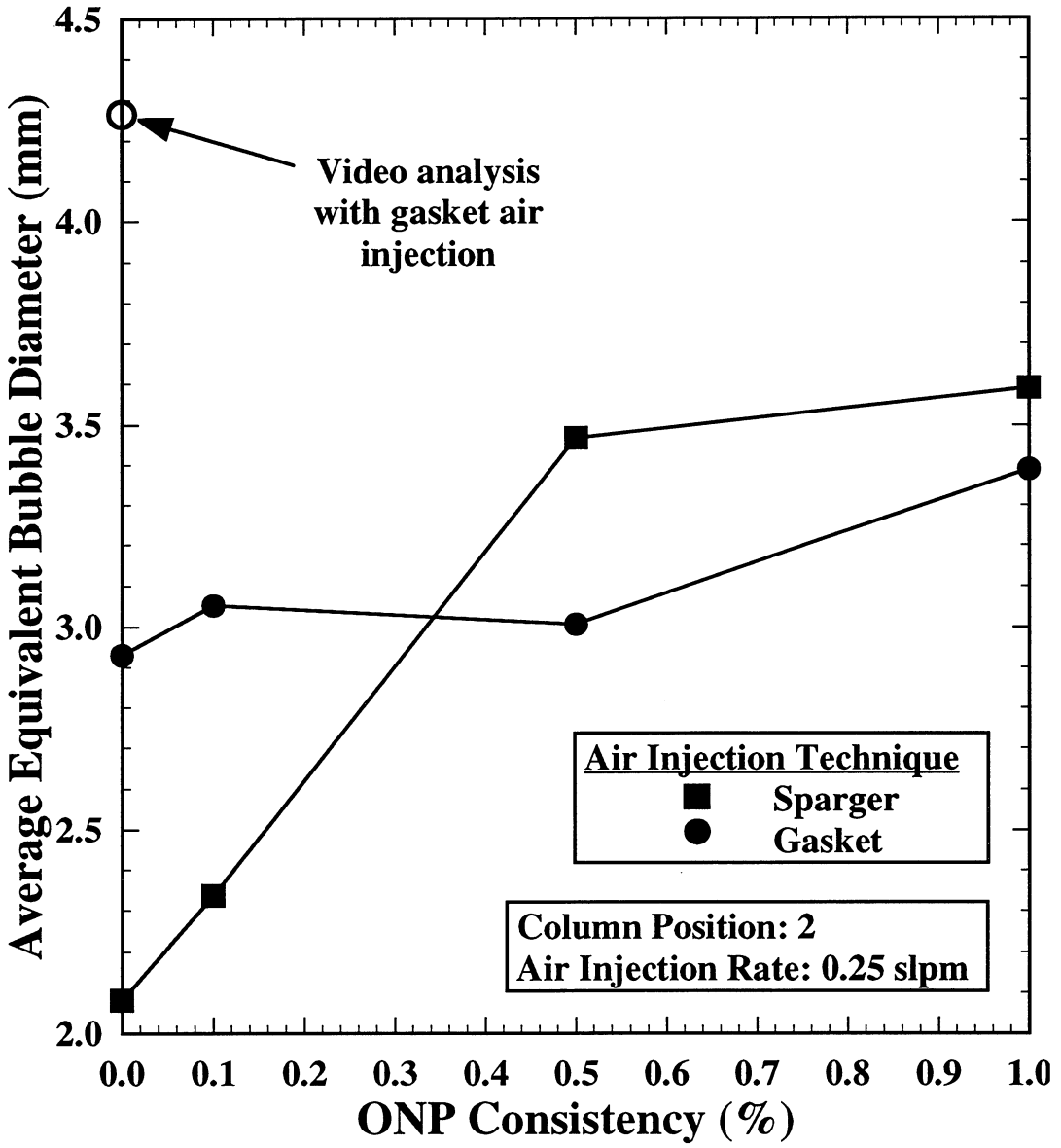

Figure 12: Effect of ONP consistency on average equivalent bubble diameter.

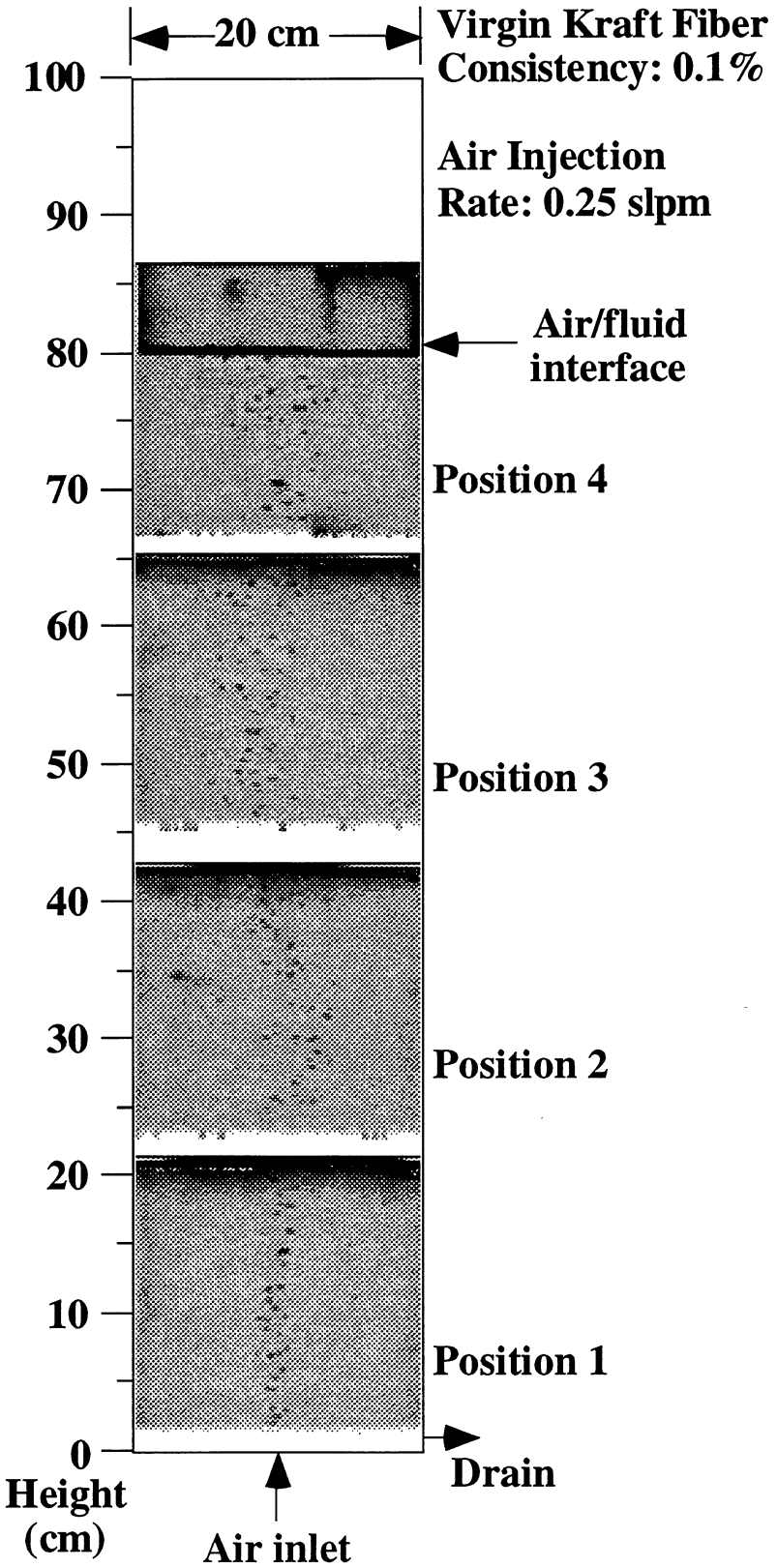

Figure 13: X-ray composite of air bubble flow patterns in an air/water/0.1% bleached kraft system with air injected through a single-holed gasket at the bottom of the column.

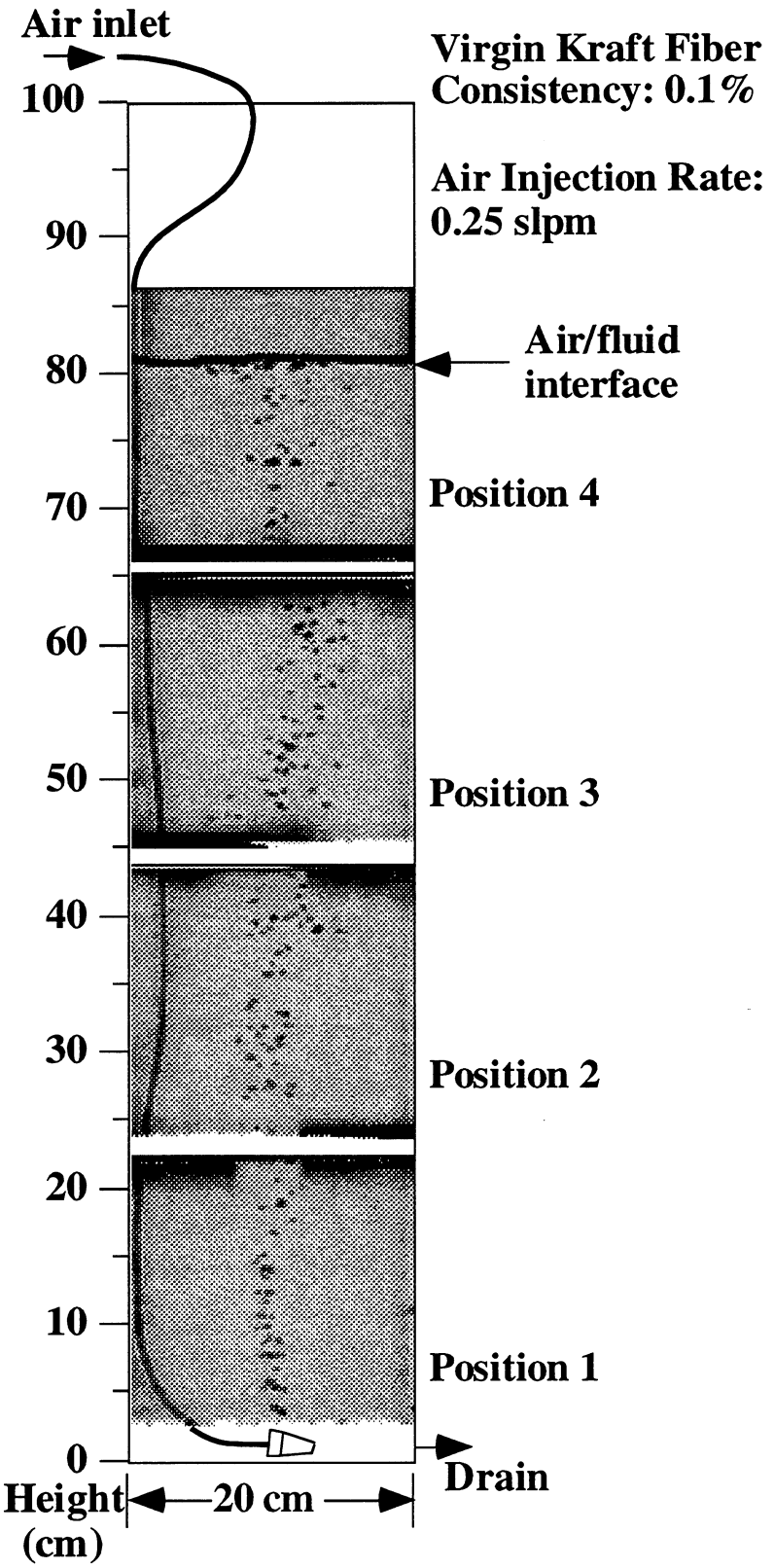

Figure 14: X-ray composite of air bubble flow patterns in an air/water/0.1% bleached kraft system with air injected through a sparger with 40 μm openings.

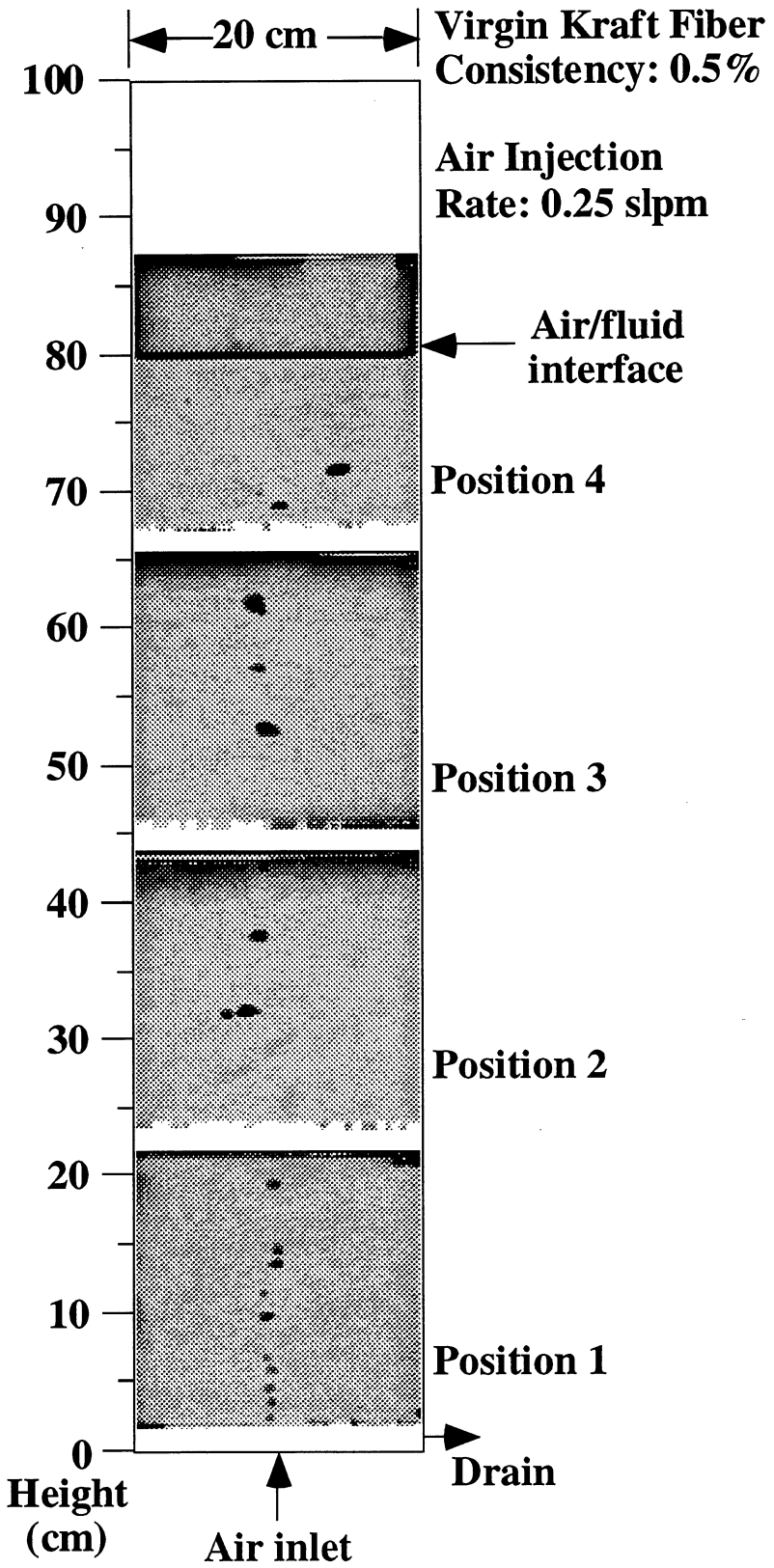

Figure 15: X-ray composite of air bubble flow patterns in an air/water/0.5% bleached kraft system with air injected through a single-holed gasket at the bottom of the column.

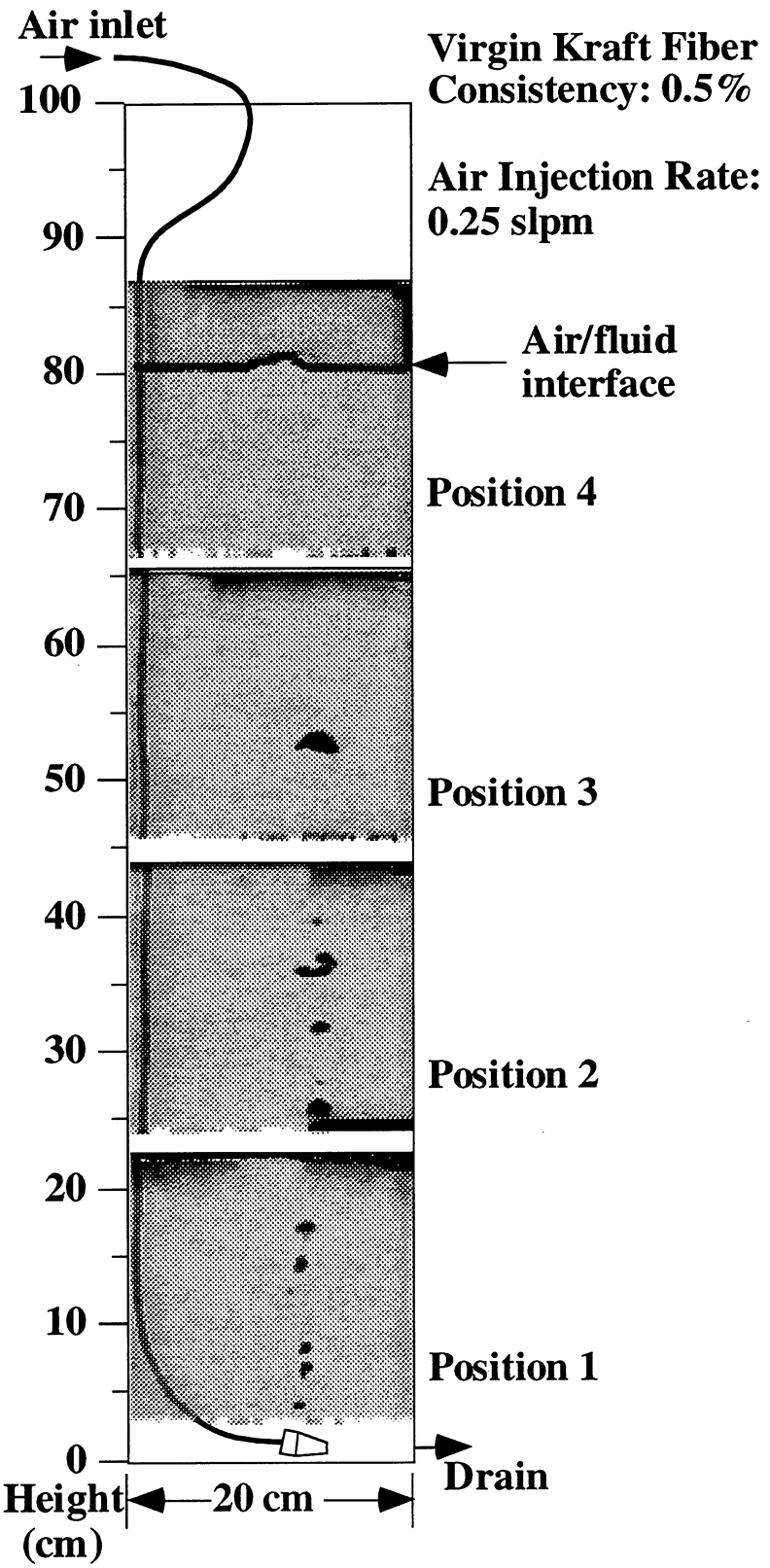

Figure 16: X-ray composite of air bubble flow patterns in an air/water/0.5% bleached kraft system with air injected through a sparger with 40 μm openings.

FIBER CARRY OVER REDUCTION IN FLOTATION DEINKING

STATUS REPORT

FOR

PROJECT E00104/F00904

Yulin Deng

March 27, 1997

Institute of Paper Science and Technology
500 10th Street, N.W.
Atlanta, Georgia

Project Title: FIBER CARRY OVER REDUCTION IN FLOTATION DEINKING
Project Staff: Yulin Deng
Budget (FY 96-97): $115,900
Reporting Period: FY 96-97
Division: Engineering and Paper Materials
Project Code: DEINK/CHEM
Project No.: F00904

FUNDAMENTALS OF SURFACE CHEMISTRY IN FLOTATION DEINKING

SUMMARY

This report is concerned with increasing utilization of recycled fiber and, more specifically, with minimizing fiber loss and maximizing deinking efficiency in flotation deinking. Although flotation deinking is considered to be one of the most effective deinking methods, many physico-chemical properties, such as ink removal efficiency, froth structure, and fiber loss mechanisms, remain unclear. To improve deinking efficiency and reduce fiber loss, the surface chemistry of ink, fiber, air bubble, and other contaminant materials in flotation deinking has to be studied.

The literature review of this report includes general information on flotation deinking and the surface chemistry of inks, air bubbles, and fibers in the process of flotation deinking. Studies on fiber surface chemistry, ink removal, and fiber loss in the flotation deinking process are also reviewed.

The RESULTS AND DISCUSSION section contains four parts: (1) the experimental method development for wetting force and contact angle measurement of wood fibers in aqueous solutions; (2) the froth stability and surface chemistry of fiber and ink in different surfactant and calcium chloride solutions; (3) the relationship among surface chemistry, ink removal, and fiber loss; and (4) the mechanisms of fiber loss in flotation deinking.

The results obtained in this research indicate that (1) both the fiber adhesion and the physical entraimment will contribute to fiber loss, but the entrainment is the

dominating factor contributing to the fiber loss; and (2) calcium ion concentration will significantly affect froth stability, ink removal, and fiber loss only when an anionic surfactant is used.

INTRODUCTION

Recycling is an important process in protecting our environment and improving raw material utilization. The flotation deinking technique has been widely used for more than a century in the mineral processing industry, and it has become one of the most effective ink separation techniques since it was introduced into the paper industry 15 years ago. Recently, the application of the flotation technique in wax removal, stickies control, and fiber fractionation has been studied. Potentially, this effective and energy saving technique will be more widely used in the paper industry. However, many significant questions remain, such as the deinking physico-chemical nature, effect of surfactant on the physical properties of deinked fibers and paper products, and the theoretical and model descriptions of the overall process.

The surface chemistry of flotation deinking has not been well-understood. The surface chemistry in flotation deinking can be divided into three categories: ink and contaminant surface chemistry, foam surface chemistry, and fiber surface chemistry. However, most of the researchers in the literature only focused on the ink surface and paid less attention to the foam stability and fiber surface chemistries. For example, it has been reported that calcium ions will increase both ink removal and fiber loss if an anionic surfactant is used, but the mechanism behind this is not clear. Because any chemicals

added into the flotation cell will affect all of the solid suspension in the pulp, the surface chemistry of ink, fiber, and foam must be studied as a whole system.

Fiber chemistry is one of the concern areas identified by technical managers of IPST Member Companies. Currently, studies on the surface chemistry of recycled fiber are not available in the literature. For example, how deinking chemicals will affect recycled fibers has not been studied. Therefore, the knowledge gained from this study would, indeed, aid not only ink removal and fiber loss, but also paper physics and papermaking wet-end chemistry, particularly when recycled fibers are used. For example, the knowledge of fiber-polymer interaction will improve fiber sizing, pulp retention, and paper physical properties.

The short-term goals of this research program are to:

* develop an effective method for fiber wettability measurement (completed);

* investigate the surface chemistry of fibers and inks in aqueous solutions and pulps (partially completed);

* investigate the effect of the hydrophobicity of fibers and inks on fiber loss and ink removal in flotation deinking (partially completed);

* determine true flotation and entrainment factors of fibers and ink particles in the flotation deinking process (partially completed);

* determine the effect of fiber length on fiber loss (will be completed in FY 97-98);

* investigate the impact of metal ions on the surface chemistry of inks and fibers (partially completed);

* investigate the effect of metal ions on foam stability (partially completed);

* study the air bubble size effect on fiber loss and ink removal (will be completed in FY 97-98);

* determine the influence of fiber contaminants on fiber loss (will be completed in FY 97-98);

* develop an effective method for reducing fiber loss in flotation deinking (will be studied from FY 97 to FY 99); and

* understand the relationship between ink and air bubble surface chemistry and ink removal efficiency, which includes the study of three types of printing materials (oil-based ink, water-based ink, and toner) and three types of surfactant (anionic, cationic, and nonionic) (will be completed from FY97 to FY 99).

The long-term goals are to:

* fully understand the mechanisms of fiber loss and ink removal in flotation deinking, and improve ink removal efficiency;

* develop an effective method to reduce fiber loss; and

* reduce the chemical consumption, fiber contamination, and pollution of process water in flotation deinking.

Possible outcomes of this research program will benefit the paper recycling industry by reducing fiber loss and increasing ink removal efficiency. It is also believed that the results obtained in this study will aid not only fiber loss, but wet-end chemistry and fiber surface chemistry.

LITERATURE REVIEW

The use of deinked fibers in the paper industry has increased dramatically in recent years, and with current environmental awareness and legislation, this trend is expected to continue. To be used as a high-value product, recycled paper must be thoroughly deinked. Three deinking processes, flotation, washing, and screening, are employed currently in the paper industry. Although flotation deinking is considered to be more effective and economical, there are still some remaining problems such as low ink removal efficiency of water-based inks, high fiber loss during flotation, and contamination of fibers by flotation deinking chemicals. Concerns with deinking efficiency and yield during flotation deinking have prompted an investigation of ink removal chemistry and fiber loss mechanisms.

Flotation as a separation technique has been practiced in the mineral processing industry since early in this century. The process has been thoroughly studied, and excellent reviews on the science and technology are available **[1,2]**. The basic principle of mineral flotation is to add a collector (surfactant), which will preferentially adsorb onto one of the minerals present. This lowers the surface energy of the mineral particle and allows it to selectively attach to the air bubbles in the flotation cell. A froth of bubbles with attached mineral particles is formed at the top of the cell and can be readily separated.

The application of the flotation technique to the deinking of wastepaper has been practiced in Europe and Japan for many years. Recently built mills in the United States have also incorporated flotation along with washing unit operations.

The chemistry of the process in flotation deinking has been reviewed **[3,4]**. In processing wastepaper with the foam flotation method, the stock suspension is composed mainly of water, fibers, ash, and ink particles. The main focus of deinking usually relates to the brightness and cleanliness of the fibers. Brightness figures without any information on the yield of the deinked fibers have only limited value because the achieved brightness strongly depends on the yield.

The separation of ink particles from a fiber surface includes three main steps: inks detach from fiber surface; inks attach to the air bubbles; and ink float and remov from the pulp suspension. However, the chemical and physical phenomenon in each step is very complicated. For example, the detached ink particles may redeposit on the fiber surface,

which will reduce paper brightness **[5,6].** Using surfactant to control the ink deposition on the fiber surface may not work because this will commonly cause a decrease of hydrophobicity of both ink and air bubble surfaces, resulting in a decrease in deinking efficiency. The ink detachment is a function of paper aging. Many researchers indicated that aged papers are more difficult to deink and will also cause a higher fiber loss during flotation **[7-9].** Ink particle size and surface chemistry are two dominate factors affecting ink removal. For example, flexoinks are very difficult to float because they have a very small particle size and high charge density **[10].**

The effect of fiber properties on the ink particle detachment has been studied **[11],** and it was found that the detachment of ink particles from fibers was not significantly dependent on the type of fiber. This implies that the surface properties of the fiber play a minor role in the detachment step. Although the detachment is not dependent on the nature of the fibers, the soluble and colloidal dispersible chemicals in different fibers will significantly affect the total flotation deinking efficiency, and may affect fiber loss in flotation deinking.

It has been well known that the surface chemistry of ink particles plays a key role in flotation deinking. The highly charged ink particles, such as water-based flexographic ink, are very stable colloidal suspensions in water, and they are difficult to attach to the hydrophobic air bubble surfaces. Even for the hydrophobic ink and toner particles, to obtain a high flotation efficiency is difficult because the flotation efficiency will be significantly affected by deinking chemicals, particularly surfactant. For example, a significant decrease in ink hydrophobicity and ink removal efficiency by the adsorption of surfactant has been well-known to papermaking chemists.

The surfactants used in flotation deinking can be divided into cationic, anionic, and nonionic. Anionic surfactants will dissociate in an aqueous solution and release positive charged ions. The negative charged organic anion together with an organic chain is responsible for the surface activities. Cationic surfactants react in the opposite way. Although ionic surfactants, particularly anionic, have been commercially used in the flotation deinking industry, the influence of the water hardness on the performance of these surfactants is significant and this influence has not been well-understood. Compared to ionic surfactants, nonionic surfactants have some advantages because they usually do not react with calcium ions.

Although ink removal efficiency is important, the fiber loss during the deinking process should also be considered because this will cause a deduction of total yield. According to Turvey **[8,9]**, the hydrophilic fibers will not adhere to a hydrophobic air bubble surface, and the fibers should not float during flotation deinking. However, reported fiber loss is in the range of 4-24 wt% depending on the processes, equipment, and chemicals used in flotation deinking. The loss across most recycled flotation deinking mills is between 5 and 12% of the gray stock, in which about 50% is high quality fibers. For highly sized or waxed fibers, such as paper board, fiber loss is extremely high, and the flotation technique cannot be used for these paper products unless a new technique is ready to increase the yield.

Although iber loss is one of the biggest problems in flotation deinking **[12]**, the mechanism of fiber loss is not clear. Most authors **[8,9,13]** have postulated that air bubbles routinely adhere to the fibers during the flotation process. In a series of studies on fiber loss in flotation deinking, Turvey **[8,9]**, and Schwinger and Dobias **[14]** indicated that 1) unprinted fibers do not float; 2) calcium ions can significantly increase fiber loss for printed fibers; 3) nonionic fatty alcohol ethoxylate surfactants cause high fiber loss;

and 4) pH plays an insignificant role in fiber loss. From these studies, Turvey **[8]** further concluded that fiber loss is due to the fact that part of the fiber becomes hydrophobic and adheres to air bubbles. However, no direct experimental measurement of fiber surface chemistry can support this assumption. The previous studies emphasized only the relationship between flotation conditions and final yield rather than the fundamental understanding. Furthermore, some of the conclusions from Turvey **[8]** are not correct. For example, many researchers indicated that unprinted fibers, even very clean bleached fibers, can still float **[13,15]** during the flotation deinking process. The opposite experimental results obtained by different researchers suggest that the mechanism of fiber loss in flotation deinking has not be well-understood.

The mechanism of fiber loss by air bubble-fiber adhesion has been questioned by Ajersch and Pelton **[15-18]**. In their experiments, no fiber-CO_2 bubble adhesion was observed for 10 different pulps. They concluded that hydrophobicity of a fiber surface does not contribute to fiber loss, and fiber loss is only due to the mechanical entrainment of fibers in the froth.

Although fiber loss in flotation deinking has been studied by many research groups, direct measurement of fiber surface hydrophobicity in flotation cells has not been performed. In this research program, both fiber surface chemistry and fiber loss in flotation deinking will be experimentally measured.

It was reported that long fibers float easier than wood fines **[13,15]**. To explain this phenomenon, Li and Muvundamina **[13]** assumed that surfactant molecules have different orientations on the fine and fiber surfaces. It has been well known that the surface of fines is more hydrophobic than long fibers because of its high lignin content. When surfactants adsorb on fines, the hydrophobic tails of surfactant molecules anchor onto the hydrophobic sites of fines and leave the charged heads (or hydrophilic parts)

toward the water phase. This leads to an increase of hydrophilicity of the surface of wood fines and prevents them from adhering onto air bubble surfaces. For long fibers, on the other hand, the surface is very hydrophilic, and surfactant adsorption is through the interaction between the hydroxyl groups of fiber surfaces and the charged heads of surfactant molecules (or hydrophilic parts of nonionic surfactant), resulting in an increase of hydrophobicity. Li and Muvundamina **[13]** believed that the increase of hydrophobicity of fine surfaces was the main reason for fiber removal. Once again, this is only an assumption, and trere is no direct experimental measurement to support it. It will be seen from this study that Li and Muvundamina's assumption is incorrect.

In addition to surfactant adsorption, many materials, such as metal ions (Ca^{2+} and Mg^{2+}), water-soluble and insoluble substances, salt concentration, and pH, will also affect the surface properties of both wood fibers and air bubbles. In some cases, these effects are significant. In addition to direct adsorption, some medal ions will interact with deinking chemicals and affect foaming ability and stability. How will the foam structure affect the ink removal and fiber loss is interesting. Therefore, it is part of the goal of this study to investigate the relationship among fiber loss, ink removal, foam stability, and concentration of metal ions.

Although the chemical compositions and surface properties are very important for fiber-air bubble adhesion, the geometry of fibers may also significantly affect the adhesion of fibers to air bubbles. However, only limited studies on the effect of fiber length on fiber flotation can be found in the literature. Li and Muvundamina **[13]** indicated that the formation of a fiber network in a pulp suspension could be an important factor and this may increase fiber loss. In contrast, Ajersch and Pelton **[18]** indicated that a network formation of fibers will reduce fiber loss. Because the fibers used in their

studies have different surface chemical properties, it is difficult to distinguish the effect of fiber length and fiber floc distribution from the effect of fiber surface chemistry.

A higher fiber loss caused by nonionic surfactant rather than anionic surfactant was reported **[8]**. The reasons behind this are not clear. One concern of this study is to examine the effects of surfactant structure on fiber loss in flotation deinking.

Among commercially available surfactants, fatty acid salt is one of the most commonly used collectors in flotation deinking. The effective ink removal using this surfactant can only be achieved in the presence of Ca^{2+}. A suggested mechanism of ink removal by this surfactant is the formation of a fatty acid-calcium complex between ink particle and air bubble. It is interesting to examine if a similar complex bridge can form between the fiber and air bubble. In this study, we will directly measure the individual and competitive adsorption of Ca^{2+} and fatty acid on fiber surfaces from various solutions. Combining the information gained from adsorption, surface tension, surface charge, air bubble stability, and contact angle measurements, the role of calcium ions in flotation deinking will be concluded.

Another important factor contributing to the fiber float may be the contamination of ink, stickies, sizing materials, and polymers. The mechanism of the bridge formation (if any) between air bubbles and fibers by ink particles and other contaminates is also of interest.

Hydrophobic/hydrophilic properties of the fiber surface are directly related to the contact angle of an aqueous solution on the fiber surface. Although the influence of adsorption and orientation of surfactant molecules on the wettability of wood fiber is very important, it has not been well-studied because of the lack of an effective method to measure the contact angle of liquid on individual fibers. The optical measurement of the

contact angle of liquid against fibers has been attempted by Foote **[19],** Jones and Porter **[20],** and Grindstaff **[21].** However, these methods are not satisfactory because (1) it is difficult to accurately measure the contact angle of liquid on very small wood fiber using an optical technique; (2) opposing curvatures between the fiber surface and observed meniscus lead to ambiguities in measuring the contact angle from the meniscus profile shape; and (3) they yield only a single θ-value, which may be highly unrepresentative of the average properties of the heterogeneous fiber. A more satisfactory approach to the determination of fiber-liquid contact angles employs the Wilhelmy principle in which the downward force upon a fiber suspended vertically through the liquid surface is measured **[22-24].** In our research program, fiber-liquid contact angle measurement was further improved.

Although both the adhesion of fiber to air bubble and the mechanical entrainment of fibers in the froth may contribute to fiber loss in flotation deinking, no study has been done to distinguish these two different contributions. Warren **[25]** studied the true flotation (adhesion flotation) and entrainment of mineral particles in flotation by measuring the particles removal against water removal. This method was used in this study to investigate the fiber loss mechanism.

EXPERIMENTAL

Receding and advancing contact angle measurements

A dynamic contact angle analyzer (Cahn DCA 312) was used to measure the surface tension of liquid and the dynamic contact angle of liquid on fibers. The instrument used for dynamic wettability experiments is shown schematically in **Figure 1,** and the theoretical consideration is given in the RESULTS AND DISCUSSION section.

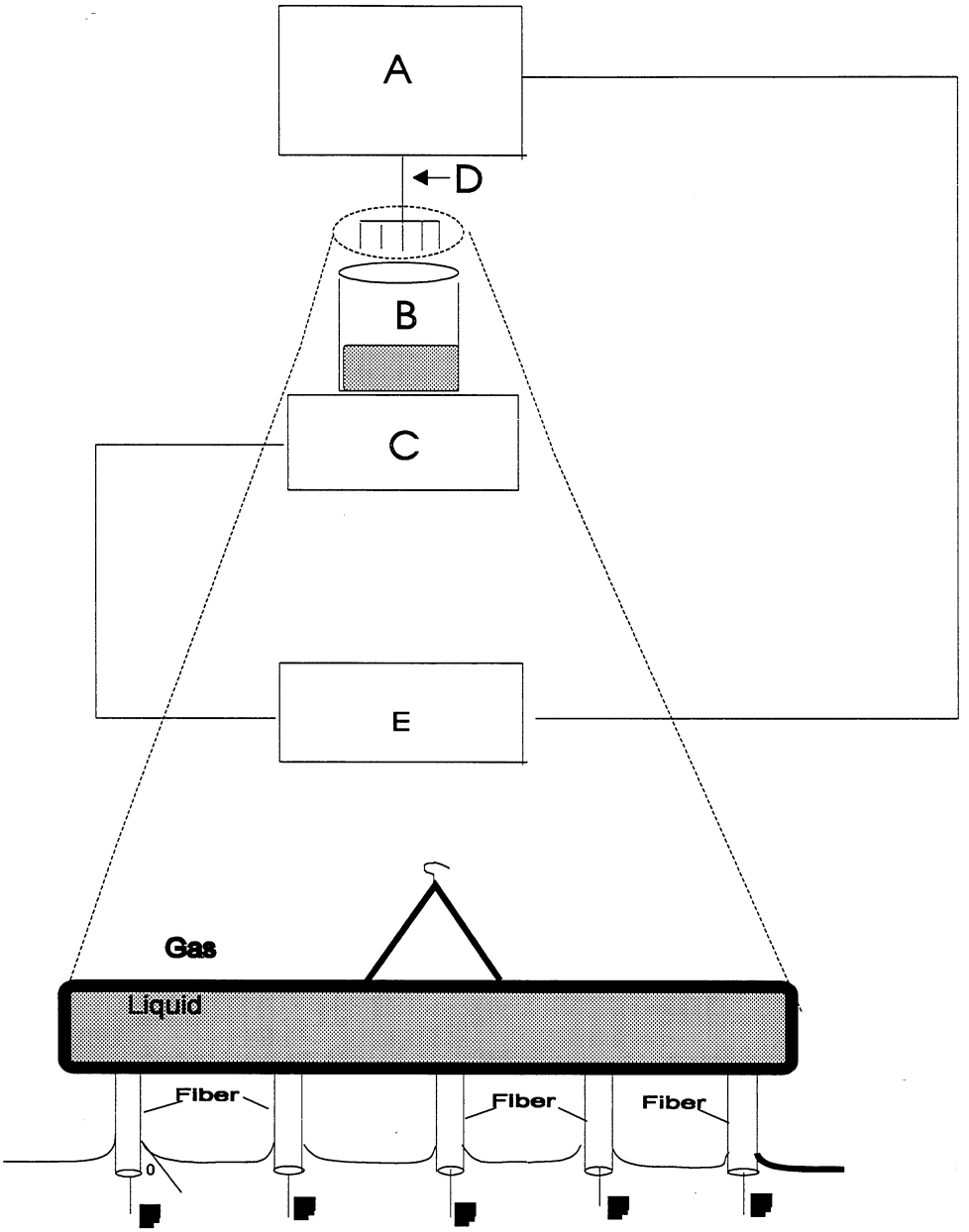

Figure 1. Schematic diagram of dynamic wetting force measurement using fiber group technique; A: electronic microbalance, B: wetting liquid, C: traveling elevator system, D: fibers, and E: computer.

The liquid is contained in a 50-ml glass beaker that can be raised up and down by a traveling elevator system, which allows the liquid to advance or recede over the sample

at a very slow, controlled rate (0.01 mm min.$^{-1}$). One end of 5-7 individual fibers was separately stuck on the adhesive tape keeping the other end in a straight line (see **Figure 1**). The ends of the fibers were carefully cut to the same level if it was necessary. The distance between individual fibers was greater than 1 mm to avoid the effect of capillary force. The dynamic wetting force on the fibers was measured by an electronic microbalance (0.1 mg resolution) and analyzed by a computer using DCA software.

Materials

The pulp properties used in this study are given in **Table 1**.

Table 1. Fiber properties.

Name	Fibers	Average length (mm)	Average perimeter (μm)	Lignin content (%)	Sizing	Freeness (ml)
HC	Holocellulose	3.02	90	0.178	no	unknown
BSP	Bleached Southern Pine	2.83	unknown	low	no	754
BK	Bleached Kraft Southern Pine	unknown	unknown	low	AKD	unknown
S-BK	Sized Bleached Kraft Southern Pine	unknown	unknown	low	no	unknown
MP	Mechanical Unbleached Pulp	2.88	91	high	no	unknown

The fiber lengths were determined by image analysis. The width and lumen diameter of fibers were measured using 400× magnification with the aid of OPTIMAS image analysis software. The fiber perimeter was calculated from average fiber width and lumen diameter.

The effect of fiber surface chemistry on fiber loss was examined using unsized and sized bleached kraft fibers that have the same geometric properties. The sized fibers were made by the reaction of fibers with varying amounts of a cationic AKD (alkyl ketene dimmer) sizing emulsion (Hercon 70, Hercules Inc.) in ~3% fiber consistency for 5 min. The furnishes were filtered and air dried about 2 hr. The air-dried fibers were heated to 100°C in a vacuum oven for ~30 min.

Surfactants, Triton X-100 (TX-100, analyze grade, J.T. Backer Inc.), cetyltrimethylammonium bromide, [$CH_3(CH_2)_{15}N(CH_3)_3Br$, CTMAB, Adrich, 95%], and sodium dodecylsulphate (SDS) (Specially pure, BDH Inc.), sodium oleic acid salt (Aldrich) were used as received. PolyDADMAC and polyacrylic acid are Nalco Inc. products.

Flotation experiments

The flotation cell used in this study is schematically shown in **Figure 2**. The flotation unit includes a polyacrylate column (variable in height) and an air inlet filter. Nitrogen was blown into the pulp at a required rate through the air inlet filter. The ultra-high pure (UHP) nitrogen was run through a digital flowmeter (Fisher product) before the flotation cell. The flow rate was first adjusted to a required value before the flotation experiment. The foam that spilled over the column was collected in a container. A burette was set up to add additional surfactant solution through an inlet tube if necessary. The distance from the pulp surface to the top of the flotation cell (froth height) was adjusted by adding extra columns to the top of the flotation cell. After the flotation experiment, the wet foam was weighed and water loss was calculated. Both removed and residue fibers were then filtered, dried, and weighed. The water loss was controlled by either changing the flotation time or the froth height.

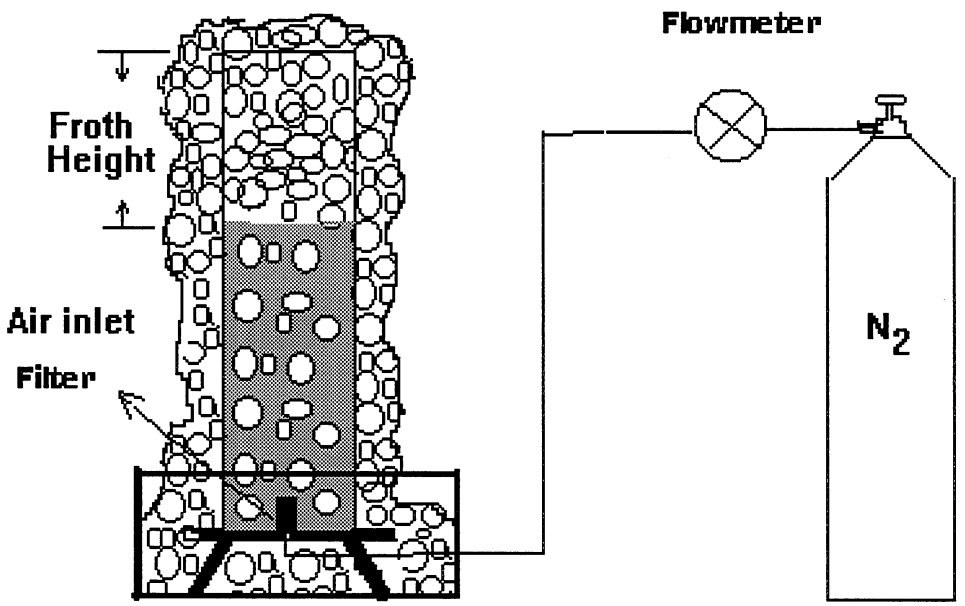

Figure 2. Schematic diagram of the graduated cylinder flotation apparatus.

The pH of the pulp was adjusted using solutions of sodium hydroxide or hydrogen chloride if necessary. After the addition of the surfactant, the pulp was mixed for ~30 minutes under slow agitation; then, the air was injected at a required flow rate.

Brightness analysis

The handsheets for brightness analysis were made on a 15-cm Büchner funnel using TAPPI standard method. The brightness of the handsheets was measured using a Shimadzu UV-VIS Spectrophotometer (UV-160A).

Foam stability

Foam stability was studied by measuring the decrease of the froth height with decay time in the flotation cell. The influence of fibers, toner particles, and calcium ions on froth stability was measured.

RESULTS AND DISCUSSIONS

Fiber Wettability

In order to study the mechanism of fiber loss in flotation deinking, and to examine the reasons for the fiber surface changing from hydrophilic to hydrophobic, the wettability of fibers must be measured. It has been well-known that the contact angle measurement carried out on a paper sheet cannot be attributed only to the fiber surface chemistry because the contact angle strongly depends on the surface roughness. Furthermore, the fibers in the flotation cell are individual fibers rather than a paper sheet. For these reasons, an effective method of wettability measurement for individual fibers in deinking pulp must be developed.

Theoretical consideration

For an object immersed in a liquid, the dynamic wetting force can be written as

$$F = P\gamma\cos\theta + mg - (\rho_l - \rho_g)V \qquad (1)$$

where F is the wetting force on the object; P is the perimeter of the wetted object; γ is the surface tension of the liquid-air surface; θ is the contact angle of the liquid on the solid surface; m is the mass of the object; g is acceleration of gravity; V is the submerged volume; and ρ_l and ρ_g are the liquid and air densities, respectively.

Because the weight and buoyancy force are negligible compared to the total force for very small wood fibers (about 1% of total wetting force) **[22,26]**, the dynamic wetting force reduces to

$$F = P\gamma\cos\theta \qquad (2)$$

However, the calculation of the contact angle of wood fiber using **Equation (2)** depends on the accurate value of the fiber perimeter. Although Young **[27]** used a light microscope equipped with a calibrated eyepiece to measure the fiber perimeter, the swelling degree of fibers in liquid, the heterogeneity of the fiber perimeter along the fiber length, and the capillary effects from fiber surface roughness and hollow structure are impossible to measure using this technique. The difficulty in obtaining an accurate value of the fiber perimeter makes contact angle measurements more complicated, and **Equation (2)** cannot be directly used. However, previous studies indicated **[22,26,28]** that the receding contact angle of water and most of the other liquids on wood fibers (unsized fiber) is zero, i.e., $\cos\theta_R = 1$, where θ_R is the receding contact angle. This leads to a relationship between advancing contact angle, θ_A, and dynamic wetting force

$$\cos\theta_A = F_A / F_R \qquad (3)$$

where F_A and F_R are the advancing and receding dynamic wetting forces of wood fibers in an aqueous solution, respectively. **Equation (3)** indicates that an advancing contact angle can be calculated from the advancing and receding forces without knowing the fiber perimeter.

Although **Equation (3)** has been used to calculate the advancing contact angle of an aqueous liquid on wood fiber, it is not clear whether the zero-receding contact angle can be generally used for systems such as fibers in surfactant or polymer solutions. In this study, the zero-receding contact angle assumption was further verified.

Although previous works provided a very useful technique for determining the wetting force of a single fiber in an aqueous solution, a large experimental uncertainty was unavoidable because the dynamic wetting force for a single fiber is too small (advancing force is less than 0.05 dyne for most unsized fibers and more less, even negative, for sized fibers in a liquid solution). Furthermore, it is a general requirement that more than 10 independent samples have to be measured due to the heterogeneity of wood fibers. These problems were solved by this study using the fiber group showed in **Figure 1**. When a fiber group is used instead of a single fiber, a relatively large force can be obtained and the heterogeneity of both fiber surface chemistry and fiber perimeter can be averaged out, resulting a more accurate measurement.

Traces of dynamic wetting forces

The typical curves of receding and advancing dynamic wetting forces measured using a group fiber technique are shown in **Figure 3**. The fibers were immersed in (advancing) or pulled out (receding) of the liquid at a constant velocity. The immersed distance shown in **Figure 3** is proportional to the immersed volume of fibers. The fiber weight was first tared out in air establishing a baseline **A.** When the fibers were immersed into the liquid, a trace of advancing force was recorded from **A** to **B**. It has been noted that the advancing wetting force obtained by a wood fiber group increases very slowly with the immersed fiber length, which is significantly different from the wetting force obtained by a glass plate in the same liquid, i.e., a sharp increase in the wetting force has usually been observed when a glass plate is immersing into the liquid. Two factors may slow the increase of advancing wetting force of wood fibers. First, the fibers swell gradually when dry fibers immerse into an aqueous solution. Because the fiber swelling will result in an increase in the perimeter and a change in the surface chemistry, the dynamic wetting force must gradually change. Second, the wood fibers

were heterogeneous along the fiber length. The heterogeneity of the fiber perimeter along its length (needle-like shape) is easy to see under a microscope, which must result in a gradual increase in the fiber wetting force when fibers are immersed into the liquids.

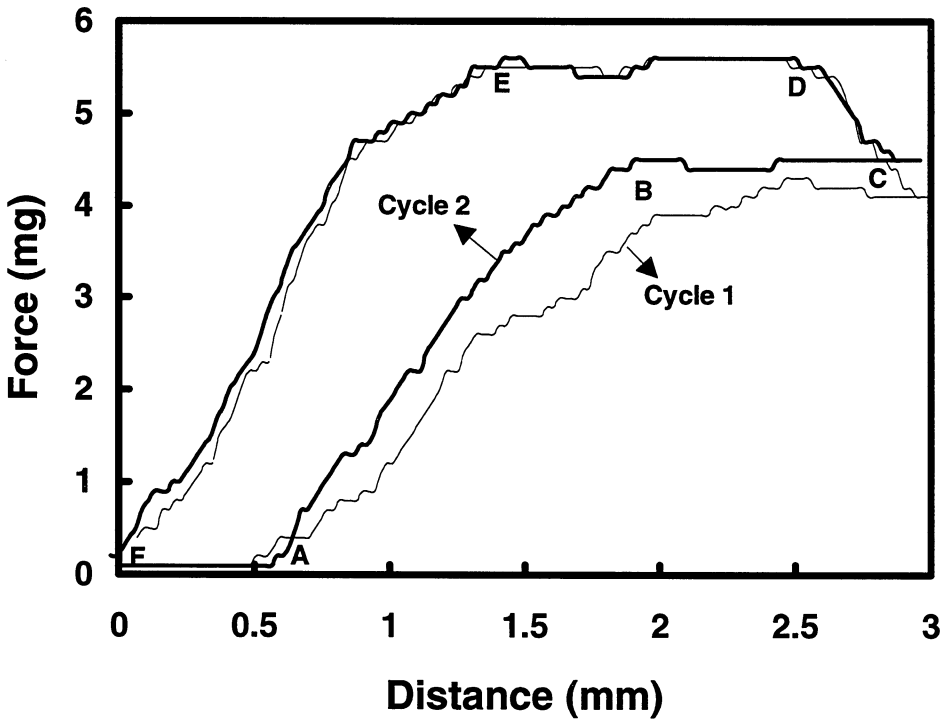

Figure 3. The traces of dynamic wetting forces of five holocellulose fibers in water.

As the fibers were immersed further from **B** to **C**, a constant advancing force was recorded. The trace of wetting force from **B** to **C** is also different from the trace of water over a glass plate. For a glass immersing into aqueous solution, the wetting force decreased with submerged volume because of the increase of buoyancy force, but a constant force was obtained when a fiber group was used. Because of this, it is necessary to extrapolate the dynamic wetting force to zero submerged volume to eliminate the buoyancy force when a glass plate is used. However, it is difficult to detect where the

zero distance is if a fiber group is used because all of the fibers may not attach to the liquid surface simultaneously. Fortunately, as discussed before, the buoyancy force may be negligible for a very small gravity force of wood fibers compared to the total wetting force. In other words, the total dynamic wetting force measured by the balance should be independent of the submerged volume for wood fibers, and it is not necessary to extrapolate the dynamic wetting force to zero contact point. This is confirmed by **Figure 3,** which shows that the wetting force is independent of the submerged volume of fibers from **B** to **C**. Comparing the calculated buoyancy force to the total wetting force showed in **Figure 3**, it was found that the buoyancy force of fibers in water was only ~1% of the total wetting force. This suggests that the total advancing wetting force of wood fibers in a solution can be directly obtained from **B** to **C,** and it is not necessary to make any correction to submersed volume. A similar conclusion can also beexpected for the receding force. In this study, the stable dynamic wetting forces (**B** to **C** for advancing, and **D** to **E** for receding) were directly used to calculate the contact angles.

After fibers reached the maximum depth at **C**, they were gradually pulled out from the liquid until reaching position **D**, at which a stable receding force was obtained. The receding force remained constant from **D** to **E** and then decreased from **E** to **F** where the fibers were totally pulled out from the liquid.

The dependence of the total force on the fiber swelling was observed in this study. It can be seen from **Figure 3** that the advancing force of the first cycle is smaller than that of the second, but the receding force is the same for both cycles. This is not surprising because the advancing wetting force was obtained by dry fibers for the first cycle, but by wetted fibers for the second cycle. Obviously, dry fibers have different perimeter and surface properties from wetted fibers. After the first cycle, the fibers were wetted and both the fiber perimeter and the wetting forces reached an equilibrium value. For the

receding force, the fibers were always wetted regardless if it was the first or the second cycle. The difference in advancing contact angles between the first and the second cycles was observed for all of the fibers and the solutions, such as BK and SBK in TX-100 solutions, and HC in different surfactant solutions. After fibers were wetted, stable wetting forces were obtained for both advancing and receding processes. All of the measurements made in this study were reproducible with an experimental error of less than ±8%.

Verification of zero-receding contact angles

Although Klungness **[26]** and Hodgson and Berg **[22]** indicated that the receding contact angle of water over a single wood fiber is zero, direct experimental proof is needed, particularly for the sized fibers in surfactant or polymer solutions.

For the same fibers in different solutions (surfactant, polymer, etc.), **Equation (2)** indicates that

$$\frac{F_R^1}{\gamma^1} = p\cos\theta_R^1$$

$$\frac{F_R^2}{\gamma^2} = p\cos\theta_R^2$$

. . . .

$$\frac{F_R^n}{\gamma^n} = p\cos\theta_R^n \qquad (4)$$

where 1, 2, and n represent the different solutions. If the assumption of zero-receding contact angle can be used for all of the solutions, **Equation (4)** can be rewritten as

$$\frac{F_R^1}{\gamma^1} = \frac{F_R^2}{\gamma^2} = \cdots\cdots\cdots = \frac{F_R^n}{\gamma^n} = \mathrm{p} \qquad (5)$$

Equation (5) indicates that if the zero-receding contact angle assumption can be used for the solutions with different surface tension, the force ratio ($\frac{F_R^n}{\gamma^n}$) should be a constant, which equals the perimeter P of the fibers. In contrast, if the receding contact angle is not zero, $\frac{F_R^n}{\gamma^n}$ must be a function of cosθ that depends on the surface tension γ (see **Equation 4**). In other words, the zero contact angle assumption can be verified by measuring the value of $\frac{F_R^n}{\gamma^n}$ in a series of solutions with different surface tensions. In this study, the receding force of different surfactant solutions over the same fiber group was measured, and the results are shown in **Figure 4**.

It can be seen from **Figure 4** that although the surface tension of TX-100 decreases as the surfactant concentration increases up to 190 mg/L (the critical micellization concentration of TX-100), the value of $\frac{F_R^n}{\gamma^n}$ is almost a constant under experimental uncertainty. This strongly suggests that although the surface chemistry of the fibers may be different before and after the surfactant adsorption, the receding contact angle of aqueous solution on the fibers is always equal to zero. The same conclusion was obtained for all of the other fibers used in this study, which includes HC, BSP, and MP in TX-100 solutions. The zero-receding contact angle assumption was further verified using different types of surfactant and polymer, such as cationic surfactant (cetyltrimethylammonium bromide, CTMAB), anionic surfactant (sodium dodecyl sulfate, SDS), and cationic polymer polyDADMAC [poly(dialyldimethylammonium chloride)]. The value of $\frac{F_R^n}{\gamma^n}$ in different surfactant and polymer solutions as a function of surface tension is given in **Figure 5**. Surprisingly, all of the results can be well-described using **Equation (5)**, which indicates that the receding contact angle of HC fibers in all of the aqueous solutions, including surfactant, anionic polymer, and cationic polymer solutions, is zero or close to zero even though the adsorption of different chemicals may

significantly change the surface properties. The uncertainty of the receding contact angle measured in this study will be discussed later.

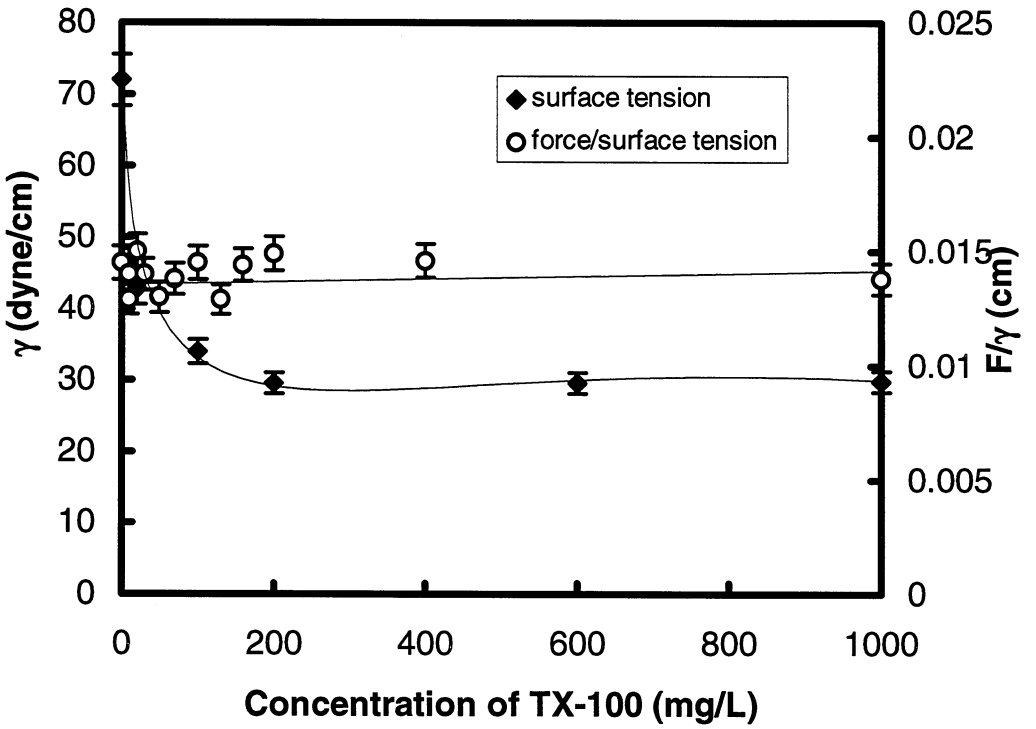

Figure 4. Surface tension γ and force ratio F_R/γ as a function of TX-100 concentration at room temperature for bleached softwood kraft fibers.

It is interesting that although the MP fibers are more hydrophobic than the bleached fibers because of the higher lignin content of the former, a zero-receding contact angle assumption can still be applied. Combining with Hodgson and Berg results [**22**], it can be concluded that the receding contact angle of water and surfactant solutions on most fibers can be treated as zero.

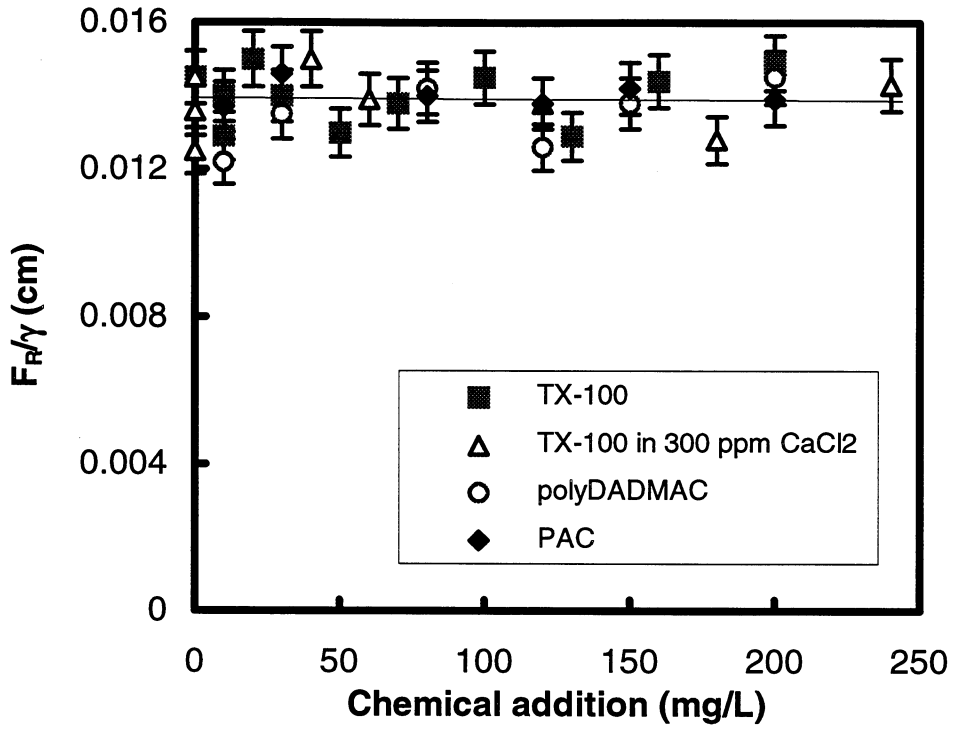

Figure 5. Force ratio F_R/γ as a function of chemical concentration of TX-100 in 300 mg/L $CaCl_2$, polyDADMAC, and polyacrylic acid solutions. Fibers: bleached softwood kraft fibers.

The perimeter of 145 ± 9 μm for a single holocellulose fiber was obtained from the data shown in **Figure 4** using **Equation (5)**. This value is 1.6 times the perimeter obtained from image analysis (90 μm). If we note that the perimeter obtained by image analysis is based on dry fibers and the perimeter obtained from the Wilhelmy principle is based on wetted fibers, the difference between these two values is not surprising. It has also been suggested from this study that although the perimeter of dry fibers can be measured by several techniques, such as image analysis and electron microscopy, it cannot be used in the Wilhelmy Equation without correcting fiber swelling. It should be

noted that the perimeter calculated from **Equation (5)** is only an apparent perimeter because the capillary and surface roughness may also affect the total force F_R.

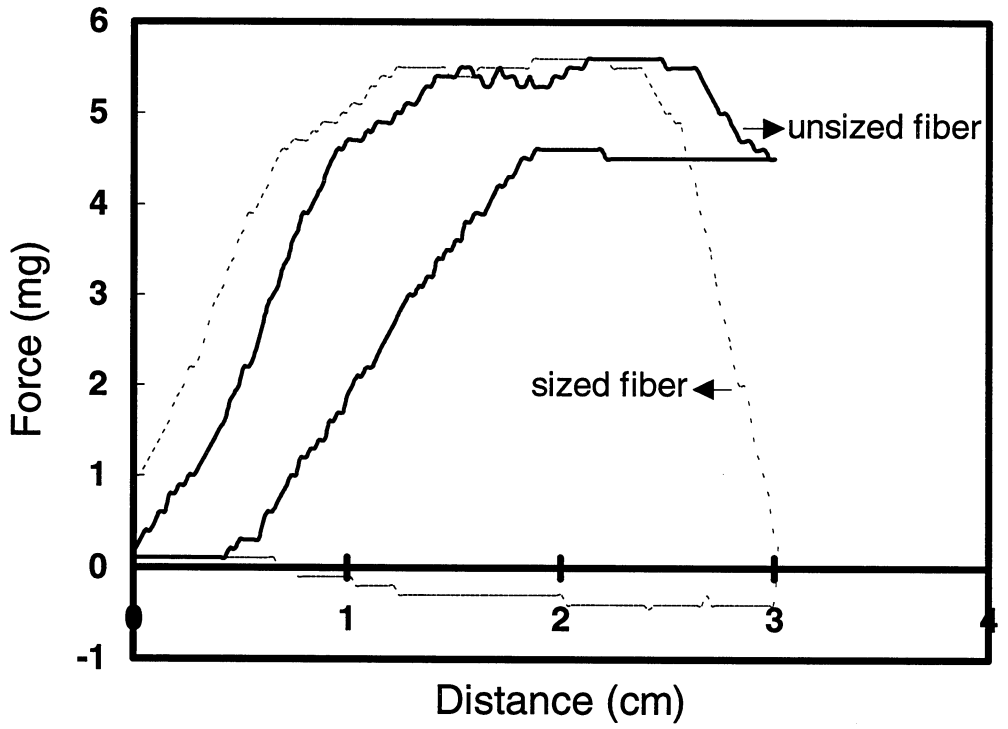

Figure 6. The traces of dynamic wetting force for sized and unsized bleached kraft fibers in water.

The receding wetting force and contact angle of highly sized S-BK fibers in TX-100 solution were also examined using **Equation (5)**. Because AKD is very hydrophobic, the sized fibers used in force measurements must be stiff enough to resist bending when fibers are immersed in the liquids. Furthermore, because the advancing wetting force may be very small, even negative, when highly sized fibers are used, the electronic microbalance must be sensitive enough. These limitations make the

measurements more difficult and lead to a high experimental uncertainty. However, after several repeated measurements, it was found that when a surfactant was added into the liquid both the hydrophobicity of sized fiber and the surface tension of the liquid decreased so that the fibers could be easily immersed into the liquid without bending. It was also noted that, in a pure water system, although the sizing materials significantly decrease the advancing force of fibers, they almost do not impact the receding force. This interesting behavior is shown in **Figure 6**. The receding forces obtained from highly sized fibers in various TX-100 concentrations were examined using **Equation 5**. Once again, a constant value of $\frac{F_R^n}{\gamma^n}$ was obtained.

The values of $\frac{F_R^n}{\gamma^n}$ obtained in TX-100 by highly sized and unsized BK fibers are (132 ± 9 μm) and (126 ± 10 μm), respectively. This very small difference suggests that even though the fibers have been highly sized the receding contact angle did not significantly change. In other words, the receding contact angle of an aqueous solution on sized fibers can also be treated as zero. According to **Equation (2)**, the difference in receding contact angle for unsized and sized fibers can be calculated by the ratio of $F_R^{unsized}$ and F_R^{sized} using

$$F_R^{sized} / F_R^{unsized} = \cos\theta_R^{sized} / \cos\theta_R^{unsized} \qquad (6)$$

where F_R^{sized} and $F_R^{unsized}$ are receding forces, and θ_R^{sized} and $\theta_R^{unsized}$ are the receding contact angles of sized and unsized fibers, respectively. Because $\cos\theta_R^{unsized} = 1$, **Equation (6)** reduces to

$$F_R^{sized} / F_R^{unsized} = \cos\theta_R^{sized} \qquad (7)$$

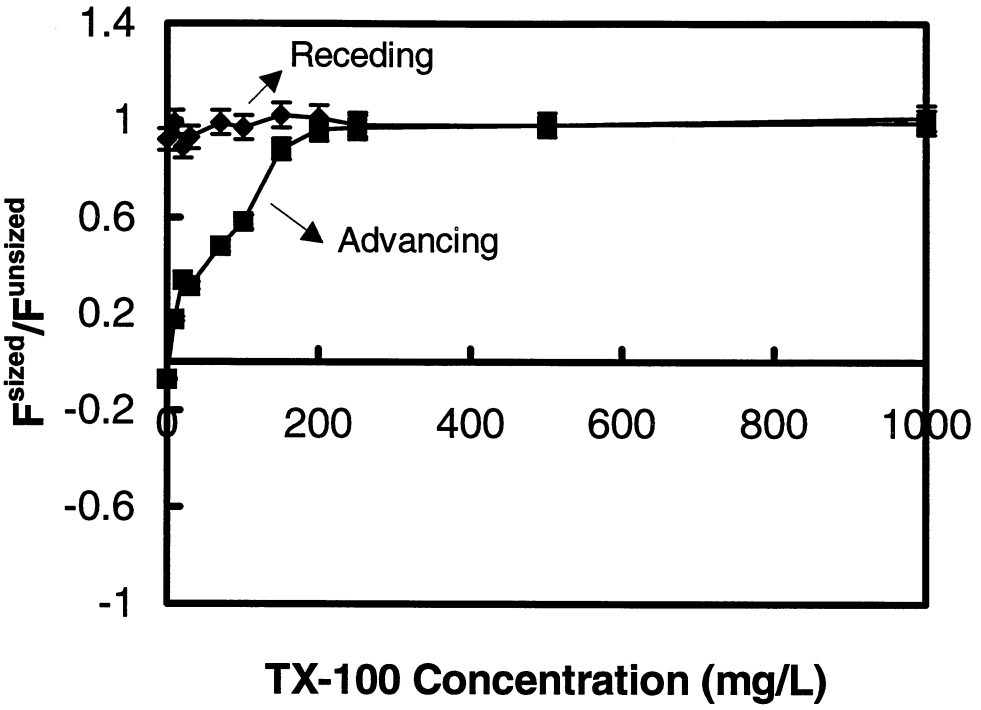

Figure 7. The ratio of the dynamic wetting forces measured from unsized (BK) and highly sized (SBK) fibers against surfactant concentration.

The values of $F_R^{sized}/F_R^{unsized}$ measured in different surfactant solutions are plotted as a function of surfactant concentration in **Figure 7**. It can be seen that all of the $F_R^{sized}/F_R^{unsized}$ values, including those obtained in pure water and in surfactant solutions, fit the unit line with an uncertainty of ± 0.12. This leads to $\cos\theta_R^{sized} / \cos\theta_R^{unsized} = 1\pm$ 0.12. It has been confirmed from the above discussion that the receding contact angle of unsized fibers in water is zero, i.e. $\cos\theta_R^{unsized}=1$. Therefore, the receding contact angle θ_R^{sized} is in the range of 0 to 23° for these sized fibers. Although this is a wide range of values, it will only give a small correction on the advancing contact angle when **Equation (3)** is used. For example, if the advancing contact angle is 60° (most sized fibers have a θ

$_A > 60^\circ$ in water), we have $F_A/F_R = \cos 60/\cos\theta_R^{sized} = 0.588/\theta_R^{sized}$. Because θ_R^{sized} is in the range of 0 to 23° for sized fibers, it leads to $F_A/F_R = 0.588 \pm 0.07$. Substituting this value into **Equation (3)** gives $\theta_A^{sized} = 60 \pm 5^\circ$. This suggests that even though the receding contact angle can be in the range of 0 to 23° for highly sized fibers the uncertainty of advancing contact angle calculated from **Equation (3)** using zero-receding contact angle assumption is small.

Although the receding force ratio of $F_R^{sized}/F_R^{unsized}$ is almost equal to one in all of the solutions, the advancing force ratio $F_A^{sized}/F_A^{unsized}$ is significantly different for sized fibers in different surfactant solutions. As surfactant concentration increases, the sized fibers sharply change from hydrophobic to hydrophilic by the adsorption of surfactant onto the fiber surfaces, but the hydrophilicity of unsized fibers changes little because they are originally hydrophilic enough. This leads to a quick increase in F_a^{sized}, but remains a constant $F_A^{unsized}$. As a result, $F_A^{sized}/F_A^{unsized}$ is sharply increased. It can be seen from **Figure 6** that the advancing force ratio, $F_A^{sized}/F_A^{unsized}$, increases from negative (in water) to positive, and finally reaches its maximum value (= 1 at the concentration above the CMC of TX-100). This suggests that the fibers, even though they are highly sized, will be fully wetted at high surfactant concentration. This will be discussed further later.

Advancing contact angle

For the fibers that have a zero-receding contact angle, the advancing contact angle can be calculated using **Equation (3)**. **Figure 8** shows the advancing contact angle of bleached soft wood kraft fibers as a function of TX-100 concentration in water and in calcium chloride solutions. It can be seen that the advancing contact angle of liquid on the cellulose fibers decreases from 39 to about 7° as the TX-100 concentration increases from 0 to ~50 mg/L. Further increase in TX-100 concentration does not significantly

change the advancing contact angle. From surface tension measurements, it has been found that the CMC of TX-100 is 190 mg/L. These results suggest that the bleached softwood kraft fibers are very hydrophilic by the adsorption of surfactant molecules even at a concentration well below the CMC.

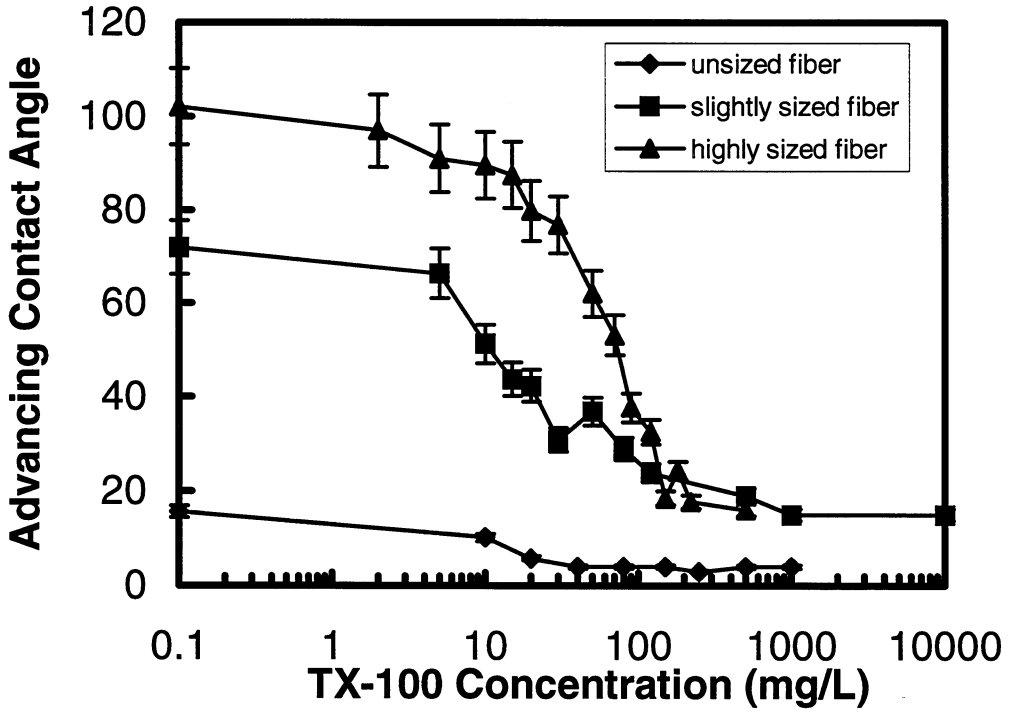

Figure 8. Advancing contact angle of unsized, slightly sized, and highly sized bleached kraft fibers as a function of TX-100 concentration.

It has been mentioned that although there is almost no difference in receding dynamic wetting forces between sized and unsized fibers the advancing wetting forces are significantly different for these two fibers. For unsized fiber, a positive advancing

dynamic wetting force was obtained, but for highly sized fiber, the advancing dynamic wetting force is negative, which leads to a $\theta_A > 90^\circ$.

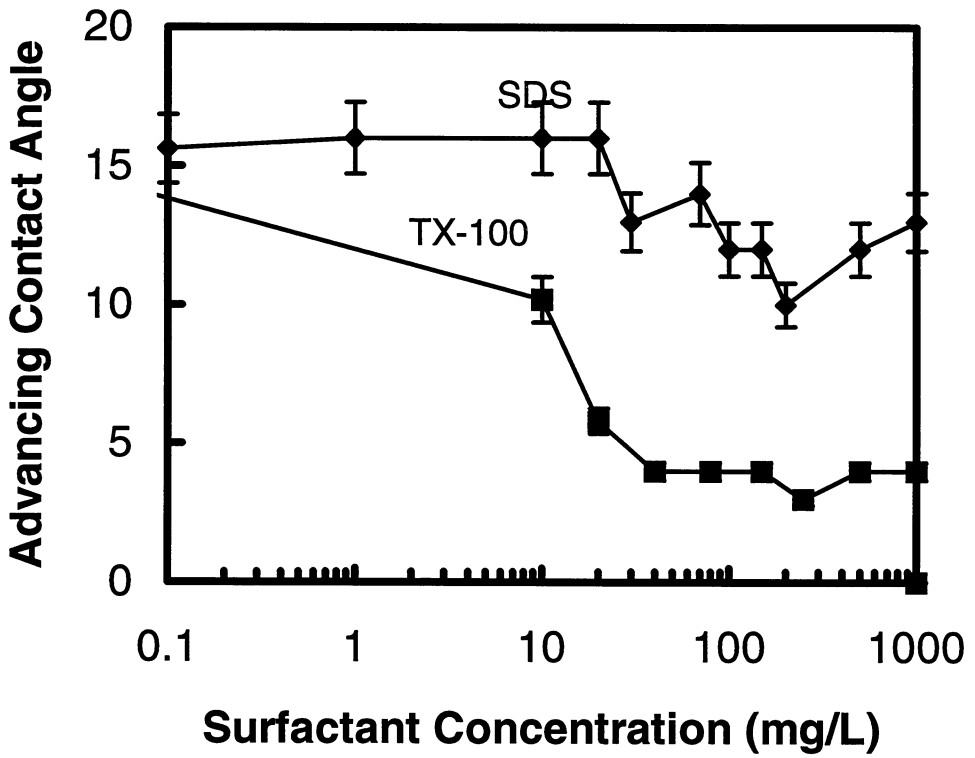

Figure 9. Advancing contact angle of unsized BK fibers as a function of surfactant concentration at neutral pH and room temperature.

It can be seen from **Figure 8** that all of the advancing contact angles of liquids on the fibers decrease as the TX-100 concentration increases regardless of whether the fibers are unsized or highly sized. For example, the advancing contact angle of liquids on highly sized fibers drops from ~ 100° in pure water to less than 20° at a surfactant concentration higher than 200 mg/L. Combining the results of holocellulose fibers in

TX-100 (**Figure 8**) with the results of BK fibers in SDS solutions (**Figure 9**), it can be concluded that the adsorbed surfactants will significantly increase the hydrophilicity of the fibers, regardless of the original fiber surface properties.

Comparison with previous results

The relationship between wettability and surfactant adsorption has been discussed by Putz et al. **[29,30]** and Li and Muvundamina **[13]**. They suggested that the hydrophilic parts of nonionic surfactant are more likely to be adsorbed by a hydrophilic solid surface leaving the hydrophobic tail toward the liquid. If this is true, the surfactant molecules on the fiber surface have different orientations when they adsorb on hydrophobic and hydrophilic fibers. For hydrophilic fibers, the adsorption of surfactant must result in an increase in fiber hydrophobicity. In contrast, the adsorption of surfactant molecules on hydrophobic fibers (such as sized fibers) must result in a decrease in fiber hydrophobicity. Li and Muvundamina **[13]** use this assumption to explain why long fibers float easier in flotation cells than fines (fines are relatively hydrophobic because of the high lignin content). The direct measurements of the advancing contact angles of different surfactant solutions (TX-100, SDS, and CTMAB) on all of the fibers (HC, BK, and SBK) in this study indicate that Li and Muvundamina's assumption is not true. Indeed, the hydrophobicity of wood fibers decreases with the increase of surfactant concentration, regardless of the nature of the surfactants (nonionic, anionic, or cationic) and the fiber properties (bleached, unbleached, sized and unsized). This suggests that the adsorption of surfactant on the fiber surface is through the hydrophobic-hydrophobic interaction rather

than hydrophilic-hydrophilic interaction. The detailed structure of the surfactant on the fiber surface will be studied further in future works.

Advantages of using the fiber group technique compared to other techniques

Several advantages could be achieved by using the fiber group technique: 1) the total wetting force of wood fibers in solution is larger than the wetting force of a single fiber in the solution, resulting in a decrease in experimental error; 2) the heterogeneity of the fiber perimeter can be averaged out by using 5 to 7 fibers simultaneously, resulting in a reproducible result and smooth curve; and 3) the capillary and surface roughness effect can be minimized compared to the contact angles obtained from a paper sheet.

Flotation Results

It has been mentioned before that both direct adhesion of fibers on air bubble surfaces and physical entrainment of fibers in the froth network have been suggested to be the mechanism of fiber loss in the literature. Because the entrainment of fibers in the froth depends on the free volume between the bubbles, the fiber loss must have a close relationship with froth structure. When froth raises up, water with fibers, ink particles, fillers, and fines, will fill up the space between bubbles. As a result, the overflow of the foam carries parts of solid materials out of the flotation cell. Because physical entrainment is nonselective and depends on the free volume between bubbles, the entrainment of fibers and ink particles must be a function of water removal during flotation. In this study, both fiber loss and water loss were examined, and the relationship between them will be discussed in the following sections.

Water loss and froth stability

The water loss as a function of the froth height was first examined using both 10- and 2-μm air inlet filters, and the results are shown in **Figure 10**.

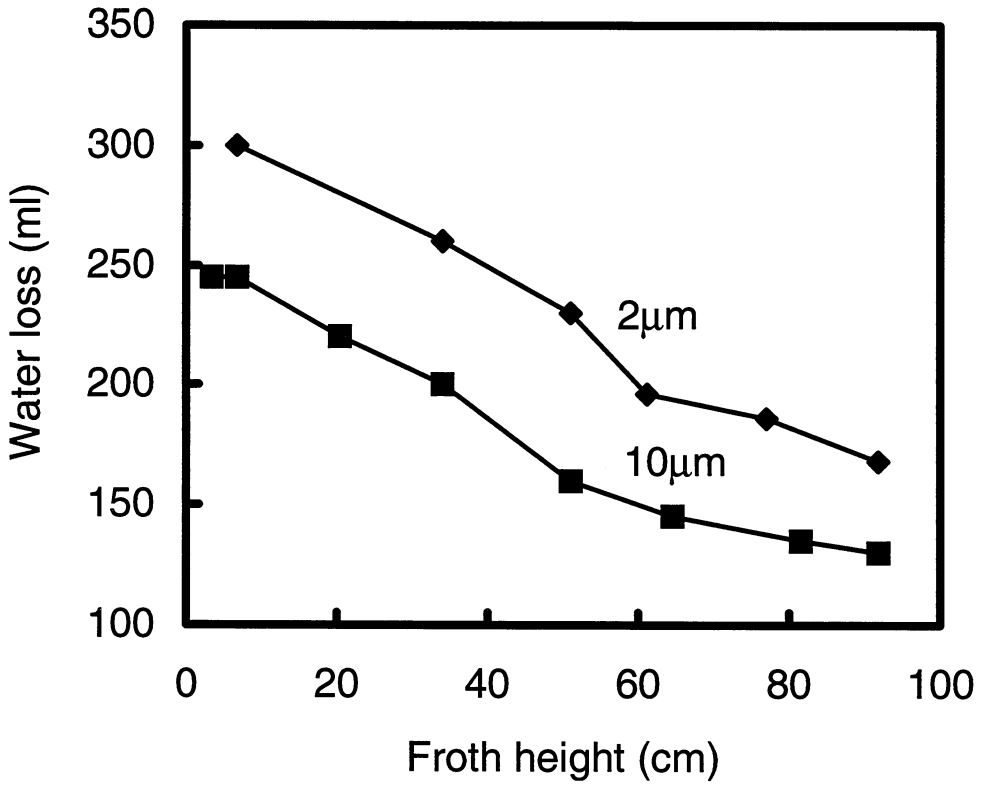

Figure 10. The influence of the pore size of the air filter inlet on the water loss. TX-100: 100 mg/L; flow rate 1800 cm^3/min; flow time: 2 min.; no fibers.

It can be seen that the water loss decreases as the froth height increases. This happens because when the froth raises up in the flotation cell, part of the entrapped water in the froth network drains back to the pulp. The drainage rate of entrapped water depends on many factors, such as the froth structure, bubble size, air flow rate, surfactant concentration, flue mechanical properties of liquid between bubbles, etc. However, if other parameters remain constant, the water loss should be dependent on the air bubble

size. **Figure 10** clearly shows that the air inlet filter with a 2-μm pore size gives much higher water loss than the 10-μm filter. This is in consistent with the geometric consideration because the froth with smaller bubbles has a higher dead volume than the larger one. The higher water loss caused by smaller bubbles should also affect the fiber loss and ink removal because more fibers and ink particles may be entrained in the froth network. The effects of air bubble size and fiber size on the fiber entrainment will be discussed later.

Figure 11 shows that, as other parameters remain constant, the water loss increases with an increase in surfactant concentration. This indicates that the entrainment of water in the froth has a close relationship with air bubble size and foam stability. As the concentration of air bubble increases, the surface tension of the solution decreases, resulting in a decrease in bubble size, an increase in froth stability, and a decrease in the water drainage rate of the froth. However, it is surprising that the water loss continually increases with a surfactant concentration up to ~400 mg/L, which is far above the critical micellization concentration (CMC, 195 mg/L). It has been well-known that both the free surfactant concentration and the surface tension of the solution are constant above the CMC, and there should not be any change in bubble size and froth structure at the surfactant concentration above the CMC. However, both water loss measurement and photographs of air bubbles indicate that air bubble size continually decreases as the surfactant concentration increases at a concentration well above the CMC. Combining the water loss measurement with the flotation deinking results obtained in this study (see below) and published results **[31],** we believe that the dynamic and reological properties of surfactant in the solution and on the air bubble surface are important factors affecting

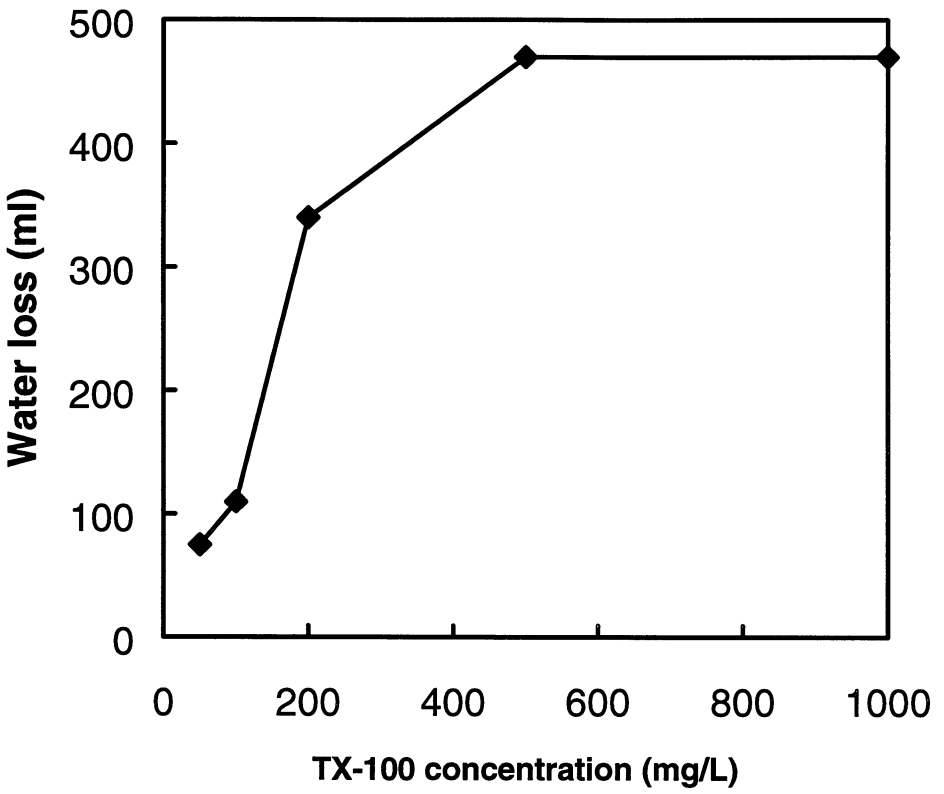

Figure 11. Water loss as a function of TX-100 concentration for 10-μm air inlet filter. Flow rate: 1800 cm^3/minute; Time: 2 minutes.

the air bubble size, stability, and solid removal. The dynamics and rheological properties of surfactant in solution are our interested research areas, and these will be studied in the future.

The calcium ions in the recycled pulp and processing water may significantly affect the flotation deinking efficiency. For example, the water hardness plays a key role in ink removal, froth stability, and fiber loss when a fatty acid is used as a collector **[3,4,10]**. However, the mechanism of how the calcium ion affects ink removal and fiber loss is not clear. In addition, how the calcium ions affect the performance of cationic and nonionic

surfactant in deinking has not been well-studied in the literature. To understand the influence of calcium ions on the whole process of deinking, froth stability as a function of calcium concentration was investigated, and the results are shown in **Figures 12** to **15.**

Some general conclusions can be drawn from **Figures 12** to **15**.

(1) The calcium concentration will increase foam stability when a nonionic or a cationic surfactant is used. It was found from surface tension measurements that the calcium concentration does not significantly affect the surface tension of the solutions of cationic and nonionic surfactant in water. Furthermore, there is no chemical reaction between calcium ion and cationic or nonionic surfactant; the increase in froth stability may be attributed to the stronger electronic repulsion force between air bubbles as calcium ions adsorb onto the air-liquid surface.

(2) The froth formed by the solution of SDS in deionized water is unstable, and it totally broke in 1.5 minute. When a calcium chloride was added into the solution, the froth broke even faster. The decrease in froth stability of SDS solution by calcium ions may be due to the complex formation between these two appositely charged materials, resulting in a decrease in the surface activity of SDS.

(3) The froth generated by oleic acid sodium salt in deionized water was very stable. However, the calcium ions will significantly reduce froth stability. It was found that even though 25 ppm calcium ions would totally destroy the froth (froth decay time was less than 10 seconds in a 25 ppm calcium ion solution), when top water was used instead of deionized water, the froth generated by 100 mg/L oleic acid sodium salt could not stay more than 15 seconds. When calcium ions were added into the oleic acid sodium solution or dissolved oleic

acid salt into top water, insoluble sodium-calcium complex particles can be clearly seen, and the particle size and concentration increased when calcium ion concentration increased. It is clear that the complex of oleic acid will reduce froth stability rather than increase it. However, many researchers indicated that deinking efficiency using fatty acid will be significantly improved by the addition of calcium ions into pulps [10]. Although the increase in deinking efficiency of fatty acid in the presence of calcium ions is attributed to the modification of ink particles by the deposition of complex of fatty acid-calcium ions, resulting in an increase in the hydrophobicity of the ink particle surface (usually called collector), it is not clear how the calcium ions will contribute to froth stability because sodium fatty acid salt cannot generate foam in the present of calcium ions. One of suggested mechanisms to explain why fatty acid salt and calcium ions can give a reasonable foam in a real deinking system may be the adsorption of calcium-fatty acid particles on the air bubble surface, which will act as a particle stabilizer. Obviously, this is not true based on our results because the adsorption of fatty acid-calcium ion complex on the air bubble surface in the absence of pulp did not contribute to froth stability. However, why a relatively stable froth can be obtained in real recycle pulps when a fatty acid and calcium ion are used is interesting, and this will be studied in our future research.

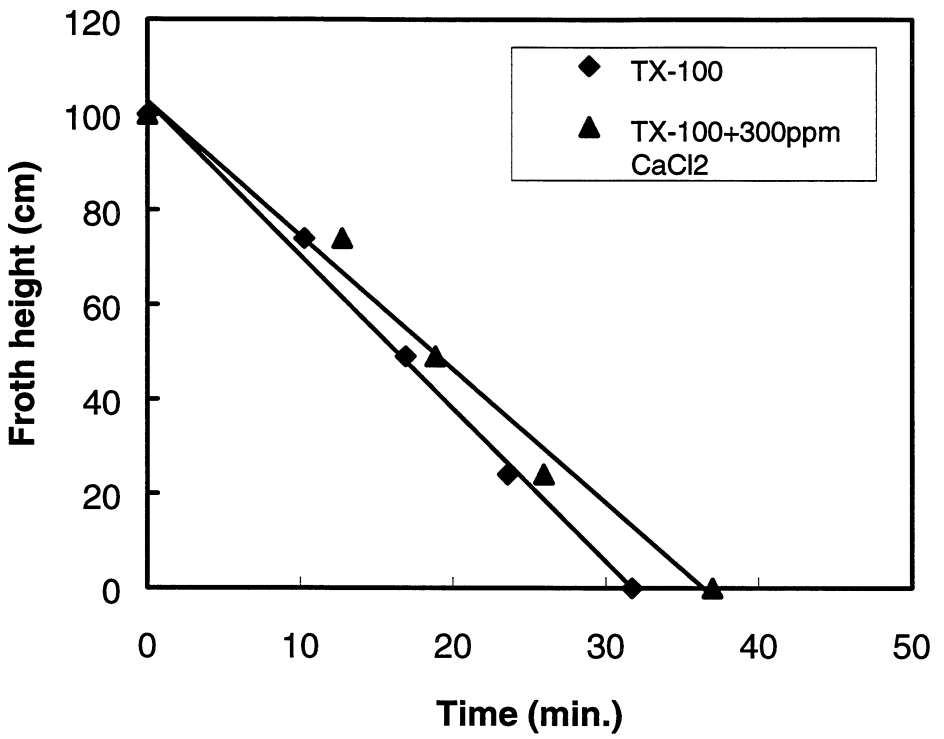

Figure 12. Effect of calcium ions on the froth decay rate. Surfactant: 100 mg/L TX-100.

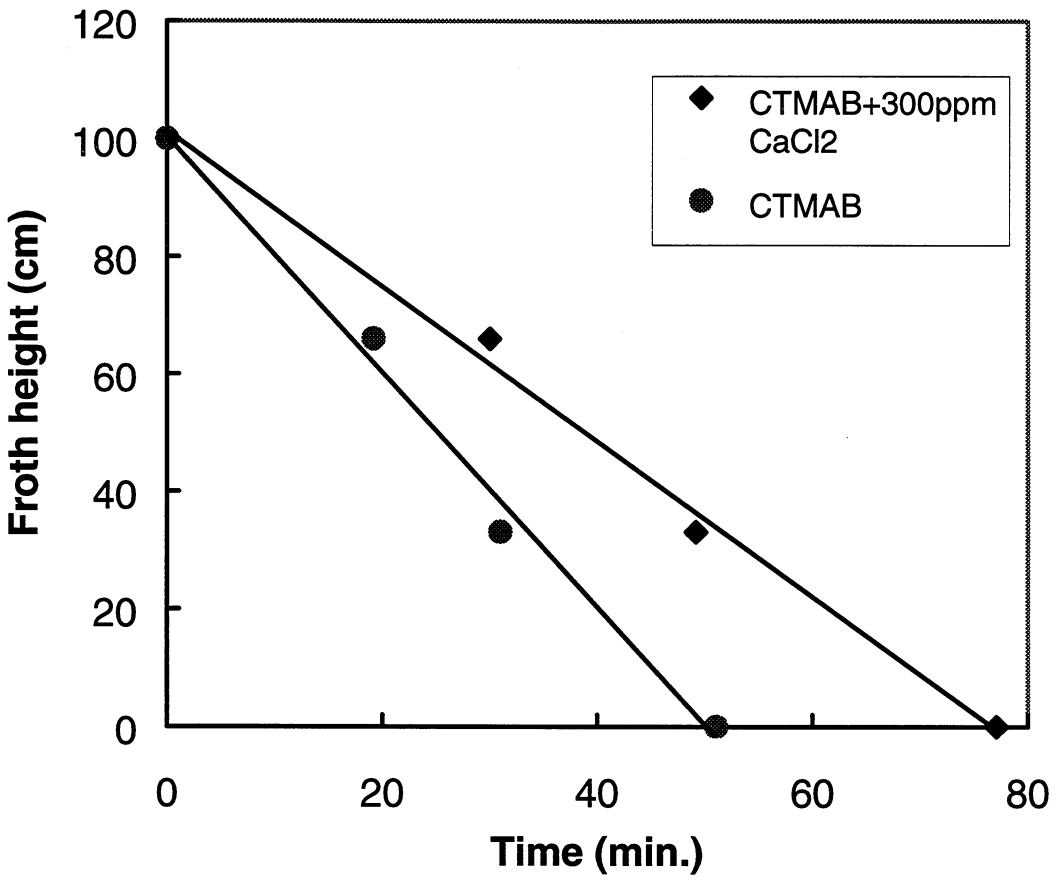

Figure 13. Effect of calcium ions on the froth decay rate. Surfactant: 100 mg/L CTMAB (cetyltrimethylammonium bromide).

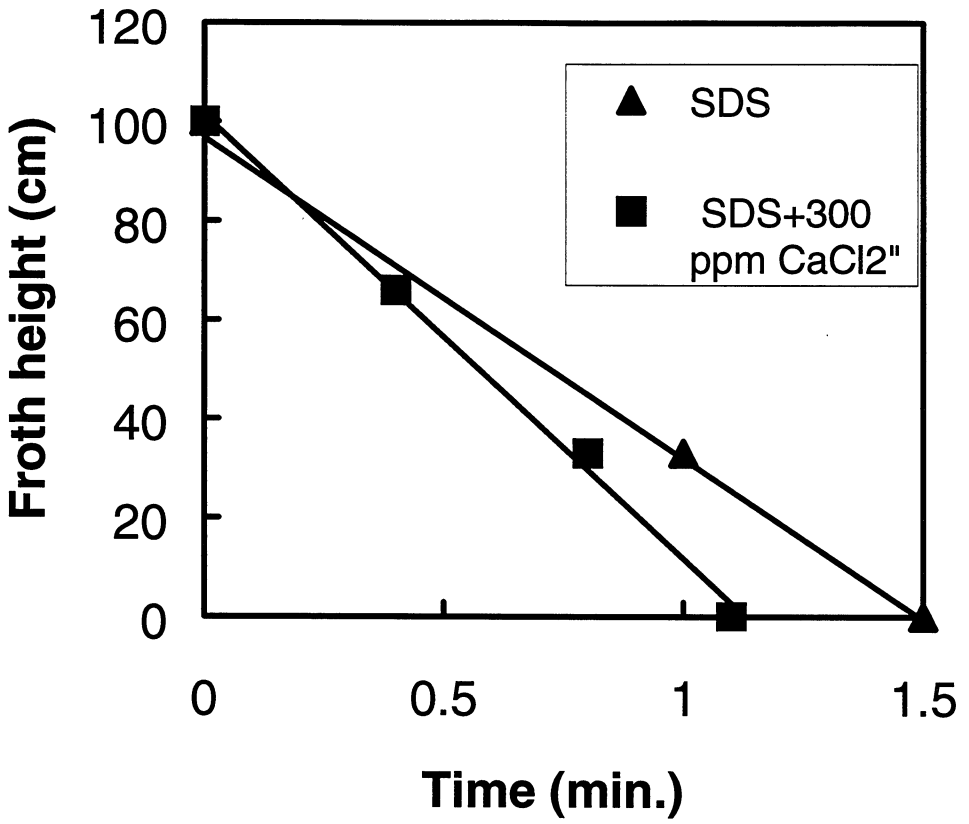

Figure 14. Effect of calcium ions on the froth decay rate. Surfactant: 100 mg/L sodium dodecylsulphate (SDS).

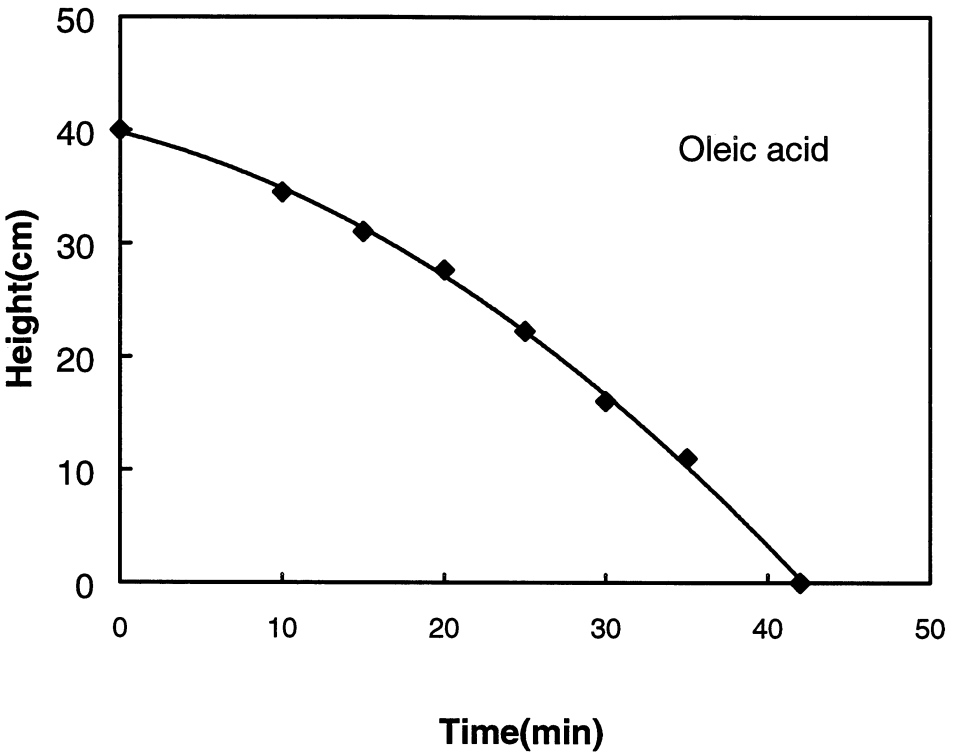

Figure 15. Effect of calcium ions on the froth decay rate. Surfactant: 100 mg/L oleic acid sodium salt in deionized water. The foam of 100 mg/L oleic acid sodium salt in top water and in $CaCl_2$ solution is unstable.

Figure 16 shows the effect of solid suspensions, such as ink and fibers, on froth stability. It can be seen that, when TX-100 was used as frother, froth stability is higher in the presence of toner particles or fibers than that without solid suspension. This indicates that toner particles and fibers (more likely fines) perform as a solid former agent in the flotation deinking process rather than a deformer. However, it should be noted that the stability of the froth may strongly depend on the solid particle size, the shape, the surface chemistry, and the concentration. Any change in the above parameters may change froth stability, even give a reverse result. The toner particles used in this study are made from

fussed toner film, and they have a three-dimensional structure with a relatively narrow distribution. However, the toner particles from copying papers have a plate structure, which may give a different effect on froth stability.

It is interesting that the froth of a cationic surfactant solution in the presence of fibers (unsized bleached soft wood pulp) is very stable compared to that without fiber suspension. For example, in a solution containing 100 mg/L CTMAB and 0.5% bleached soft wood fibers, there was no significant decrease in froth height in more than an hour, even though most of the entrained water had drained back to the pulp phase leaving a stable froth with very thin water film between the bubbles.

It can be seen from the above discussion that froth stability is very complicated, which depends on many factors, such as the type of surfactant, the presence of calcium ions, solid suspension, etc. Obviously, ink removal efficiency will strongly depend on froth stability. However, most of the researchers reported in the literature is focused on the interaction of ink particles with air bubbles in the pulp suspension, and there is little research on the relationship between ink removal efficiency and froth stability. We believe that ink removal will not only be controlled by interactions among the materials in recycling pulp, but will also be controlled by all of the physico-chemical phenomenan in the froth. Therefore, the froth structure is an important area of flotation deinking.

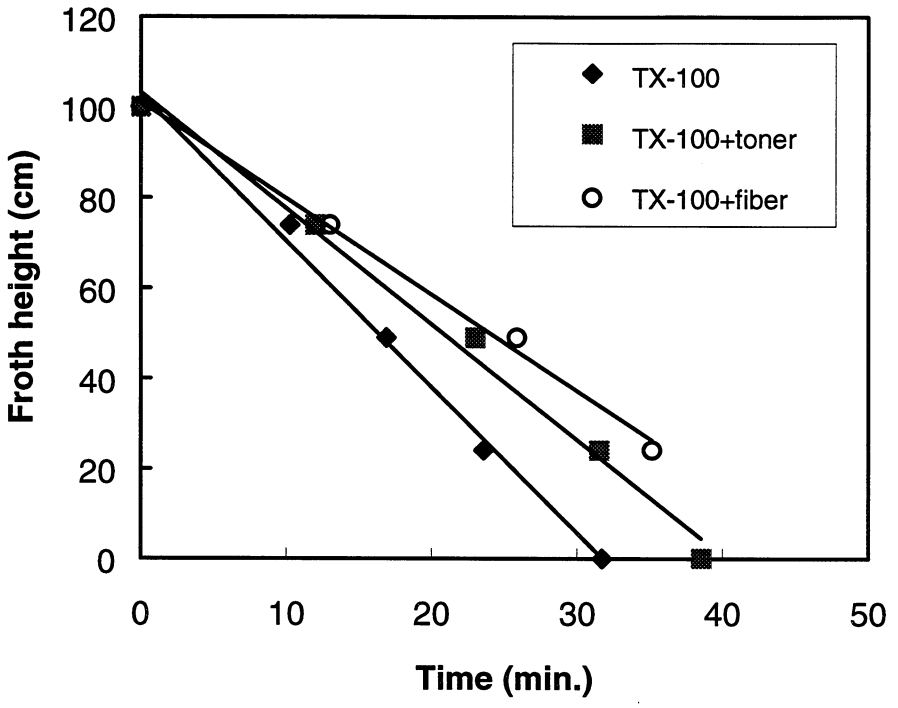

Figure 16. Effect of toner and fibers on the froth decay rate. Surfactant: 100 mg/L TX-100.

In the flotation process, some water and solid suspension will be removed out from the pulp by entrapping them in the froth network. Obviously, solid removal by this entrainment is a function of water loss. The water loss obtained using different systems is shown in **Figure 17**. The results are very complicated. For example, **Figure 17** shows that toner particles give a higher water loss than that without toner particles, which is consistent with the froth stability measurement shown in **Figure 16,** i.e., the more stable the froth, the higher the water entrainment in the froth network. However, in **Figure 16** the presence of any type of the fiber reduced water loss (foam should be less stable) than that without fiber, but an enhancement of the froth stability by 0.5% fibers was observed. Although the results of **Figure 17** are complicated, they clearly show that the effect of

solid suspension on water loss is not significant, and for all of the systems, the water loss is decreased as the froth height is increased.

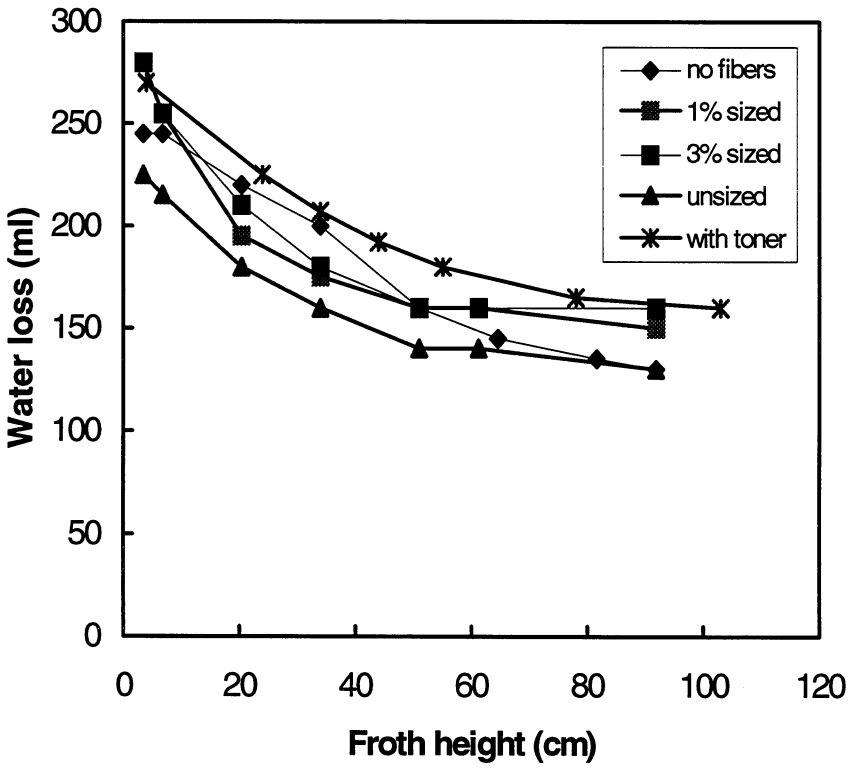

Figure 17. Water loss as a function of froth height in both the presence and absence of fibers. Air inlet pore size: 10-μm; Fiber concentration: 0.52%; TX-100: 100 mg/L; Air flow rate: 1500 cm^3/min.; Time: 2 minutes.

True flotation and entrainment

The flotation of solid materials can be divided into "true flotation" and "entrainment." True flotation occurs when solids attach to air bubbles and are floated

with them. A basic requirement for true flotation is that the solid particles must be hydrophobic enough so that they can strongly adhere onto the bubble surface. However, entrainment occurs when particles enter the froth with the water and occupy the spaces between the bubbles. When froth raises up, part of the water and particles entrapped in the froth will drain back into the pulp, but the remainder is carried upwards and scraped off.

Entrainment is a problem in flotation deinking because it is nonselective. Generally speaking, the clean fibers, such as uncontaminated bleached kraft pulp, have a very hydrophilic surface. On the other hand, the ink particles are hydrophobic or can be modified to hydrophobic. If true flotation is the only manner removing the solid materials from pulp in the flotation deinking process, and the ink particles can be separated easily from fibers by adhering to the air bubble surface. However, many experimental and industrial results indicate that part of the fibers, even though the fibers are very clean hydrophilic fibers, will be entrapped into the froth network and removed during flotation. This was also confirmed in this study by direct measurements of fiber loss and the contact angle of fibers in a pulp supernatant. **Figure 18** shows fiber loss as a function of water loss for bleached kraft pulp, which has a zero-receding contact angle and a 7° advancing contact angle in a 100 mg/L TX-100 pulp solution. If fiber removal is caused only by adhesion of the fibers onto the air bubbles, these very hydrophilic fibers should not float. However, **Figure 18** indicates that up to 13% (which may vary with froth height) of unsized fibers was removed in a 2-minute flotation process under our experimental conditions.

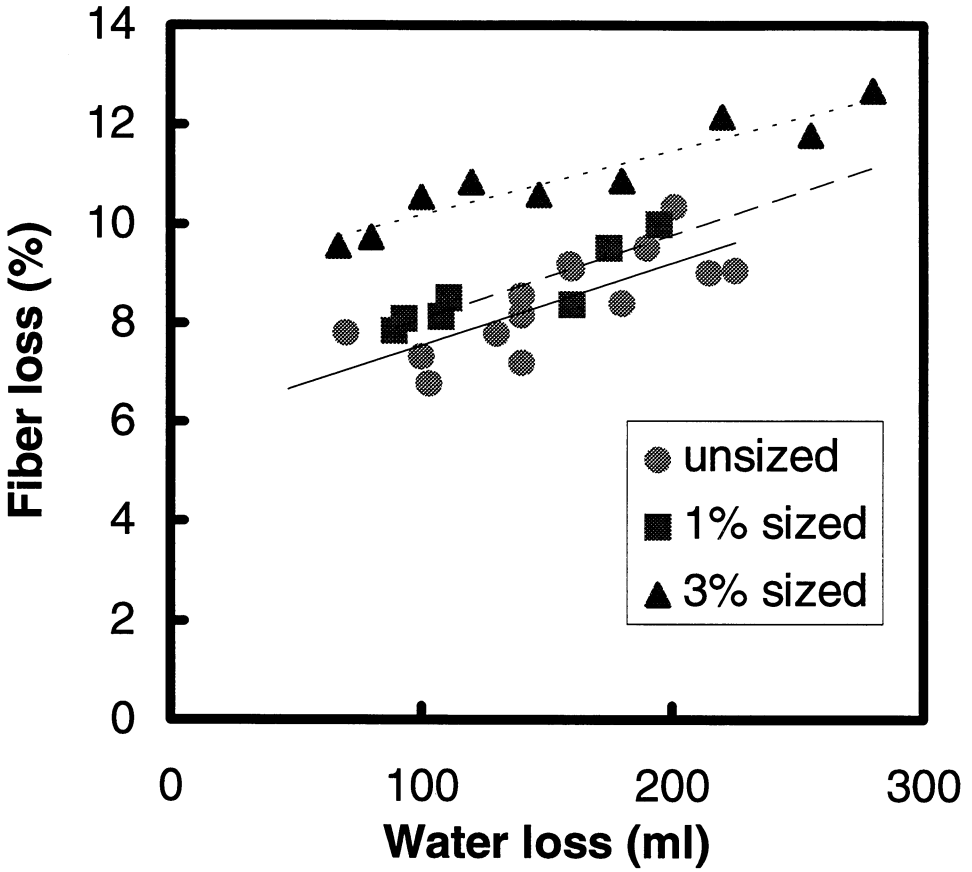

Figure 18. Fiber loss as a function of water loss for unsized and AKD sized BK fibers. Pore size of air inlet filter:10 μm; fiber consistency: 0.52%; concentration of TX-100: 100 mg/L; air flow rate: 1800 cm^3/minute; flotation time: 2 minutes.

As discussed above, fiber removal by physical entrainment should be a function of water removal, and at ideal conditions, a linear relationship between fiber removal and water removal is expected. This suggests that, if there was no water loss, the fiber loss by entrainment should be zero and all of the fiber losses should be attributed to true flotation. The contributions of true flotation and entrainment in mineral flotation have been discussed, and the following equation has been used **[25]**:

$$R = f + g\mathrm{W}_{\mathrm{water}} \qquad (8)$$

where R is the total recovery of the given solid suspension at experimental conditions; f is the recovery of the solid by true flotation; g is the entrainment factor; and $\mathrm{W}_{\mathrm{water}}$ is the weight of removed water. At ideal conditions, the fractions of true flotation and entrainment can be obtained from the intercept and the slope of suspension removal, against water removal respectively.

It can be seen from **Figure 18** that fiber loss, regardless of sized or unsized fibers, has a liner relationship with water loss. This is consistent with the expectation of **Equation (8)**. According to **Equation (8)**, the intercept of the curve shown in **Figure 18** should correspond to the fiber adhesion on the bubble surface, and the slope should correspond to the entrainment of fibers in the froth network. It should be noted that the amount of true flotation is not only a function of fiber hydrophobicity, but also a function of air bubble size, air flow rate, total flotation time, surface tension, fiber size, surfactant type, surfactant concentration, surface tension, etc. As other parameters remain constant, true flotation should depend only on the hydrophobicity of the fiber surface. Furthermore, if all of the floated fibers are caused by physical entrainment, the intercept of fiber loss against water loss should be zero. In contrast, if all of the removed fibers are adhered fibers, the slope of the curve should be zero. The results in **Figure 18** clearly show that both the slope and the intercept are not zero for all of the fibers, which strongly suggests that both the entrainment and adhesion will contribute more or less to total fiber loss.

Equation (8), which was used for the mineral flotation system, may not work well for fiber loss in flotation deinking. This is because to use this equation, it has to be assumed that all entrapped (rather than adhered) particles can be washed away if all the entrapped water flows back to the pulp phase. This may be almost true if entrapped

particles are small, such as mineral or ink particles, but is not the case when the particle size is large. The drainage of solid suspension and water from a froth is very similar to a filtration process in that small particles can pass through the screen holes but large particles will be retained on the screen. Because fibers have a much larger size than mineral and ink particles, some fibers cannot pass through the microchannels during the water drainage, which results in an unrecoverable fiber entrainment. The water drainage and fiber retention in a raising up froth network are schematically shown in **Figure 19**. It can be seen that there are three different fibers that may be removed in flotation processing: adhered fiber A that floats through the true flotation mechanism, unrecoverable fiber B that cannot wash away from the froth because of either its orientation or large size, and recoverable fiber C that can easily flow back to the pulp phase during water drainage. In terms of the above discussion, **Equation 8** should be further modified if it is used to describe the fiber loss in the flotation:

$$R = A + B + Cw_{water} \qquad (9)$$

where A and B are the fiber loss caused by true flotation and unrecoverable entrainment, respectively; C is recoverable fibers removed during the drainage of entrapped water; and w_{water} is the water loss at fixed flotation conditions. **Equation (9)** indicates that the sum of the true flotation and unrecoverable fiber $(A + B)$ equals the slope of total fiber loss R against total water removal, and it is independent of total water removal at a fixed flotation time.

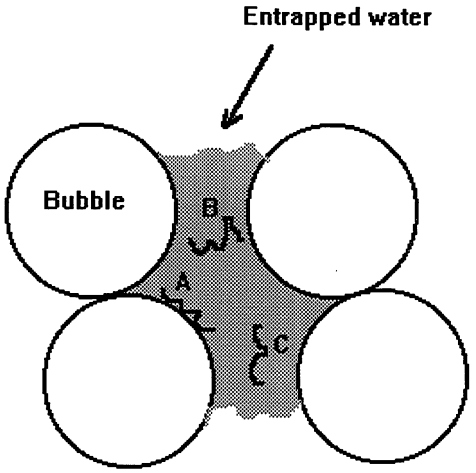

Figure 19 A

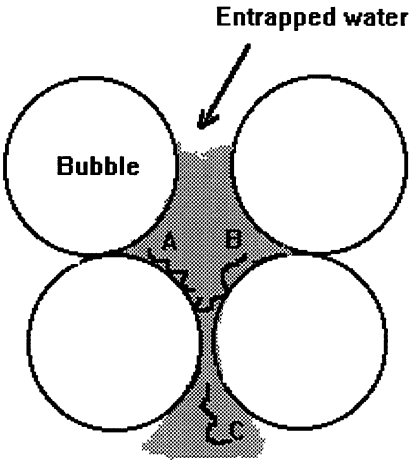

Figure 19 B

Figure 19. Three different fibers in the flotation froth. A: adhesion fiber; B: unrecoverable fiber that cannot be washed back to the pulp even if all of the entrapped water has drained; C: recoverable fiber that can be washed back to the pulp during the drainage of entrapped water.

It is clear that true flotation is closely related to fiber surface hydrophobicity, and a fully hydrophobic fiber should not adhere to the air bubble surface. The contact angle measurement (see **Figure 8**) indicated that the receding and advancing contact angles of unsized bleached fibers in a 100 ppm TX-100 solution are zero and < 7°, respectively. This suggests that unsized bleached softwood fibers are very hydrophilic in this solution and they cannot adhere to air bubbles by hydrophobic force in the flotation process. In other words, the loss of these highly hydrophilic fibers in the flotation cell is caused solely by the physical entrainment, and the true flotation A in **Equation (9)** is zero. Therefore, fiber loss for unsized bleached softwood fibers can be described by

$$R = B + C w_{water} \qquad (10)$$

By plotting total fiber loss of unsized fiber against water removal, the factors of B (0.29 g) and C (7.5×10^{-4} g/ml) were obtained, respectively.

Because both the sized and unsized fibers used in the flotation study have the same fiber length, it is reasonable to assume that the entrainment factors B and C for all three fibers are a constant at the same water remove level. In other words, the difference in fiber loss between unsized and sized fibers is attributed only to the true flotation A. This assumption is confirmed by the results shown in **Figure 18**, in which three different fibers have a very closed slope C.

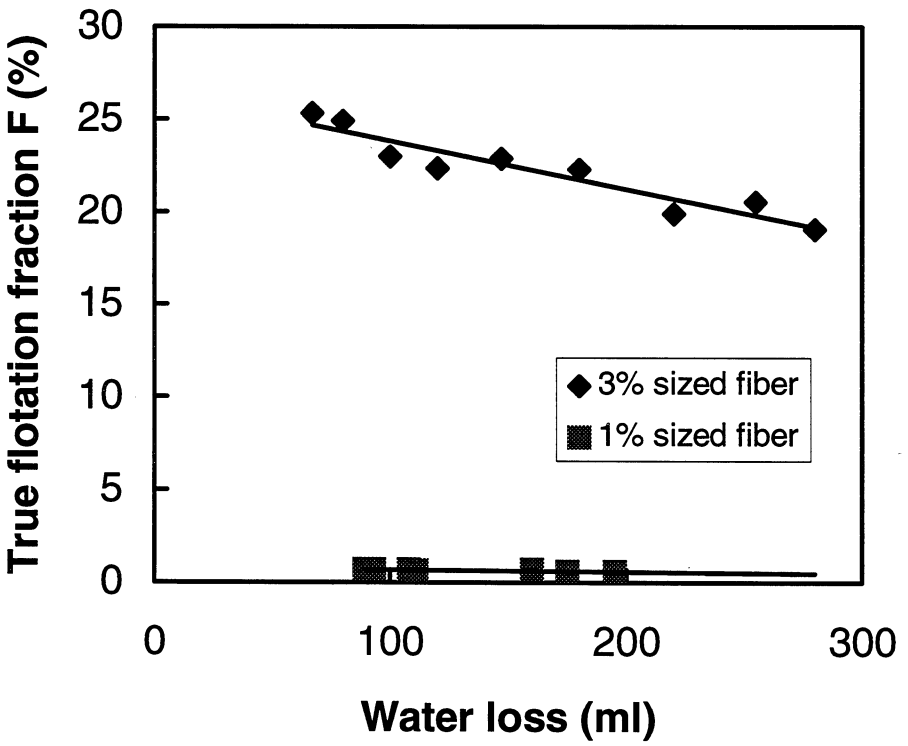

Figure 20. True flotation factor F as a function of water loss. The true flotation factor for unsized bleached softwood fiber is assumed as zero. Pore size of air inlet filter:10 μm; fiber consistency: 0.52%; concentration of TX-100: 100 mg/L; air flow rate: 1800 cm^3/minute; flotation time: 2 minutes.

In terms of the above assumption, by applying $B = 0.29$ g and $C = 8.3 \times 10^{-4}$ g/ml to **Equation (9)**, the true flotation A for 1 and 3% AKD sized fibers is 0.025 and 0.15 g, respectively. It can been seen that true flotation factor A is much smaller than entrainment factor B even for highly sized fibers. Because total fiber loss is a function of total water removal and froth height, the true flotation factor at the flotation time t

$$F = A/R \tag{11}$$

is plotted against water loss and froth height in **Figures 20** and **21**.

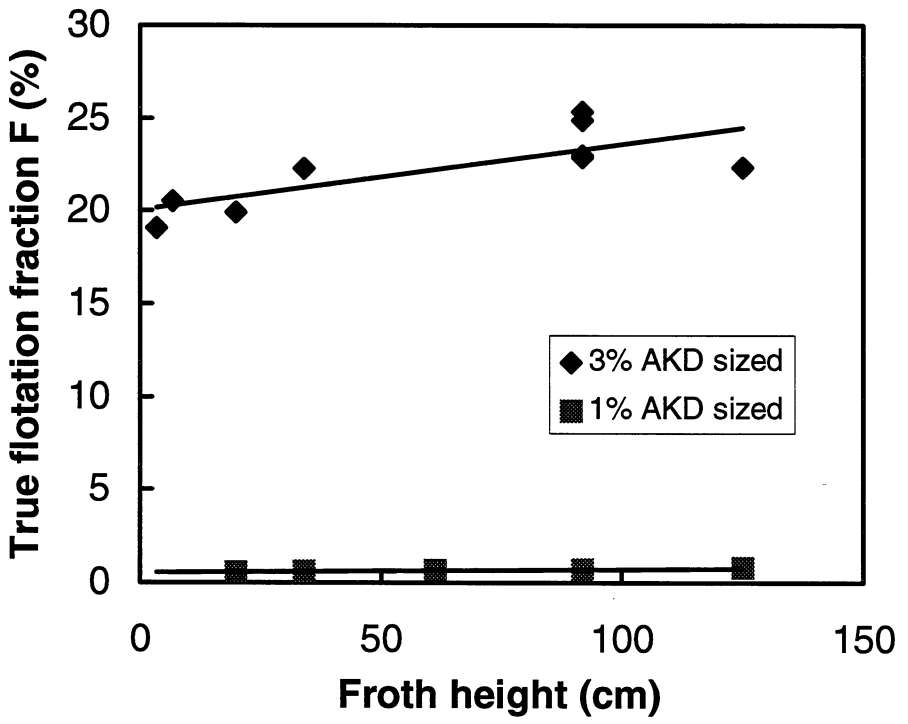

Figure 21. True flotation fraction as a function of froth height. The true flotation fraction of unsized fibers is assumed as zero. Pore size of air inlet filter:10 μm; fiber consistency: 0.52%; concentration of TX-100: 100 mg/L; air flow rate: 1800 cm^3/minute; flotation time: 2 minutes.

It can be seen from **Figure 20** that the true flotation fraction *F* for 1% AKD sized fiber is only about 0.8% of total lost fiber at all froth heights measured in this study, which suggests that almost all of the fibers removed from this pulp at our experimental conditions are attributed to physical entrainment. Even for 3% AKD sized fibers, the true flotation fraction *F* is still less than 25% of total fiber loss. The results shown in **Figure 20** clearly indicate that physical entrainment is the main cause of fiber loss in flotation deinking. This is consistent with Ajersch and Pelton's results **[18]**. Although the role of fiber hydrophobicity in fiber loss has been argued for many years, no direct experimental observation has been obtained in previous research. Our results clearly show that both the hydrophobicity of fibers and physical entrainment will contribute to total fiber loss, but entrainment is much more important than true flotation for all types of fibers.

Some people believe that ink contaminated fibers may result in a higher fiber loss in flotation deinking. Although this has not been directly measured in this study, our results obtained using AKD sized and unsized fibers suggest that the hydrophobic contamination is not a dominant factor for fiber floating. The most effective method to reduce fiber loss in flotation deinking should rely on the reduction of entrapped fibers rather than the modification of fiber surface chemistry to reduce hydrophobicity.

Figure 21 shows that the true flotation factor *F* increases as the froth height is increased. This is because total fiber loss is decreased, but true flotation remains a constant when froth height is increased. For highly sized fibers, the true flotation factor *F* decreases from 25 to 19% when water loss increases from ~ 80 to 280 ml (or the froth height decreases from 5 to 125 cm).

The effect of froth height on total fiber loss can be further seen in **Figure 22**. On average, the total fiber loss is reduced by ~2% if the froth height is increased to 125 cm, regardless of the type of fiber. This is because the increase in froth height will increase

the time for water drainage so that more fibers will be washed away from the froth. Comparing the results shown in **Figures 18** and **22**, two important conclusions can be obtained: a) both fiber loss and water loss in flotation deinking can be reduced by increasing froth height, and b) some entrapped fibers can be washed away from the froth.

Although water loss in flotation deinking has not been thought of as a problem in the paper mill, the energy saved by reducing water loss can also benefit the paper industry. Even for a fully closed flotation deinking mill, water loss by removing the froth from the top of the flotation cell can still be as high as 10% of the total water circulated in the flotation cell, which corresponds to a water loss of ~10 tones/(tone pulp). Because the discharged water contains many deinking chemicals, such as surfactant and basic materials, reducing water removal will protect our environment. The result of this study indicates that properly controlling the froth height is a cost-effective method to reduce both water consumption and fiber loss. However, how froth height will affect ink removal is not clear, and this will be further studied in our laboratory. It has been noted that the increase in drainage time will reduce only entrapped solids but not significantly affect the removal of adhered hydrophilic materials. As a result, fiber loss can be reduced, but ink removal efficiency may not be significantly affected because ink removal is based on the true flotation rather than entrainment.

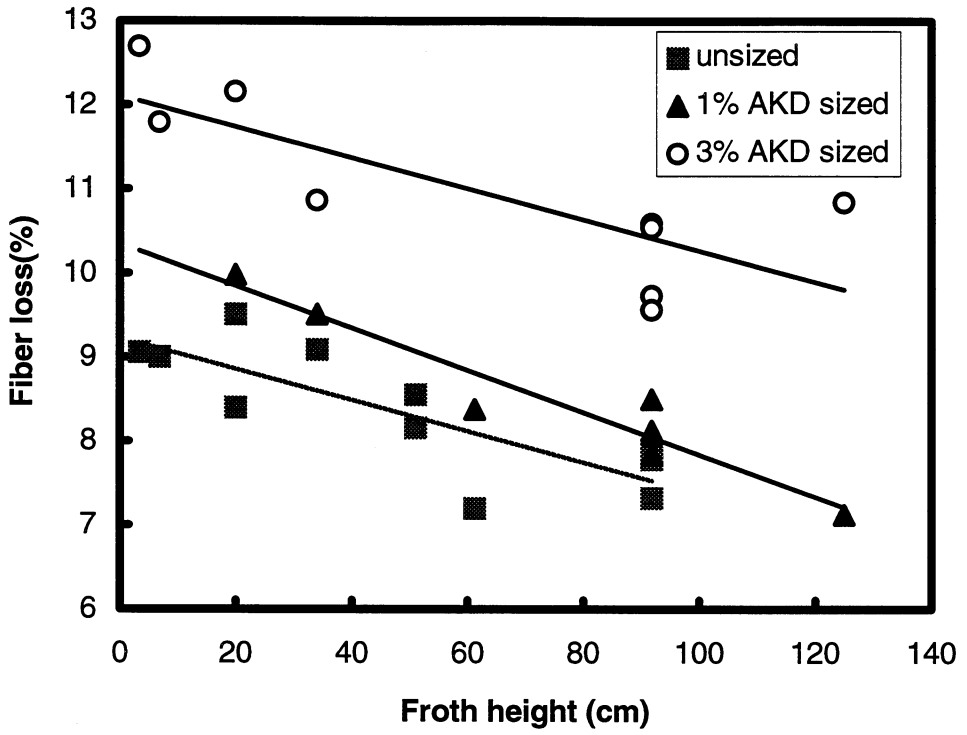

Figure 22. Fiber loss as a function of froth height for unsized and AKD sized BK fibers. Pore size of air inlet filter:10 μm; Fiber consistency: 0.52%; concentration of TX-100: 100 mg/L; air flow rate: 1800 cm^3/minute; flotation time: 2 minutes.

Figure 23 shows the effect of flotation time on total fiber loss and water loss. It can be seen that the intercept of fiber loss against water loss increases with flotation time, but the slope remains almost a constant. The increase in the intercept as the flotation time is increased suggests that both the true flotation and the removal of recoverable fibers are increased in parallel. This is reasonable because the more air bubbles injected into the pulp, the higher the probability of fiber adhering onto the air bubbles. Although the intercept was different for the curves obtained at 7 minutes and 2 minutes, the same slope of fiber loss against water loss was obtained. This suggests that the slope (i.e., the rate of

removing recoverable fiber C) depends lineally on the rate of water removal. According to **Equation (9)**, the slope C is not a function of total water loss W_{water} or flotation time t, but the intercept $(A + B)$ is a function of total water removal or the flotation time t. The fiber losses as a function of total water loss obtained at 2 minutes and 7 minutes shown in **Figure 18** support the above assumption. However, the ratio of the intercepts obtained at 7 minutes and 2 minutes is about 2:1, which is less than the theoretical predicted value of 7:2. Many reasons, such as the decrease in fiber consistency and the surfactant concentration with flotation time, may cause the difference between experimental data and theoretical prediction.

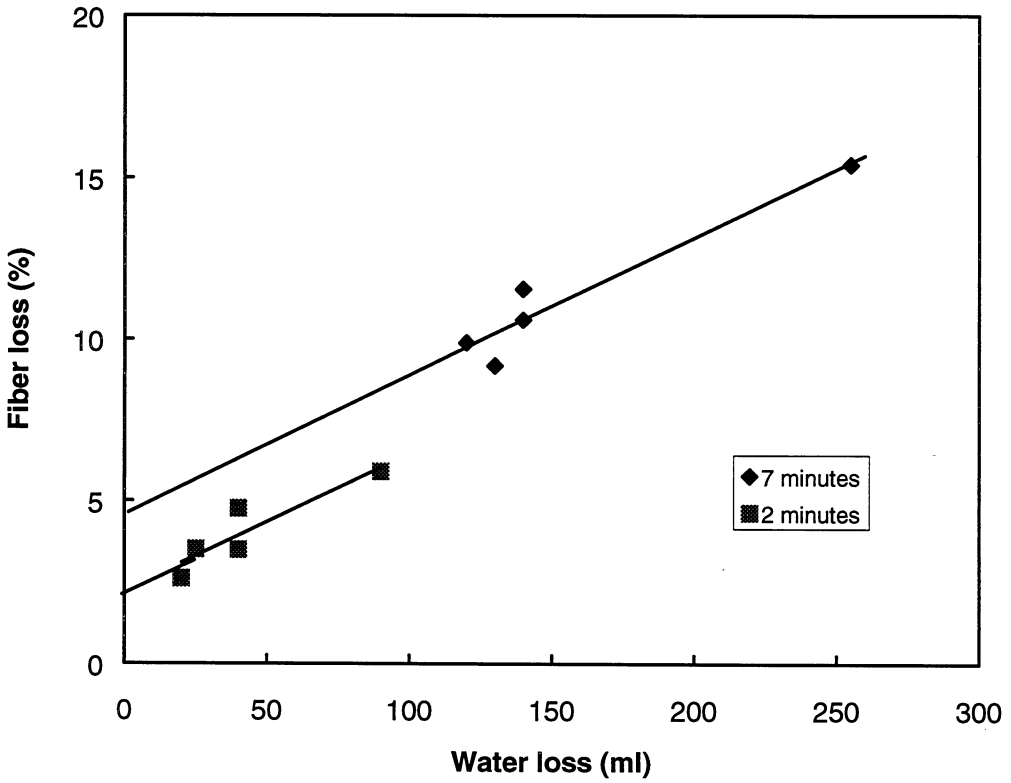

Figure 23. Fiber loss as a function of water loss obtained at 2 and 7 minutes. Fibers used are 0.45% unbleached softwood fibers (without sizing agent). Pore size of air inlet filter:10 μm; concentration of TX-100: 100 mg/L; air flow rate: 1500 cm^3/minute.

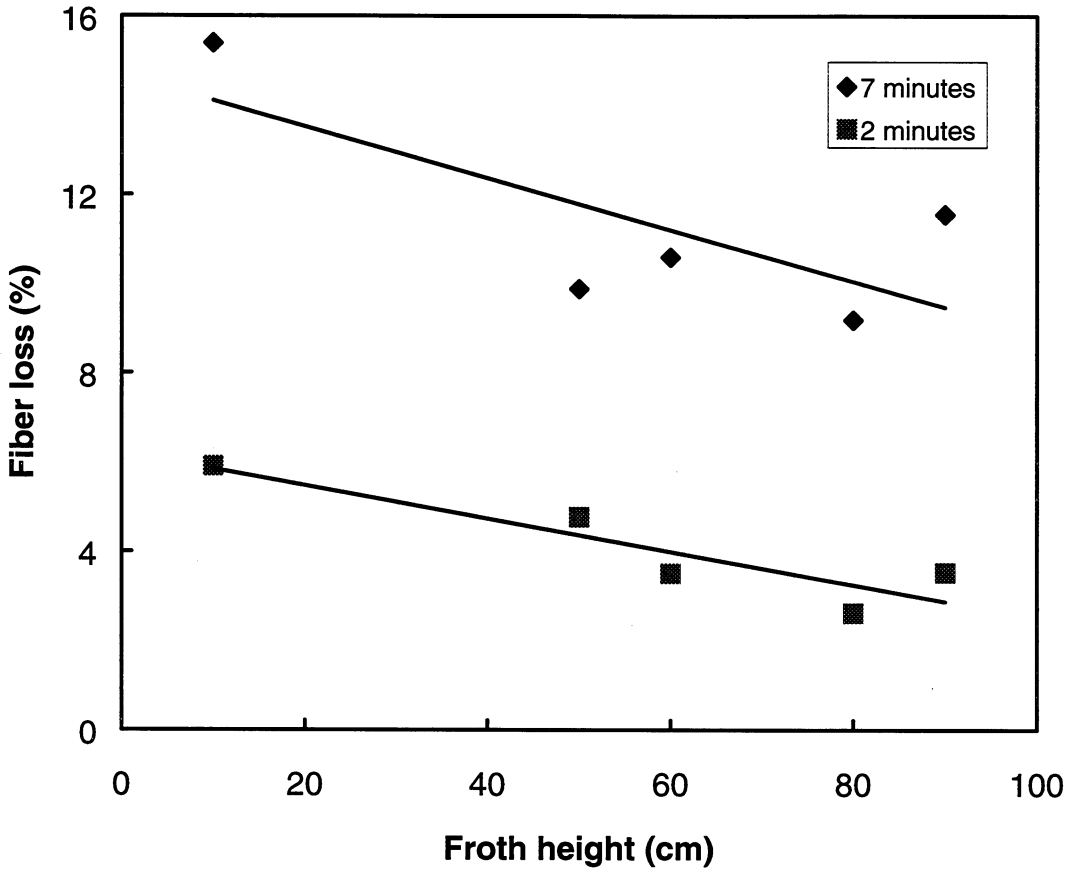

Figure 24. Fiber loss as a function of froth height obtained at 2 and 7 minutes. Fibers used are 0.45% unbleached softwood fibers (without sizing agent). Pore size of air inlet filter:10 μm; concentration of TX-100: 100 mg/L; air flow rate: 1500 cm^3/minute.

Figure 24 shows the fiber losses obtained after 2- and 7-minute flotation as a function of froth height. Once again, a decrease in fiber loss as froth height increases was obtained for both the flotation conducted at 2 and 7 minutes.

Figure 25 shows the consistency of fibers in the froth as a function of froth height. It can be seen that, in most cases, the consistency of fibers in the froth is lower than the original pulp, regardless of which fibers are hydrophilic (unsized) or hydrophobic (sized).

The total fiber consistency is decreased as the froth height is increased because some fibers were washed away from the froth.

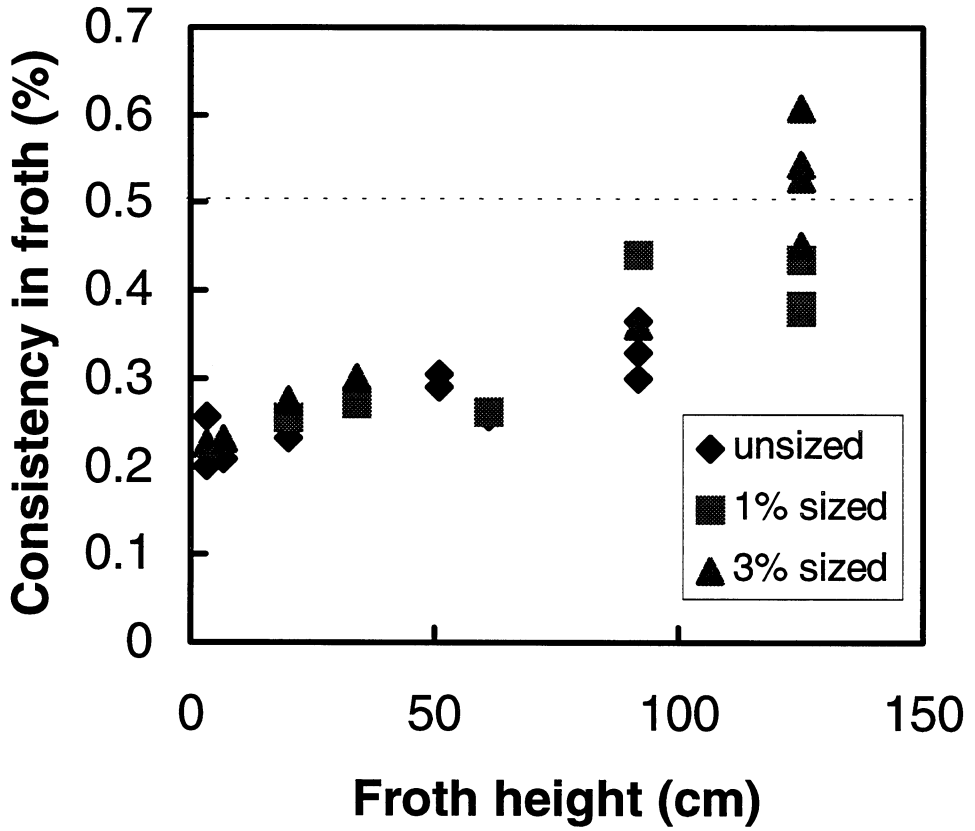

Figure 25: Fiber consistency in the froth as a function of froth height. Dashed line is the original pulp consistency in the flotation cell. Fibers: 0.52% unsized BKP; pore size of the air inlet filter:10 μm; TX-100: 100 mg/L; air flow rate: 1800 cm^3/minute; flotation time: 2 minutes.

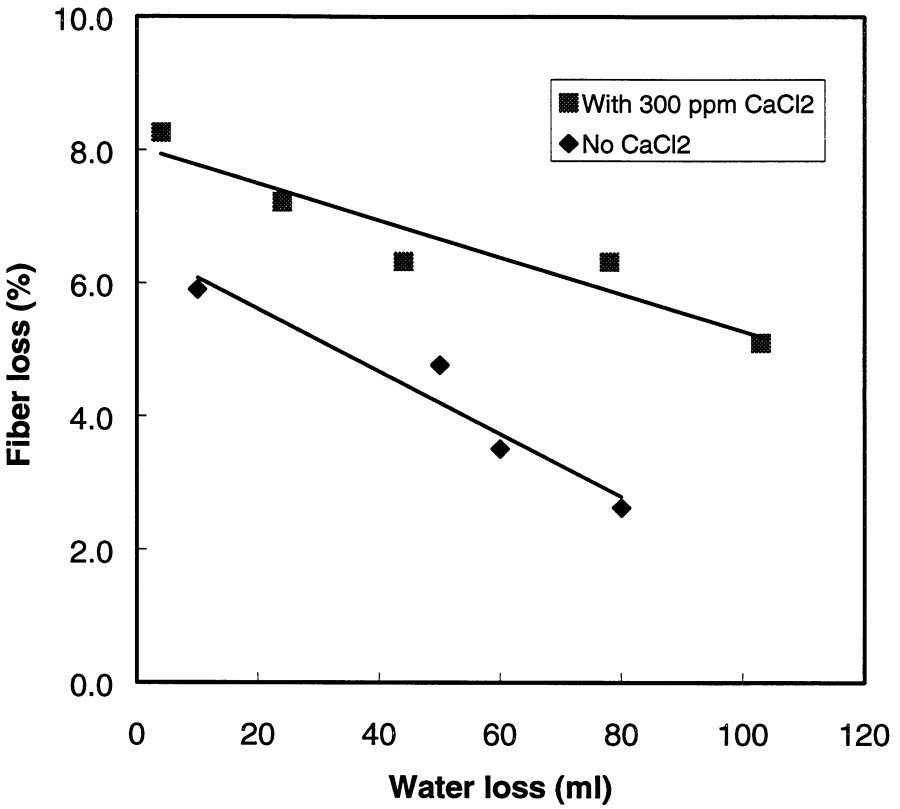

Figure 26. Effect of calcium chloride concentration on fiber loss at different froth heights. Pore size of the air inlet filter:10 μm; TX-100: 100 mg/L; air flow rate: 1800 cm^3/minute; flotation time: 2 minutes; fibers: 0.52% unsized bleached soft kraft.

Although many researchers indicated that calcium ions will affect both the ink removal and fiber loss, the results are inconsistent. **Figure 26** shows the effect of calcium ions on fiber loss when TX-100 was used as a surfactant. Although calcium ions have only a small effect on the froth stability of TX-100 (see **Figure 12**), the increase in fiber loss at the same froth height can be clearly seen from **Figure 26**. Furthermore, our experimental results also indicated that the calcium ions will increase water removal

when other parameters are the same. Once again, the cause of high fiber loss in the presence of calcium ions for the TX-100 system are not clear. How the calcium ions will affect fiber loss and ink removal when a fatty acid or a cationic surfactant is used will be one of our ongoing research projects.

Air bubble size effect

Generally speaking, both true flotation and physical entrainment are air bubble size-dependent. Many factors, such as surfactant concentration, gas flow rate, pore size of the air inlet filter, pulp concentration, soluble and colloidal materials in pulp, etc., may affect bubble size. Qualitative results showed that both fiber loss and ink removal are air bubble size-dependent. For example, the rate of toner particles removal is much lower using a 2-μm air inlet filter than using a 10-μm air inlet filter at the same flotation conditions. When a 2-μm filter was used, some of the very small air bubbles were adsorbed onto the fiber surface, which resulted in fibers floating to the top of the flotation cell after the flotation experiment. This phenomenon was significant only when sized fibers were used. When unsized furnish or a 10-μm filter was used, the fibers sank to the bottom aft the flotation experiment.

The primary results about the bubble size effect on the total fiber loss are given in **Figure 27**. As discussed before, the small bubbles gave higher water loss compared to the large bubbles in a pure surfactant system. The same result was obtained when fibers were added. For example, at a froth height of 7 cm, air flow rate 1500 ml/min, 100 mg/L TX-100, and 0.45% BK fibers, the water loss was 330 ml/minute if a 2 μm-air filter was used. However, the water loss was only 140 ml/minute when a 10 μm-air filter was used. The relationship between fiber loss and air bubble size has not been systematically studied, and this is an important objective of our ongoing studies.

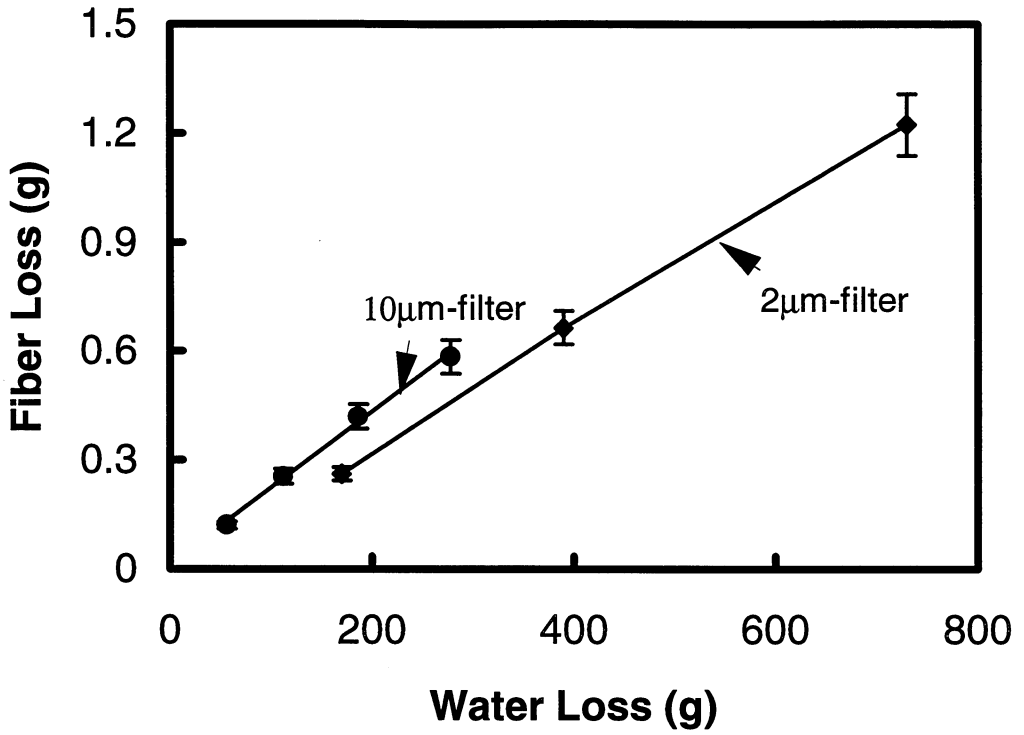

Figure 27. The total loss of unsized BK fibers as a function of water loss. The froth height: 7 cm; TX-100 concentration: 100 mg/L; flow rate: 1500 cm^3/minute. The water loss was obtained by changing the flotation time at a fixed froth height.

It should be noted that the water loss and fiber loss shown in **Figure 27** were measured by changing the flotation time at a fixed froth height, which has a different mean from the curves shown in **Figure 18**. It can be seen that the two curves in **Figure 27** have a closed slope, which means that the fiber entrapped in the same amount of water is a constant, although the froth structure may be significantly different when 10 and 2-μm filters are used. However, at a fixed flotation time, the total fiber loss caused by small bubbles was higher than that caused by large bubbles because smaller bubbles remove more water than larger ones.

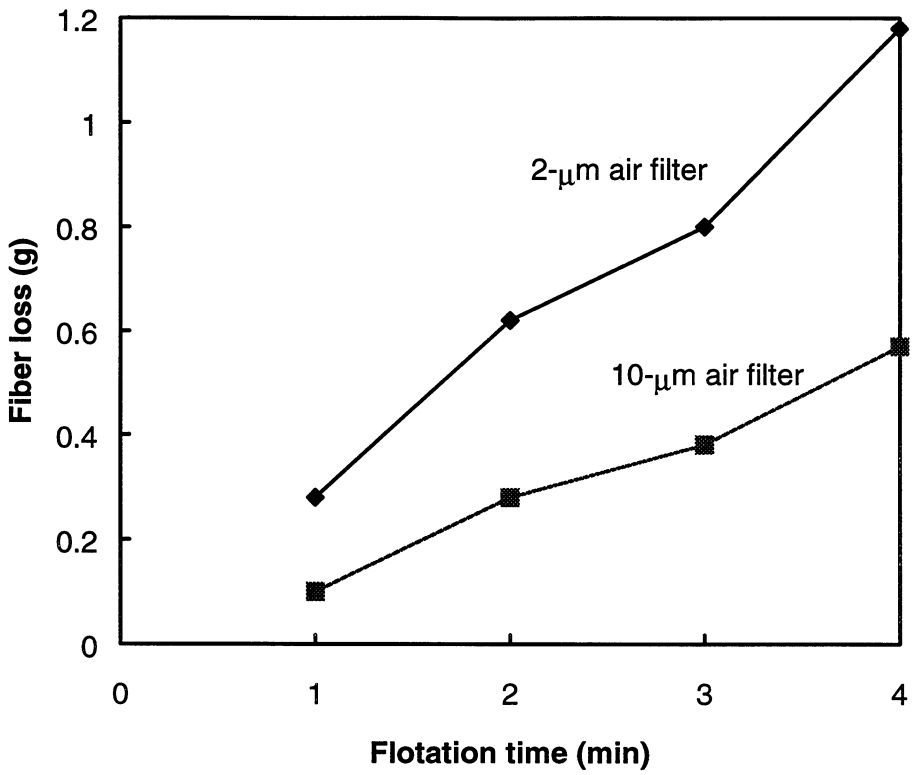

Figure 28. The total loss of unsized BK fibers as a function of flotation time at fixed flotation time. The froth height: 7 cm; TX-100 concentration: 100 mg/L; flow rate: 1500 cm^3/minute.

Figure 28 shows fiber loss as a function of flotation time. It can be clearly seen that, at the same flotation time, the fiber loss is much higher for a 2-μm air filter than a 10-μm filter. The major reason for higher fiber loss caused by small air bubbles is that the small bubbles will entrap more water than the large bubbles.

Toner deinking

The flotation efficiency of toner as a function of surfactant concentration was examined using the copied paper pulp. The toner removal efficiency was determined by measuring the brightness of the handsheets made from the residue fibers in the flotation

cell, and the results are showed in **Figure 29**. At low surfactant solution, the removal of toner particles initially increased then decreased as the surfactant concentration increased. The increase of ink removal efficiency at low concentrations may be attributed to the increase in froth stability and the decrease in air bubble size. The decrease in flotation efficiency above the CMC is a little surprising because all of the surface properties, such as the concentration of free surfactant in the solution, the contact angle of liquids against toner surface, and the surface tension of the solutions, are independent of the total surfactant concentration above the CMC. A similar phenomenon was found in the water loss measurement (see **Figure 11**). The reason for this may be the interaction kinetics between toner and air bubbles, which will be investigated further in our future work.

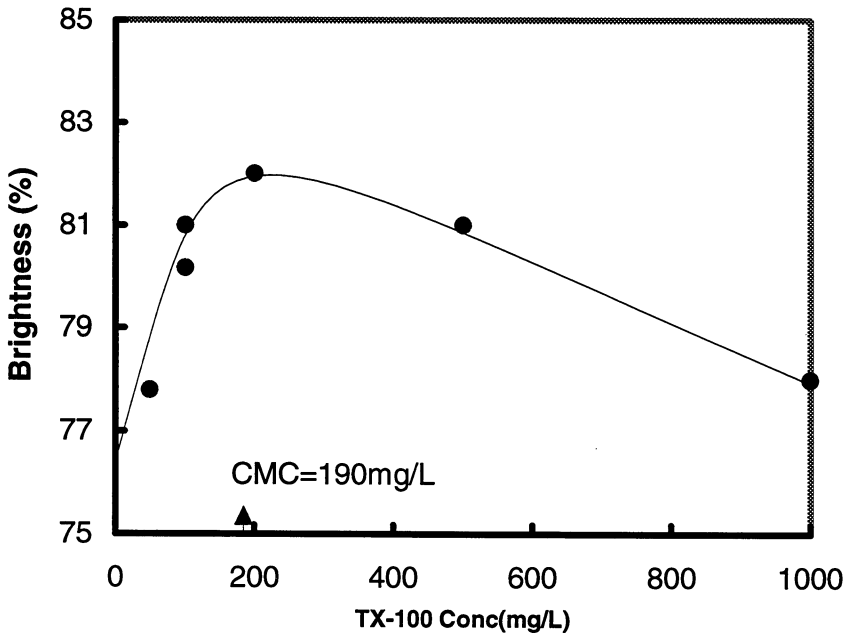

Figure 29. Brightness as a function of concentration of TX-100 after flotation deinking using bench flotation cell. Air flow rate: 3000 cm^3/L; time: 10 minutes.

CONCLUSIONS

1. The wetting force and contact angle of individual fibers in various solutions can be measured using a fiber group technique.

2. The receding contact angle of an aqueous solution on all of the fibers, including bleached, unbleached, and sized fibers, is zero or close to zero. The advancing contact angle decreases as the surfactant concentration increases up to the critical micellization concentration.

3. Fiber loss in the flotation process is attributable to two different mechanisms: fiber-bubble adhesion and froth entrainment, but the fiber adhesion is less important compared to the entrainment.

4. Increasing froth height can decrease fiber loss and water loss. By increasing froth height, water loss and fiber loss can be reduced.

5. Calcium ion concentration will significantly affect froth stability, ink removal, and fiber loss only when an anionic surfactant is used.

6. Toner and fines will contribute to air bubble stabilization, but this contribution is not significant.

REFERENCES

1. N. Ramakrishnan and C. Balaraman, Mineral processing, recent trends, *J. Mines, Metals & Fuels*, **37** (10) 437 (1989).

2. H.J. Schulze, Fundamentals of flotation deinking in comparison to mineral flotation, *1st Research Forum on Recycling*, Montreal, Canada, 161 (1991).

3. L.D. Ferguson, Deinking chemistry: Part 1, *Tappi J.*, **75(7),** 75 (1992).

4. L.D. Ferguson, Deinking chemistry: Part 2, *Tappi J.*, **75(8),** 49 (1992).

5. A. Larson, P. Stenius, and L. Oderg, Surface chemistry in flotation deinking, Part III, Svensk PAPPER, **88,** (3), R2 (1985).

6. R.W. Turvey, An overview of the deinking process, *22th International Symposium on Wet End Chemistry Developments for the 90's*, Miami University, (1991).

7. A. Larson, P. Stenius, and L. Oderg, Surface Chemistry in flotation deinking, Part II, Svensk PAPPER, **87,** (18), R165 (1985).

8. R.W. Turvey, Why do fibers float, *J. Pulp Paper Sci.*, **19**, 52 (1993).

9. R.W. Turvey, Stock loss as a function of water hardness in flotation deinking, *Paper Techn. and Ind.*, 366 (1987).

10. G.M. Dorris and N. Nguyen, Flotation of model inks, Part II: Flexo ink dispersions without fiber, *2nd Research Forum on Recycling*, 13, (1993).

11. L. Sjostrom and A. Calmell, Detachment of printing ink from different types of fibers, Proceedings of Research Forum on Recycling, Montreal, 1 (1995).

12. J. D. Fallows, *Deinking Seminar Notes,* Atlanta, GA, TAPPI Press, June 22-24 (1992).

13. M. Li and M. Muvundamina, Fractionation of recycled pulp obtained from mixed paper, *1994 TAPPI Recycling Symp.*, Atlanta, TAPPI Pres. 303 (1994).

14. K. Schwinger and B. Dobias, The influence of calcium ions on the loss of fiber in the flotation deinking process, *1st Research Forum on Recycling,* Montreal, Canada, 1 (1991).

15. M. Ajersch and R. Pelton, The growth of bubbles on pulp fibers and on carbon black dispersed in supersaturated carbon dioxide solution, *3rd Research Forum on Recycling,* Vancouver, Canada, 27 (1995).

16. M. Ajersch and R. Pelton, The growth of bubbles on pulp fibers and on carbon black dispersed in supersaturated carbon dioxide solution, *2nd Research Forum on Recycling*, Montreal, Canada, 129 (1993).

17. M. Ajersch, R. Pelton, S. Loewen, and A. Chan, Measurement of dispersed air in newsprint pulp suspensions, *Tappi J.* **75** (2) 125 (1992).

18. M. Ajersch and R. Pelton, Mechanisms of pulp loss in flotation deinking, *J. Pulp and Paper Sci.*, 22, 9 (1996).

19. J.W. Foote, A method for the measurement of the angle of contact formed between a liquid surface and a fiber, and the application of this and swelling data to pore diameter measurements, *Paper Trade J.,* October: 40 (1939).

20. W.C. Jones and M.C. Porter, A method for measuring contact angles on fibers, *J. Colloid Interface Sci.,* **24**, 1 (1967).

21. T.H. Grindstaff, A simple apparatus and technique for contact-angle measurements on small-denier single fibers, *Textile Res. J.* **39**, 958 (1969).

22. K.T. Hodgson and J.C. Berg, Dynamic wettability properties of single wood pulp fibers and their relationship to absorbency, *Wood and Fiber Sci.,* **20**, 3 (1988).

23. J.J. Krueger and K. T. Hodgson, The relationship between single fiber contact angle and sizing performance, *Tappi J.,* **78**, (2), 154 (1995).

24. J.J. Krueger, and K. T. Hodgson, Single-fiber wettability of high sized pulp fibers, *Tappi J.* **77** (7), 83 (1994).

25. L.J. Warren, Determination of the contributions of true flotation and entrainment in batch flotation tests, *Int. J. Min. Proc.* **14**, 34 (1985).

26. J.H. Klungness, Measuring the wetting angle and perimeter of single wood pulp fibers: a modified method, *Tappi J.* **64** (12), 65 (1981).

27. R.A. Young, Wettability of wood pulp fibers, applicable of methodology, *Wood and Fiber*, **8** (2), 120 (1976).

28. T.H. Daugherty, Dynamic wetting of single pulp fibers, M.S. thesis, University of Washington (1981).

29. H. Putz, H. Schaffrath, and L. Göttsching, Deinking of oil- and water-born printing inks. A New Flotation Deinking Model, *1st Research Forum on Recycling,* Montreal, Canada, 183 (1991).

30. C. Ackermann, H. Putz, and L. Göttsching, Deinkability of waterborne flexo inks by flotation, *2nd Research Forum on Recycling,* Montreal, Canada, 201 (1993).

31. M. Epple, D. Schmidt, and J. Berg, The effect of froth stability on the flotation of a xerographic toner, *Colloid Polym. Sci.,* **272**, 1264 (1994).

UTILIZATION OF RECYCLED FIBERS-STICKIES

STATUS REPORT

FOR

PROJECT F00902

Sujit Banerjee
Sonal Patel
Thomas Merchant

March 27, 1997

Institute of Paper Science and Technology
500 10th Street, N.W.
Atlanta, Georgia

Project Title: UTILIZATION OF RECYCLED FIBERS-STICKIES
Project Staff: Sujit Banerjee, Sonal Patel, Thomas Merchant
Budget (FY 96-97): $56,000
Reporting Period: FY 96-97
Division: Engineering and Paper Materials
Project Code: STICKIES
Project No.: F00902

Effect of Shear on Stickie Deposition and Agglomeration

Introduction

Stickies are frequently found on shear-sensitive surfaces. In order to understand how shear influences PVAc deposition, Britt jar measurements were made where polyvinyl acetate (PVAc) or wax was added to water or a pulp slurry, and the material deposited on the blade measured. Since the flow is laminar at the stirring speed used, the fluid in the immediate vicinity of the blade moves at roughly the same velocity as the blade. Hence, the blade surface is in a low-shear region, as compared to the walls which experience the highest shear. The stickie or wax deposits on the blade since it is the most quiescent region in the system. Since the deposit forms a smooth sheath on the blade which easily detaches, the importance of molecular weight, temperature, shear, and consistency can be easily evaluated. In a separate set of preliminary experiments, we have induced the agglomeration of an acrylate in water by shear alone. This report presents the complete deposition results, and provides preliminary data on agglomeration.

Effect of PVAc molecular weight on fiber:water distribution

PVAc was melted on linerboard (15 g.) which was then slushed in a British disintegrator with 1.5L of water at 60°C at 50,000 revolutions. The slurry was processed at 600 rpm at 50°C for 15 min., drained through a 200 mesh screen, and the filtrate dried at 105°C. For the 0.5% consistency work, the slurry was diluted with an equal volume of water. The residue was Soxhlet extracted with toluene for 2 hours, and the toluene filtered, dried and weighed. The results in Table 1 for both pure and mixed stickies indicate that the amount of stickie transferred to the filtrate is not influenced by molecular weight. The absence of a molecular weight dependence can be rationalized if the residue was principally composed of stickie-fiber aggregates that broke off the furnish as opposed to discrete stickie and fiber entities. An important observation that initiated much of the remaining study was that a small amount of material deposited on the blade. Accordingly, deposition of stickie on the blade from an aqueous suspension was studied in the absence of fiber.

Blade deposition of stickies on shear sensitive surfaces in the absence of fiber

Pure PVAc

Ten mL of a 2 percent solution of PVAc in methanol was injected slowly into 600 mL of water in a Britt jar stirred at 200-800 rpm, so that a total of 0.2 gm of PVAC was added to the system. The Reynolds number at 400 rpm is 7.88E3. The material deposited on the blade was removed, dried and weighed; the results are listed in Table 2.

Deposition increases cleanly and substantially with increasing molecular weight as illustrated in Figures 1 and 2 for the 50°C and 70°C experiments, respectively. The effect of temperature is more variable, with deposition changing only slightly with increasing

Table 1: Effect of molecular weight on the distribution of PVAc				
run	PVAC (MW, wt.)	filtrate residue (g.)	extract wt. (g.)	avg. percent stickie recovered[1]
0.5% consistency				
6815A	12,800 (1 g.)	0.0735, 0.0946	0.0020, 0.0013	0.85
6815B	90,000 (1 g.)	0.0963, 0.0425	0.001, 0.0014	0.60
6815C	500,000 (1 g.)	0.0856, 0.0434	0.0015, 0.0036	1.3
6816A	12,800 (1 g.) & 90,000 (1 g.)	0.0393, 0.0538	0.0012, 0.0019	0.4
6816B	12,800 (1 g.) & 500,000 (1 g.)	0.0678, 0.0790	0.0035, 0.0013	0.6
6816C	90,000 (1 g.) & 500,000 (1 g.)	0.0744, 0.0865	0.0013, 0.0009	0.28
1% consistency				
6823A	12,800 (2 g.)	0.1534, 0.2046	0.0009, 0.0015	0.3
6823B	90,000 (2 g.)	0.2016, 0.1936	0.0018, 0.0046	0.8
6826A	500,000 (2 g.)	0.1560, 0.1719	0.0009, 0.0012	0.25
6826B	12,800 (2 g.) & 90,000 (2 g.)	0.0688, 0.2115	0.0023, 0.0038	0.75
6826C	12,800 (2 g.) & 500,000 (2 g.)	0.1940, 0.1969	0.0014, 0.0019	0.83
6826D	90,000 (2 g.) & 500,000 (2 g.)	0.1668, 0.1923	0.002, 0.001	0.38
[1]of original amount of stickie added; ± 25%				

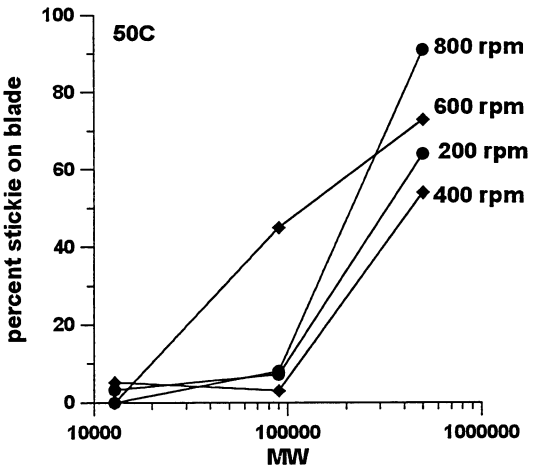

Figure 1: Stickie deposition at 50°C

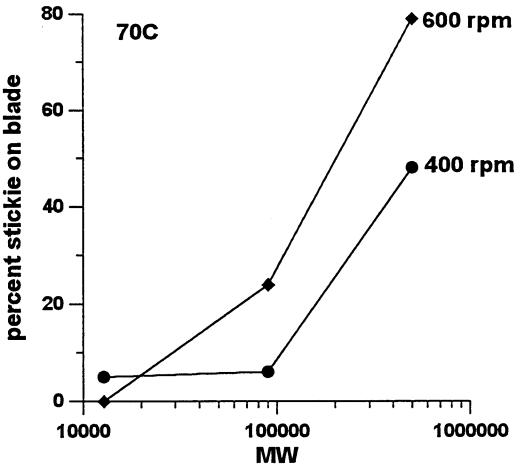

Figure 2: Stickie deposition at 70°C

Table 2: Blade deposition of PVAc (no fiber)				
run	**PVAc MW**	**temp (°C)**	**stickie on blade (g.)**	**avg. percent stickie on blade (g.)[1]**
200 rpm				
61015A	12,800	50	0.0069, 0.0057	3.2
61015C	90,000	50	0.0144, 0.0147	7.3
61015E	500,000	50	0.1218, 0.1322	64
400 rpm				
61017A	12,800	25	0.0366, 0.0364	18
6513A	12,800	50	0.0102, 0.0108	5.3
6605A	12,800	70	0.014, 0.0065	5.0
61017C	90,000	25	0.0072, 0.0095	4.2
6513B	90,000	50	0.0606, 0.0628	3.1
6604A	90,000	70	0.0123, 0.0118	6.1
61017E	500,000	25	0.1485, 0.1050	63
6510D	500,000	50	0.1040, 0.1101	54
6604B	500,000	70	0.1007, 0.0915	48
600 rpm				
61017B	12,800	25	0	
6426A	12,800	50	0	0
6426B	12,800	70	0	0
61017D	90,000	25	0	0
6429A	90,000	33	0.1195, 0.0461	41
6424B	90,000	50	0.079, 0.1014	45
6424A	90,000	70	0.0446, 0.0503	24
61017F	500,000	25	0.1518, 0.1227	69
6426C	500,000	50	0.1261, 0.1658	73
6426D	500,000	70	0.1637, 0.1542	79
800 rpm				
61015B	12,800	50	0	0
61015D	90,000	50	0.0154, 0.0166	8
61015F	500,000	50	0.1641, 0.192	91
[1]of original amount of stickie added; ± 10%				

temperature. There are two exceptions. Deposition of the MW 12,800 PVAc falls threefold over the 25-50°C interval at 400 rpm, and that of the MW 90,000 PVAc is reduced by half over the 50-70°C range at 600 rpm. The effect of stirring speed on the MW 12,800 material is consistent in that deposition does not occur at rpm values of over 600. The MW 90,000 polymer is influenced strongly by rpm. Note that in Figure 1, deposition is low for all condi-

tions except 600 rpm, i.e. deposition reaches a maximum at this speed, and falls of in either direction. A similar but smaller increase also occurs between 400 and 600 rpm at 70°C.

Since the flow is laminar at the stirring speed used, the fluid in the immediate vicinity of the blade moves at roughly the same velocity as the blade. Hence, the blade surface is in a low-shear region, as compared to the walls which experience the highest shear. The stickie or wax deposits on the blade since it is the most quiescent region in the system, i.e. deposits on the walls tend to be washed out. Most of the variability on temperature and rpm can be reconciled through consideration of PVAc viscosity. Deposition increases with increasing molecular weight, since the viscosity increases concomitantly, and the more viscous material resists washout from the blade. Since increasing temperature lowers viscosity, deposition is either unaffected by or decreases with temperature. The effect of stirring speed is straightforward for the MW 12,800 material in that the higher speed increases the washout tendency. The MW 90,000 polymer exhibits more complex behavior (which is presently not understood) rising between 400 rpm and 600 rpm, but decreasing on either side of the 600 rpm value in Figure 1.

Deposition on a Teflon blade

In order to determine the extent to which the blade material influences deposition, the metal blade of the Britt jar was substituted with a Teflon-coated replacement. The blade assembly consists of three circular paddles connected to a shaft. The metal paddles were of 1.96" diameter; those for Teflon were of 2.00". Hence, the Reynolds numbers were marginally higher with Teflon. Ten mL of a 2% solution of PVAc in methanol was injected slowly into 600 mL of water in a Britt jar at 50°C, so that a total of 0.2 gm of PVAC was added to the system. Deposition is lower on Teflon as shown in the comparison in Table 3. The trend is reasonable since Teflon is more oleophilic than metal.

Table 3: Deposition of PVAc on Teflon (no fiber)

run	MW	rpm	stickie on blade (g.)[1]	avg. percent stickie on blade	metal blade values (Table 2)
61125A	12,800	400	negligible	0	5.3
61125B	12,800	600	0.0093, 0.0109	5.0	0
61202A	90,000	400	0.0363, 0.0314	2.7	3.1
61202B	90,000	600	0.0939, 0.0839	4.9	45
61204A	500,000	400	0.1808, 0.1818	9.5	54
61204B	500,000	600	0.1640, 0.1646	8.2	73

[1]of original amount of stickie added

Mixtures of PVAcs

The above measurements were repeated for equal mixtures of two stickies, which were prepared together in methanol and then added to the Britt jar. The results are presented in Table 4 and illustrated in Figures 3-5. For example, Figure 3 presents data on mixtures of the MW 12,800 polymer with either the MW 90,000 material or the MW 500,000 stickie. Except for one case, the 90,000 and 500,000 mixture at 400 rpm in Figure 5, deposition decreases with temperature. Again, the effect of stirring speed alone is uncertain, with no clear trend emerging. For example deposition increases with rpm in Figure 3; the opposite is true in Figures 4 and 5. In general, the property of the mixture is intermediate between those of its constituents. While this is not true for all mixtures (as will be shown later for wax), it seems that the deposition properties of a polymer with components of different degrees of polymerization can be tailored through mixing. For example, the properties of a MW 90,000 polymer can be approximated by a mixture of MW 12,800 and MW 500,000 polymers.

An attempt was made to separate deposits of stickie mixtures with size exclusion chromatography which separates different molecular weight fractions. The individual stickies were run initially to establish response factors. Columns in the size fraction of 500-10,000 and 20K-300K were used in tandem, and a UV detector was set at 230 nm. The response curves of the individual PVAcs (12,800, 90,000, 500,000) were linear. However, mixtures of stickies could not be separated, since the nominal molecular weight of the stickie was only an average covering a wide range of molecular weights.

Table 4: Blade deposition of PVAc mixtures in the absence of fiber

run	PVAc MW (1:1 mixtures)	temp (°C)	rpm	stickie on blade (g.)	avg. percent stickie on blade (g.)[1]
6614A	12,800, 90,000	50	400	0.0135, 0.0261	9.9
6614D	12,800, 90,000	70	400	0.0066, 0.0166	5.8
6614B	12,800, 90,000	50	600	0.0589, 0.0584, 0.0435	27
6614C	12,800, 90,000	70	600	0.0097, 0.0251	8.7
6614E	12,800, 500,000	50	400	0.0384, 0.0538	23
6614H	12,800, 500,000	70	400	0.0188, 0.0326	13
6614F	12,800, 500,000	50	600	0.0712, 0.0825	38
6614G	12,800, 500,000	70	600	0.0465, 0.0553	25
6614I	90,000, 500,000	50	400	0.0471, 0.0859	33
6614L	90,000, 500,000	70	400	0.1465, 0.0801	57
6614J	90,000, 500,000	50	600	0.0295, 0.0896	30
6614K	90,000, 500,000	70	600	0.0393, 0.0762	29

[1]of original amount of stickie added, ± 29%

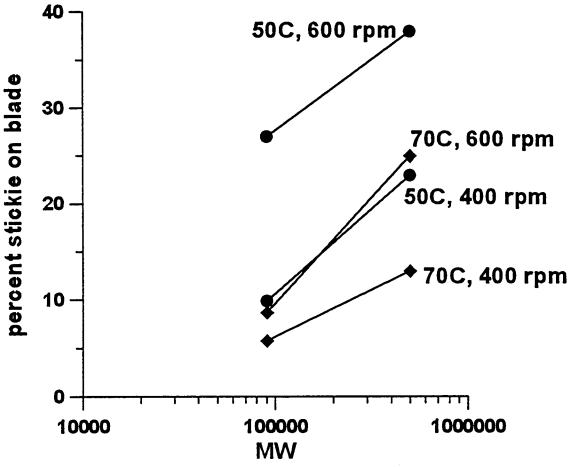

Figure 3: Deposition of MW 12,800 & (MW 90,000 or MW 500,000)

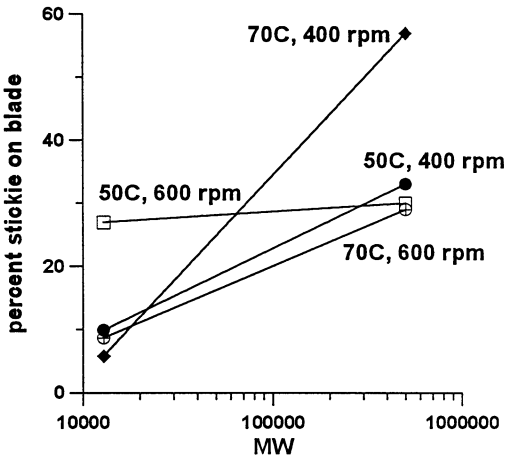

Figure 4: Deposition of MW 90,000 & (MW 12,800 or MW 500,000)

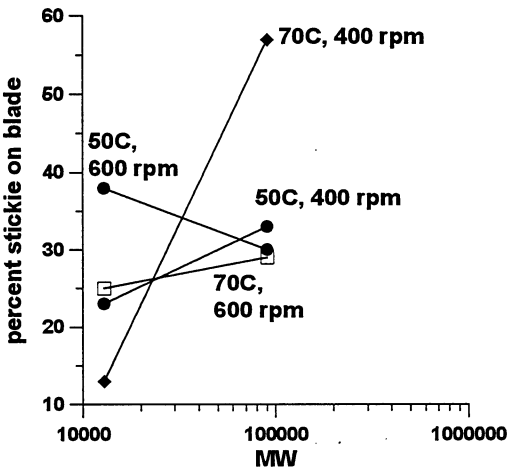

Figure 5: Deposition of MW 500,000 & (MW 12,800 or MW 90,000)

Effect of the sequence of addition on blade deposition

Each pair of stickies used above was dissolved in methanol, and were, therefore, completely mixed when they deposited out of solution. Conceivably, separate addition of the stickies to the solution could alter deposition behavior; e.g. one stickie could attach to the blade first, with the other then depositing on the attached stickie. Hence, 0.1 g of each PVAC separately dissolved in 10 mL of methanol was added sequentially to 600 mL of water in the Britt jar kept at 50°C with the rotor set at 400 rpm. The results shown in Table 5 demonstrate that deposition in independent of the sequence of addition.

Table 5: Effect of addition sequence on blade deposition			
run	**addition sequence**	**stickie on blade (g.)**	**avg. percent stickie on blade (g.)**
6904B	90,000, 12,800	0.0215 g	11
6909C	12,800, 90,000	0.0174 g	8.7
6909A	90,000, 500,000	0.0718 g	36
6909B	500,000, 90,000	0.0503 g	25
6909D	12,800, 500,000	0.0534 g	27
6909E	500,000, 12,800	0.0358 g	18

Table 6: Deposition of wax in the absence of fiber				
run	**rpm**	**temp (°C)**	**avg. percent wax on sides**	**avg. percent wax on blade**
6617A	400	50		7.2
6617D	400	70	16.5	2.5
6617B	600	50	45	0.8
6617C	600	70	11	0.9
			toluene extracted	
61023A	400	50	62, 84	7.2
61023B	600	50	67, 73	5.5

Wax

The above approach was extended to 3040 Amber wax (used in curtain coating), 1 g. of which was melted and added to 600 mL of water in a Britt jar. Unlike the PVAc work, most of the wax was found on the sides of the container as shown in Table 6. Initially, the sides were physically scraped off, and wax recovery was poor, as shown in the first four entries of Table 6. Later, warm toluene was used to dissolve the wax, and much more material was recovered. In any case, blade deposition of the wax was minimal.

A PAC member suggested that wax deposition on the Britt jar walls might be induced by a relatively cool wall temperature. Hence, comparisons were made with and without insulation of the Britt jar sides. The insulation used was foam material taken from beverage can "coozies". Temperatures of both the water, and the region between the jar exterior and the insulation were recorded. The temperature of the water was found to higher than that of the exterior surface of the jar by about 7°C after a typical 15 minute run. However, the plastic wall material is an excellent insulator, and the corresponding difference between water and the interior surface should be much narrower. A pair of experiments were done where the deposition of the wax added as above was measured at 400 rpm and 50°C with and

Table 7: Deposition of wax/PVAc mixtures in the absence of fiber					
run	MW of PVAC mixed with wax	rpm	temp (°C)	avg. percent wax on blade	avg. percent wax on sides
6618D	12,800	400	50	21	30
6618C	12,800	600	50	1.6	32
6618A	12,800	400	70	1.9	10
6618B	12,800	600	70	2.9	18
6619A	90,000	400	50	2.7	11
6619B	90,000	600	50	13	50
6619D	90,000	400	70	1.2	67
6619C	90,000	600	70	0.5	10
6620A	500,000	400	50	4.2	13
6620B	500,000	600	50	1.6	28
6620C	500,000	400	70	0.5	22
6620D	500,000	600	70	0.2	18

without insulation. For the uninsulated experiments, 95% of the wax was recovered from the walls. Immeasurable amounts were attached to the stirrer shaft and temperature probe, and nothing deposited on the blade surface. A 65% recovery was realized from the insulated work; as before virtually all of the material was attached to the sides.

The behavior of wax differs from that of PVAc in that it preferentially attaches to the sides. Because of its high molecular weight, the wax will resist washout, and will attach to the first receptive surface it encounters. Since the area of the surface greatly exceeds that of the blade, the wax preferentially deposits there.

Mixtures of wax and PVAc were studied next in order to determine the extent to which PVAc modified the behavior of wax. Equal amounts (0.5 g.) of wax and PVAc were melted together and added to 600 mL of water in the Britt jar and processed for 15 minutes. The results shown in Table 7 demonstrates complex behavior. For example, blade deposition of either pure wax or the 12,800 MW PVAc alone is small, whereas a substantial amount of a mixture of the two attaches to the blade. It would appear that the mixed material exhibits properties that are not necessarily intermediate between the behavior of its components. We hypothesize that the stickie softens the wax to the point where it is washed off the sides and transferred to the blade.

Deposition of stickies on shear sensitive surfaces in the presence of fiber

Stickie attached to fiber

PVAc (1 g.) was melted on different amounts of linerboard and the material was slushed with 1L of water in a British disintegrator. The pulp (300 mL) was diluted with an equal volume of water and processed in the Britt jar at 50°C for 15 minutes. The material on

Table 8: Deposition of 12,800 MW PVAc at 50°C in the presence of fiber			
run	**consistency (%)**	**rpm**	**percent stickie on blade**
6709B	0.025	600	0.0
6708I	0.05	400	0.0
6708J	0.05	600	9.9
6628A	0.10	400	0.0
6628B	0.10	600	0.0
6628C	0.20	400	14
6628D	0.20	600	20
6628E	0.30	400	18
6629A	0.30	600	1.3
6629B	0.40	400	2.6
6629C	0.40	600	2.9
6629D	0.50	400	5.0
6629E	0.50	600	16
6701A	0.60	400	8.2
6701B	0.60	600	6.4

Table 9: Deposition of 90,000 MW PVAc at 50°C in the presence of fiber			
run	**consistency (%)**	**rpm**	**percent stickie on blade**
6708C	0.025	400	17
6708D	0.025	600	71
6708A	0.05	400	0
6708B	0.05	600	118
6625A	0.10	400	0
6625B	0.10	600	0
6625C	0.20	600	11
6625D	0.20	400	0
6625E	0.30	400	0
6625F	0.30	600	23
6625G	0.40	600	34
6625H	0.40	400	0
6626A	0.50	400	0
6626B	0.50	600	0
6626C	0.60	600	0
6626D	0.60	400	0

Table 10: Deposition of 500,000 MW PVAc at 50°C in the presence of fiber			
run	**consistency (%)**	**rpm**	**percent stickie on blade**
6708H	0.025	600	0
6708E	0.05	400	38
6708F	0.05	600	0
6627A	0.10	400	0
6627B	0.10	600	0
6627C	0.20	400	0
6627D	0.20	600	42
6627E	0.30	600	0
6627F	0.30	400	0
6627G	0.40	400	0
6627H	0.40	600	0
6627I	0.50	400	0
6627J	0.50	600	0
6627K	0.60	400	0
6627L	0.60	600	0

the blade was then measured, and the results are presented in Tables 8-10. Deposition of the 12,800 material increases slightly with increasing fiber content. For example, Table 2 shows no deposition at 50°C at 600 rpm in the absence of fiber, whereas appreciable amounts are found on the blade in Table 8 at the higher consistencies. We attribute the difference to the fact that the fiber adds "body" to the stickie, in effect increasing its viscosity. In other words, when the fiber-stickie aggregate contacts the blade, the stickie bonds to the blade, and the fiber provides resistance to washout.

Deposition of the MW 500,000 molecular weight polymer is reduced in the presence of fiber. This polymer has a sufficiently high viscosity to withstand shear, and the added fiber only serves to scour the stickie off the blade. The behavior of the MW 90,000 polymer is inconsistent. Under some conditions, the fiber induces greater deposition; in others the amount is reduced. Recall, however, that the deposition of this polymer was highly variable in the absence of fiber (Figure 1). The fiber adds an additional level of complexity, and we attribute the variability in Table 9 to a combination of the strengthening and scouring action of the fiber.

Stickie free from fiber

In order to determine the scouring effect of fiber on stickies, measurements were made where the stickie was added to a pulp suspension. PVAc (0.2 g.) in 10 mL of methanol was added dropwise to a 600 mL pulp suspension in a Britt jar at 50°C. The mixture was

Table 11: Effect of consistency on the blade deposition of PVAc				
run	PVAc MW	rpm	stickie on blade	average percent stickie on blade
consistency: 0.033%				
61010A	12,800	400	0, 0	0
61010B	12,800	600	0, 0	0
61010C	90,000	400	0.0146, 0.0117	6.6
61010D	90,000	600	0.0144, 0.0134	7.0
61010E	500,000	400	0.0098, 0.00108	5.1
61010F	500,000	600	0.0058, 0.0336	9.9
consistency: 0.067%				
61011A	12,800	400	0.0046, 0	0.0046
61011B	12,800	600	0, 0	0
61011C	90,000	400	0.0142, 0.0140	0.0141
61011D	90,000	600	0,0	0
61014A	500,000	400	0.0570, 0.0724	0.0647
consistency: 0.133%				
61014B	500,000	600	0.0484, 0.0425	0.0455
61002A	12,800	400	0, 0	0
61002B	12,800	600	0, 0	0
61002E	90,000	400	0.0029, 0.0035	0.0032
61002F	90,000	600	0, 0	0
61003C	500,000	400	0.0066, 0.0092	0.0079
61003D	500,000	600	0, 0	0
consistency: 0.25%				
61002C	12,800	400	0, 0	0
61002D	12,800	600	0, 0	0
61003A	90,000	400	0.0042, 0.044	0.0043
61003B	90,000	600	0, 0	0
61004A	500,000	400	0.0050, 0.0060	0.0055
61004B	500,000	600	0, 0	0

stirred for 15 minutes and the material deposited on the blade weighed. Although stickies comprised most of the deposits, fiber was also trapped on the blade. The deposits were dissolved in methanol, filtered to remove fiber, and the dried filtrate reweighed to give the stickies content. The results listed in Table 11 show that even at low consistency, the amount deposited is decreased substantially from the "no-fiber" result in Table 2. The effect is particularly strong for the 500,000 MW PVAc. The most likely explanation lies in the abrasive nature of the fiber referred to above. A less likely scenario is that the number of stickie-blade collisions will be decreased by the presence of fiber, and stickie deposition could also

Table 12: Effect of surfactant (BRD2360) on PVAc deposition				
run	PVAc MW	rpm	stickie on blade (g.)	average percent stickie on blade
61029A	90,000	400	0.0187, 0.0222	10
61029B	90,000	600	0.0345, 0.0090	11
61031A	90,000	200	0.0211, 0.0226	11
61103A	500,000	400	0.1847	92
61103B	500,000	600	0.1334, 0.1868	80

Table 13: Effect of surfactant hydrophobicity on PVAc deposition			
run	rpm	stickie on blade (g.)	average percent stickie on blade
LHB=2			
61120A	400	0.0459, 0.0261	18
61120B	600	0.0347, 0.0211	14
LHB=16			
	400	0.0215, 0.0373	12
	600	0.0411, 0.0158	14

decrease on this account.

Effect of surfactant on blade deposition of PVAc

PVAc (0.2 g.) in 10 mL of methanol was added dropwise to 600 mL of water at 50°C containing 0.0410 g. of surfactant BRD2360 in a Britt jar. This material is sold by Buckman as a flotation aid for secondary fiber recovery, and is a blend of fatty acids. A comparison of the results shown in Table 12 with those run without surfactant in Table 2 shows that the surfactant has a significant but relatively small effect.

In order to determine whether surfactant hydrophibicity played a role a set of surfactants of different LHB values were obtained from ICI. An material with an LHB value of 2 was prepared from 8% span 80 (sorbitan monooleate) and 92% of span 85 (sorbitan trioleate). An LHB 16 material was prepared by mixing 60% of Tween 20 and 40% of Tween 80; both Tween formulations are polyoxyethylene 20 sorbitan monolaurate. The surfactant (0.04 g.) was added to water (50°C) before introduction of the 90,000 PVAc (0.2 g./10 mL methanol). As shown in Table 13, deposition appeared to be independent of stickie hydrophobicity.

Measurements were also made with whitewater from Riverwood's coated board and

Table 14: PVAc deposition out of whitewater				
run	**whitewater**	**rpm**	**stickie on blade (g.)**	**avg. percent stickie on blade**
61115A	#1 coated board	400	0.0593, 0.0589	29
61115B	#1 coated board	600	0.0756, 0.0552	32
61118A	#2 linerboard	400	0.0198, 0.0246	11
61118B	#2 linerboard	600	0.0252, 0.0282	13

linerboard lines at Macon. The PVAc (0.2g, 90,000 MW) in methanol was added dropwise to the filtered white water (600 mL) at 50°C in the Britt jar and maintained for 15 minutes. Comparison of the results shown in Table 14 with the Table 2 baseline data shows that surfactant only has a relatively small effect. Hence, our results in water should at least qualitatively apply to a mill situation. We caution that these results only apply to PVAc, and should not be generalized across all stickies.

Preliminary work on inducing a controlled stickies outbreak

All of our previous work was done with a Britt jar. We had acquired a mixing chamber through another project where temperature, pH and stirrer speed is computer-controlled, and gas or liquid can be automatically introduced. The original purpose of the equipment (New Brunswick Bioflow 3000, illustrated in Figure 6) was for fermentation in a biotechnology project. The glass tank has a total volume of 5L, and a working volume of 2.5L. Inserted into the center of the tank is a metal shaft stirrer with a radial flow impeller that can be controlled to 50-1000 rpm. Four removable metal baffles are placed to reduce solid body rotation and minimize vortex formation. The bottom of the tank is jacketed with a controlled temperature water bath. A probe placed into the liquid in the tank monitors the temperature, which is regulated at 25-80°C by a microprocessor. The reactor also accommodates a pH probe, and pH can be automatically adjusted. Air can be introduced through a ring-shaped sparger placed directly beneath the impeller.

Since we had the luxury of automatically adjusting a variety of conditions, we set out to create a stickies outbreak. A Carbotac 26171 latex (5 mL) which is approximately half latex and half water was added to 2L of water at 50°C, and the pH and impeller speed was varied. Sticky globs floated to the surface at high rpm (10,000) and low pH (≈2). Small amounts also adhered to the surfaces of the submerged baffles and impeller blades and shaft. The disappearance of the latex from the suspension could be measured with a spectrophotometer at 650 nm, the wavelength typically used for turbidity measurements. Absorbances of latex suspensions were linear with concentration which allowed the water clarification to be followed progressively.

The results of two such experiments are presented in Figures 7 and 8, which differ in that air at 5 lpm was bubbled through the system in the Figure 8 work. The suspension was

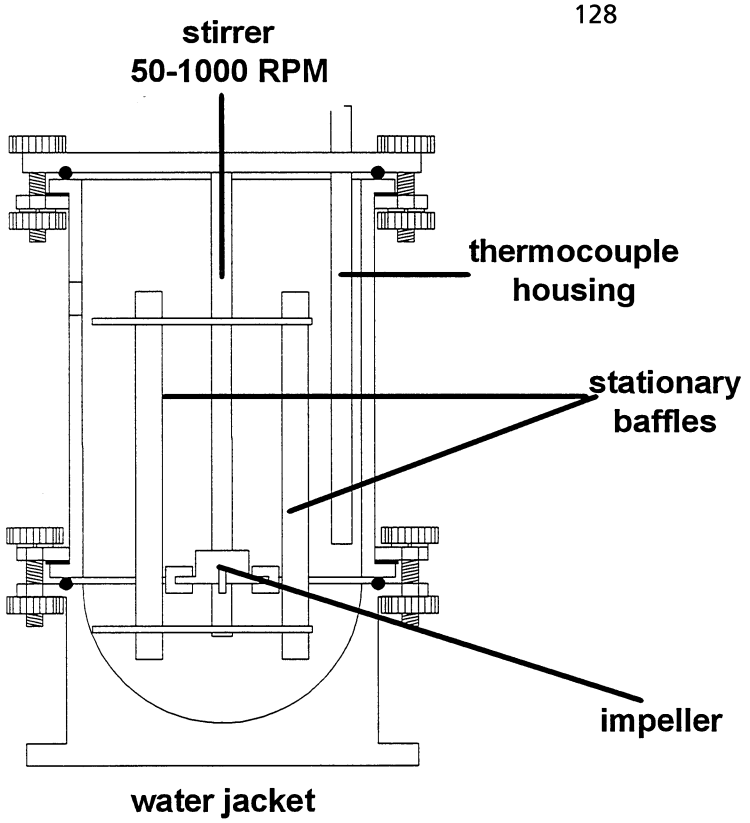

Figure 6: Schematic of the Bioflow 3000 fermenter

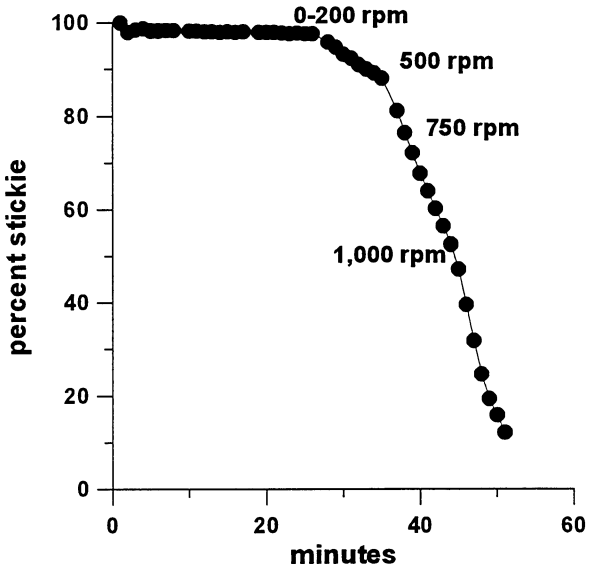

Figure 7: Water clarification at 50°C

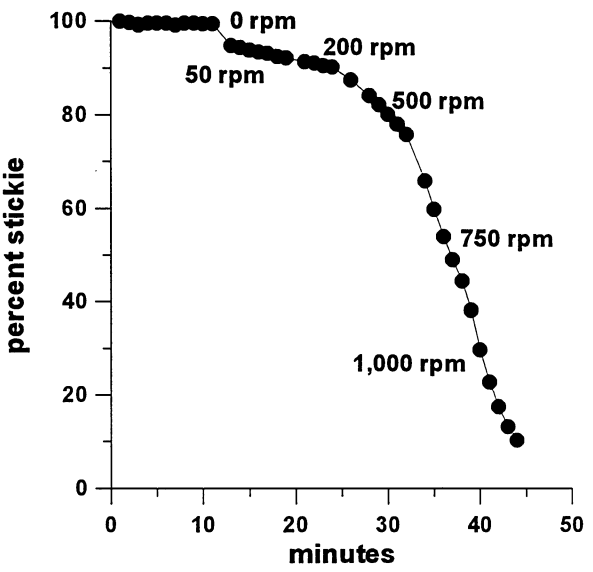

Figure 8: Water clarification at 50°C, with a 5 lpm air flow

initially stirred at 50 rpm with samples being drawn every minute, and the speed was then progressively increased to 1000 rpm. Appreciable agglomeration occurs at or above stirring speeds of 500 rpm, and the water is substantially clarified at 1,000 rpm where the agglomerated stickie floats to the surface. Agglomeration did not occur in neutral solutions even at 1,000 rpm and under aeration, suggesting that the polymer needed to be destabilized before it could grow. Evidently, the repulsion among negatively charged polymer molecules is sufficient to overcome the agglomerating influence of turbulence.

Since air was entrained at the higher speeds, the additional effect of aeration was examined in Figure 8, where the Figure 7 procedure was repeated under an airflow of 5 lpm. Air enhances agglomeration at the lower rpms, but not at higher agitation. Presumably, the contribution of the added turbulence provided by aeration is significant only at low rpms where the turbulence is proportionately smaller.

Conclusions

Two opposing forces appear to govern the deposition of stickies. At low shear, the stickie tends to deposit on a surface on account of its tack. As shear increases, the stickie tends to get washed off the surface. The presence of fiber accelerates the process probably through physical abrasion. Hence, for deposition to occur, the stickie must have enough tack to attach to a surface, and a high enough viscosity to resist washout.

Since a low molecular weight stickie will be of lower viscosity than a higher molecular weight analog, it will tend to be washed out. On the other hand, the softening point of a high molecular weight material such as wax may be higher than the system temperature, in which case it may not have enough tack to attach to a surface. As observed, a mid-molecular weight substance may have the optimum tack and viscosity to deposit out. These properties may be best combined through a mixture. For example, while MW 12,800 PVAc or wax deposits only marginally, appreciable deposition occurs with a mixture of the two. It appears that the low molecular weight PVAc provides the tack and the high molecular weight wax contributes viscosity to the mixture. The presence of fiber can add "body" to a low molecular stickie thereby imparting some resistance to wash-out. Hence, fiber can have a dual effect. Although it's major effect is abrasion, it can also strengthen low-viscosity tacky stickies.

While it is certainly possible for a single stickie to have optimal properties for deposition, it is more likely that these properties can be reached through mixtures. By this logic, stickie deposits in mills will usually be comprised of mixtures. This could explain why stickie outbreaks in mills occur suddenly and are usually difficult to trace back to a particular load of furnish. Our findings suggest that a contaminant may destabilize a stickie suspension by reinforcing the tack or viscosity of the stickie by mixing with it. Hence, it could induce deposition while only being present in small proportions. Through the wax PVAc analogy discussed above, it is possible that two contaminants that are relatively innocuous when pure may combine to be troublesome.

Many of these conclusions should also apply to stickie-stickie agglomeration. For instance, the abrasive effect of fiber on stickie should apply regardless of whether the stickie is attached to a surface or suspended in water. For an outbreak to occur, the stickie agglomerate should have enough viscosity to withstand both shear and fiber abrasion. The effect of shear, however, is complex. On the one hand, shear could disrupt stickie particles; on the other, it could force contact among particles and induce agglomeration as exemplified by the fermenter work. The likely explanation is that turbulence overcomes the repulsive interactions among the stickies, which is diminished at low pH. However, if fiber is present, turbulence would accelerate stickie break-up by accelerating abrasion.

One of the unique attributes of the fermenter work is that it allows us to create a controlled outbreak. It appears that the factors contributing to an outbreak are viscosity, tack and shear response, both formative and disruptive. A control strategy that controls one or more of these factors should prove the most effective. The fermenter could also provide a means for testing dispersants. Polymers that inhibited agglomeration at high rpm at low concentrations would be judged as optimum. Turbulence could also be used to advantage in whitewater cleanup. For example, if dissolved air flotation is contemplated, then maximizing turbulence should improve agglomeration and floatability.